# CRITICAL HEAT FLUX FOR A DOWNWARDS FACING DISK IN A SUBCOOLED POOL BOILING ENVIRONMENT

**CRITICAL HEAT FLUX FOR A DOWNWARDS FACING DISK IN A SUBCOOLED POOL BOILING ENVIRONMENT**

By
M. Gočmanac,

A Thesis
Submitted to the School of Graduate Studies
in Partial Fulfillment of the Requirements for the Degree
M. A. Sc. in Engineering Physics

McMaster University
©Copyright by M. Gočmanac, 2011

MASTER OF APPLIED SCIENCE (2011)
(Engineering Physics)

MCMASTER UNIVERSITY
Hamilton, Ontario, Canada

Title: Critical Heat Flux for a Downwards Facing Disk in a Subcooled Pool Boiling Environment

Author: Marko Gočmanac, B. Eng. (McMaster University)

Supervisor: Dr. J. C. Luxat

Number of Pages: xiv, 94

## Acknowledgments

This work is an accomplishment by many. I'd like to thank all the positive, selfless people that I made the acquaintance of and inspired me throughout my studies at McMaster. I was fortunate to have learned from people with diverse talents and interests and have on more than one occasion witnessed excellence. Being a student at McMaster has been a privilege.

Most of all I would like to thank Dr. John Luxat. Dr. Luxat has always been willing to spend his time discussing things with me. He was very flexible in his approach and management style. I would like to thank him for having the vision that students too can perform experiments relevant to industry and for his idea in generating one.

I would like to acknowledge Clee and Jim for their guidance in the successful machining and construction of the heated element. Anytime I needed a hand with construction or experimentation my colleagues and friends from Engineering Physics were always up for it—especially Dave Trudell and Mike McDonald. I would like to acknowledge the work of B. A. Statham, particularly in development of the LabView temperature measurement application and his willingness to partake in illuminating discussions relating to pool boiling.

Lastly, I would like to say that I am very grateful to my company, AMEC NSS, for allowing me to take a leave of absence in an effort to complete my degree.

~

Za moju familiju i prijatelje, tamo daleko, i ovde blizu.

For my friends and family—near and far.

August 2011

## Abstract

An experimental investigation of the physical feasibility of thermal creep failure of the Calandria Vessel under a severe accident load is presented in this thesis. Thermal creep failure is postulated to occur if film boiling is instigated in the Shield Tank Water surrounding the Calandria Vessel. The objective of this experimental study is to measure the Critical Heat Flux (CHF) for a representative geometry in environmental conditions similar to those existing in the CANDU Calandria Vessel and Shield Tank Water.

Two geometries of downwards facing surfaces are studied. The first is termed the 'confined' study in which bubble motion is demarcated to the heated surface. The second is termed the 'unconfined' study where individual bubbles are free to move along the heated surface and vent in any direction.

The method used in the confined study is novel and involves the placement of a lip surrounding the heated surface. The level of confinement is adjusted by varying the inclination angle. Data has been obtained for Bond Numbers (*Bo*) 0, 1.5, 3, 3.6 and 11.8 with corresponding $q_{CHF}$ 596, 495, 295, 223, and 187 kW/m$^2$, respectively. A correlation relating the CHF to level of confinement is stated. The CHF results are in good agreement with Theofanous *et. al.* (1994), as is the observation that a transition angle is observed in the correlation. The transition angle in this study is found to be ~5.5°. The obtained nucleate boiling curves are compared to Su *et. al.* (2008) data for similar *Bo* and excellent agreement is achieved in the medium to high heat flux regions.

The unconfined study consists of a downward facing plate in a pool of subcooled water. The obtained nucleate boiling curve is compared with the Stephan-Andelsalam correlation and agreement is not observed. There were visibly different trends in the convective heat transfer coefficient with a mean difference of 31%. The experimental data is compared to data obtained by Nishikawa *et. al.* (1984) and is found to be in acceptable agreement. The power requirement to instigate film boiling was not met, meaning that the CHF is greater than 1 MW/m$^2$. Visual observations are made and an argument is based on the premise that the phenomenon of dryout for a downwards facing surface is similar to that of an upwards facing surface. The theory and current acceptance of CHF for an upwards facing surface is discussed—in particular Zuber's "Hydrodynamic Limit" of 1.1 MW/m$^2$, Dhir (1992) and recent experimental evidence from Theofanous *et. al.* (2002). These three studies were found to be in agreement with results presented here.

The experimental evidence presented herein supports the statement that thermal creep failure of the Calandria Vessel is physically unreasonable under analyzed severe accident loads.

# List of Figures

# List of Tables

# Table of Contents

# Nomenclature

| | |
|---|---|
| A | Cross-sectional Area |
| B | Subcooled CHF correction factor |
| Bo | Bond number |
| C | Specific Heat Capacity |
| D | Diameter of Disk or Heated Rod |
| $e_q$ | Systematic Error in heat flux, 95% confidence |
| $e_{q,CHF}$ | Systematic Error in CHF, 95% confidence |
| $e_{q,combined}$ | Combined Error in heat flux, 95% confidence |
| $E_s$ | Energy Stored |
| $e_{T,combined}$ | Combined Error in Temperature, 95% confidence |
| $e_{\sigma T}$ | Systematic Error in Temperature, 95% confidence |
| $e_{\sigma y}$ | Systematic Error in Separation Distance, 95% confidence |
| f | Bubble departure frequency |
| g | Acceleration due to gravity |
| $h_{Data}$ | Data calculated convective heat transfer coefficient |
| $h_{fg}$ | Enthalpy of vaporization |
| $h_{predicted}$ | Correlation predicate convective heat transfer coefficient |
| k | Thermal conductivity |
| L | Length of heated rod |
| M | Mass of vapour slug |
| $P_{CHF}$ | Input power at CHF |
| $P_{NB}$ | Input power at last known Nucleate Boiling Data Point |
| q | Heat Flux |
| $q_{CHF}$ | Critical Heat Flux |

| | |
|---|---|
| $q_{CHF}^{T\Delta_{sub}}$ | Subcooled Corrected Critical Heat Flux |
| $Q_{in}$ | Energy Input |
| $q_{NB}$ | Heat flux at last known Nucleate Boiling Data Point |
| $Q_v$ | Volumetric Heat Generation Rate |
| s | Gap size |
| T | Temperature |
| $T_1$ | Average Thermocouple Temperature Near Wall |
| $T_{1,2}$ | Arithmetic Mean of $T_1$ and $T_2$ |
| $T_2$ | Average Thermocouple Temperature Far Wall |
| $T_\infty$ | Pool Temperature or Bulk Fluid Temperature |
| $T_{avg}$ | Average Device Temperature |
| $T_{sat}$ | Temperature of Saturation for water at 1 atm |
| $T_w$ | Surface wall temperature |
| V | Volume |
| v | Velocity |
| y | Non-Recoverable Kinematic Energy Lost in Wall Collision |
| μ | Viscosity |
| $\Delta_{c\text{-}c}$ | Centre to Centre Vertical Separation Distance |
| ΔT | Difference between surface wall temperature and saturation temperature |
| $\Delta T_{sub}$ | Difference between saturation temperature and pool temperature |
| Δy | Thermocouple vertical separation distance |

**Greek Symbols**

| | |
|---|---|
| Δρ | Density difference between the liquid and vapour phases |
| θ | Angle of inclination |
| ρ | Density |

| | |
|---|---|
| $\rho_g$ | Density of the vapour phase |
| $\rho_l$ | Density of the liquid phase |
| $\sigma_{rq}$ | Random error in Heat Flux, 68% confidence |
| $\sigma_{rT}$ | Random error in Temperature, 68% confidence |
| $\sigma_{T1}$ | Random error in $T_1$, 95% confidence |
| $\sigma_{T2}$ | Random error in $T_2$, 95% confidence |

# 1 Introduction

The focus of this thesis is to report on an experimental study aimed at investigating whether or not wall-melt-through of the CANDU Calandria Vessel is a physically reasonable failure mode in the event of a severe accident. This chapter proceeds to provide the adequate background in operating CANDU reactors, severe accidents and boiling heat transfer in order to make the thesis self-contained and information presented within it accessible to readers.

## 1.1 The CANDU Reactor

The CANada Deuterium Uranium (CANDU) reactor is used in nuclear power plants to generate heat through the control of nuclear fission reactions. The CANDU reactor was developed in a partnership between Atomic Energy of Canada Limited and Ontario Hydro beginning in the 1950s with the first unit going operational in 1976. Significant design differences can be found in operating CANDU reactors, but all CANDUs can be adequately described by referring to the CANDU 6 design. Note, however, that the conclusions in that the work presented in this thesis are equally applicable to all CANDU designs.

The CANDU 6 reactor is a horizontal pressurized heavy water reactor. There are 380 fuel channels that contain 12 fuel bundles each. A fuel bundle is composed of 37 fuel elements comprised of natural Uranium Dioxide cylindrical pellets in a Zircaloy cladding. Spacers and bearing pads within the fuel bundle ensure separation between individual fuel bundles and the fuel channel. Each fuel channel is approximately 6 m long and is of Zircaloy material. Pressurized heavy water at an inlet pressure of 10 MPa transfers heat from the fuel to separate loop U-tube type steam generators.

Within the reactor core, Zircaloy Calandria Tubes (CT) surrounds the Pressure Tubes. Carbon Dioxide gas circulates between the annulus of each PT and CT in an effort to thermally insulate the primary heat transport system from the moderator system.

A unique feature of the CANDU design is that the moderator and coolant systems are distinct, separate and independent. The moderator in CANDU 6 reactors is heavy water which is maintained at approximately 70 ˚C and is only slightly pressurized relative to atmosphere. The moderator system is enclosed in the Calandria Vessel (CV).

The Calandria is made of stainless steel and has an inner diameter of approximately 7.6 m and a wall thickness of 29 mm. The Calandria Vessel is housed in and supported by a light water filled steel-lined concrete vault.

The most significant design feature of the CANDU reactor is that fresh nuclear fuel utilized is natural Uranium (0.73% U-235 wt%). To maintain the reactor critical at high powers, fresh fuel must be frequently inserted. Thus, CANDUs are designed to operate at full power while individual channels are re-fuelled. This design feature eliminates fuelling outages and can yield impressive capacity factors.

CANDU 6 reactors are equipped with two independent fast acting shutdown systems as well as an emergency core coolant injection system. Shut-Down System 1 (SDS1) is a system of 32 spring-loaded neutron absorbing rods that are poised above the reactor. Upon clutch de-energization the rods are accelerated by the force of gravity and, initially, the compressed spring. The rods fall through the moderator and rapidly reduce the reactor power. Shut Down System 2 (SDS2) injects dissolved Gadolinium Nitrate at a high pressure into the moderator. Each shutdown system uses separate neutron detectors and circuitry to initiate a reactor trip. Lastly, the Emergency Core Cooling System (ECCS) is a further heat sink in the event of a large or sustained Loss-of Coolant Accident (LOCA). This system will inject light water into the primary heat transport system and cool the fuel.

The CANDU reactor is a successful and safe technology that has been employed worldwide. As can be ascertained from the earlier discussion, the CANDU reactor has a significant number of heat sinks, safety systems and barriers that make radioactive release to the public an acceptably low risk.

## 1.2 Calandria Vessel Behaviour under Severe Accident Conditions

Severe accidents are defined as accidents that involve core degradation due to insufficient heat removal. Core degradation is defined as damage to fuel or structures within the reactor core. Severe accidents are an interesting and fruitful area of study for CANDU reactors. Modeling and experimental difficulties arise in severe accidents for a number of reasons. Sample sources of difficulty include: loss of geometry of the core, spatial and temporal variance in decay heat, complex reactions between Uranium-Zirconium and steam, and a large number of failure modes that can be caused by different sources that are not necessarily independent of each other.

The CANDU design has a number of heat sinks that make progression to a severe accident a very unlikely scenario and one that proceeds very slowly. One example of an initiating event that results in a particularly challenging severe accident is a LOss of Coolant Accident (LOCA) coincident with a loss of heat sinks. Broadly, damage to the CANDU reactor is expected such that fuel channels collapse and form a Corium pool (Corium is an alloy of Uranium-Zirconium-Oxygen). A solid Corium crucible is formed at the bottom of the Calandria Vessel and around the molten Corium. The Corium continues to heat up due to decay heat. At the top of the Corium pool most of the heat transfer is through radiation to the surrounding Calandria Wall. At the bottom of the Corium pool a quasi-equilibrium state is reached where the internal volumetric heat generation rate is matched by conduction through the Calandria Vessel wall and into the Shield Tank Water. The long term behaviour of the Corium pool is shown in Figure 1.1.

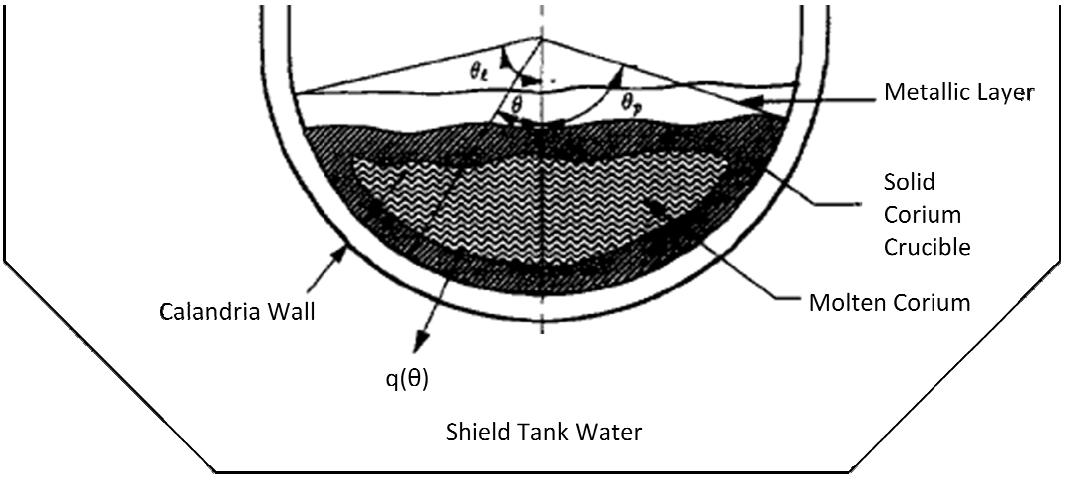


**Figure 1.1: Long Term Behaviour of Core Melt, Adapted from Theofanous *et. al.* (1997) and altered for Application to CANDU Reactors**

The potential failure modes of the Calandria Vessel have been analyzed by D. Luxat and J. Luxat (2007) and severe accident progression in CANDU reactors has also been studied in detail in the open literature (Luxat (2007), Dupleac *et. al.* (2009), Matthew *et. al.* (2008)). The motivation of this thesis is derived from a potential failure mode identified by D. Luxat and J. Luxat (2007). In particular, the identified failure mode of the Calandria Vessel is due to wall melt-through brought on by an excessive heat load from the Corium debris bed and pool. The Calandria Vessel can fail due to creep deformation if the wall temperatures are too high. At temperatures approaching the

melting temperature of A304 Stainless Steel, the Calandria Vessel will rupture under the modest load of the Corium pool.

There is evidence that the temperatures on the Calandria Vessel wall will be sufficiently low such that creep deformation does not occur. If, during the course of the accident, the Shield Tank Water surrounding the Calandria Vessel wall is removing heat while in the nucleate boiling regime, then the wall temperatures of the Calandria Vessel wall will be sufficiently low to prevent rupture. This thesis aims to experimentally determine this safety limit and measure the Critical Heat Flux (CHF) for a representative geometry. If it can be shown that the CHF is higher than heat fluxes that will be experienced through the Calandria Vessel wall then it can be inferred that failure due to creep is physically unreasonable. Alternatively, if the CHF for the representative geometry is lower than heat fluxes through the Calandria Wall then rupture and release of the Corium to the Reactor Vault is probable.

### 1.2.1 Conservative Experimental Representation of the Calandria Wall

The CHF will vary as a function of azimuthal angle along the Calandria Wall. At the stagnation point of the Shield Tank Water, located at $\Theta$=0° on Figure 1.1, the CHF will be at some minimum value. Since the Calandria Vessel has a large radius, in the limit, the stagnation point and immediate vicinity can be adequately represented by a flat disk. Thus, the CHF will be measured for a flat disk in a pool boiling environment at pool temperatures representative of those seen in the Shield Tank Water.

It is also of interest to study the effect that obstructions have on the CHF. Near the stagnation point are large pipes belonging to the moderator re-circulation system. These obstructions can affect the movement of vapour and can lower the CHF. Experimentally determining the effect obstructions have on CHF can be studied by introducing objects that will perturb the movement of vapour. Conservatively, placing a lip around the disk will confine boiling only to the surface and will significantly influence the CHF as it does not allow for venting of the vapour slug. In this geometry, it is also of interest to study the impact that inclination angle has on the CHF. Thus, the CHF will be measured for a disk where bubble motion is confined to the heated surface by the presence of a surrounding lip. Multiple experiments will be performed where the bulk fluid temperature is varied along with the inclination angle.

## 1.3 Boiling Heat Transfer in a Pool Boiling Environment

Boiling is a ubiquitous process used routinely in a variety of heat exchange systems. It is to this day an elusive and not fully understood process. The definition of boiling is a phase change where fluid in the liquid phase is heated to form vapour bubbles. Some variety of a heated surface is needed to form vapour bubbles. The motion of bubbles, whether they coalesce or not, and how they leave the heated surface is still a problem without an accepted solution. There is debate within the academic community on whether these vapour bubbles are formed directly on the heated surface or in a superheated liquid layer adjacent to the heated surface (Dhir 1998). The impact that water purity and heater surface oxidation have on boiling and CHF is to this day debated (Theofanous *et. al.* (2002)). Commonly accepted engineering practice is to correlate the applied heat flux as a function of the wall superheat—the so-called "Boiling Curve". The heat flux is the controlled quantity if applied through constant electrical heating of the heated element. The wall superheat is the independent quantity and is defined as the difference between surface wall temperature and saturation temperature of the liquid at the system pressure. A qualitative Boiling Curve for an upwards facing surface is shown in Figure 1.2.

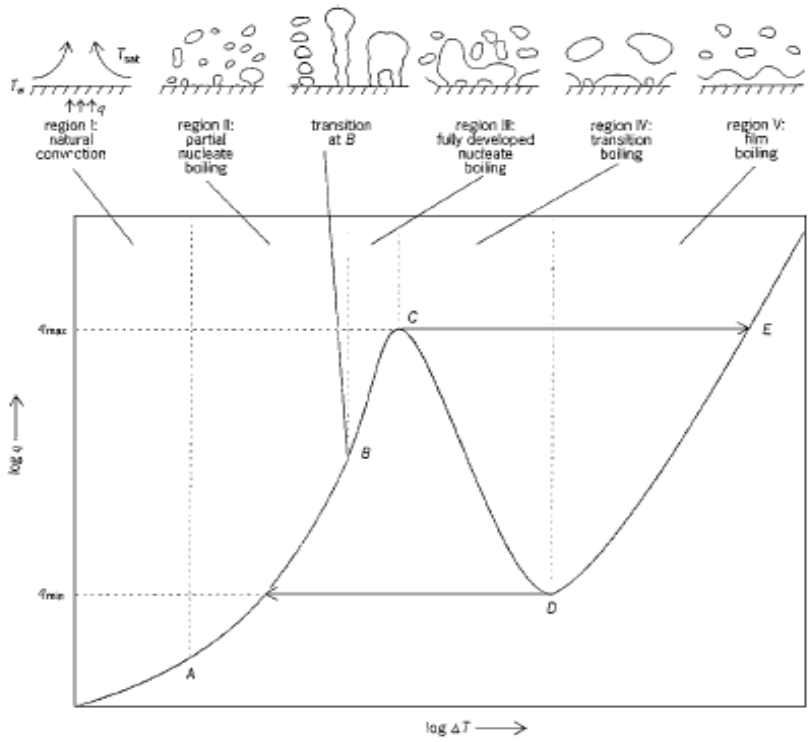


**Figure 1.2: Qualitative Boiling Curve, Reproduced from Dhir (1998)**

The work presented here utilizes distilled water as the working fluid at atmospheric pressure. This poses some challenges as water has a high heat capacity as well as a large enthalpy of vaporization. Performing experiments using water as the working fluid is preferred because water is used extensively in industrial settings – including the CANDU reactor.

Pool boiling refers to boiling under natural convection conditions where the surface between the liquid-air interface is a free surface. In the CANDU reactor, the Shield Tank Water is a system under normal operation that can be classified as a mixed system with natural convective circulation due to buoyancy forces and small forced convective cooling. If circulation of the Shield Tank Water system is unavailable then it is classified as a subcooled pool boiling environment in the short term and a saturated pool boiling environment in the long term.

In all thermal-hydraulic CANDU systems the heated element's wall temperature is required to be maintained to the left of point C on Figure 1.2 with adequate margin. Region I is the natural convection region where heat transfer is dominated by buoyancy induced flows due to density differences in the liquid. Points A to C demarcate what is termed nucleate boiling. Operating a heated device in this mode of heat transfer is very efficient, but safe and reliable operation can be compromised if adequate attention in design or operation is not exercised.

### 1.3.1 Nucleate Boiling and Critical Heat Flux

Regions II and III are called partial nucleate boiling and fully developed nucleate boiling, respectively. The former is characterized by discrete sites where vapour bubbles appear. In partial nucleate boiling for an upwards facing flat plate, a vapour bubble will appear at or near the heated surface and after some time detach and transfer heat to the pool of water. This is an effective mode of heat transfer because the vapour bubble is superheated. When it leaves the surface it will transfer heat to the pool of water through conduction or potentially collapse, thereby releasing the energy input into vaporizing the water earlier. Fully developed nucleate boiling is characterized by the formation of vertical jets and the coalescence or merger of adjacent bubbles. There may be a change in the slope of the boiling curve when nucleate boiling goes from partial to fully developed. As can be seen from Figure 1.2, fully developed nucleate boiling is also an effective mode of heat transfer as the wall temperature stays relatively small for high heat fluxes.

Point C on Figure 1.2 is approached as the heat flux is increased. Point C is termed the Critical Heat Flux (CHF) and is the upper limit of safe operation of equipment. Exceeding the CHF will result in a large and rapid temperature excursion. Physically this temperature excursion is explained by the new presence of a vapour blanket that has enveloped the surface. The heat transfer rate of vapour is much smaller than liquid since the mean free path is much greater. This mode of boiling heat transfer is termed film boiling and is shown as Region V on Figure 1.2. Point C is a point of instability. Exceeding point C from the left side (i.e. raising the input heat flux) causes a temperature excursion. In the steady state, the heated surface will reach a wall temperature defined at point E. This temperature value is usually greater than the melting temperature of the device and will therefore lead to catastrophic failure—this is the so called "Boiling Crisis" or "Burnout".

### 1.3.2 Methods of Boiling Curve Measurement: Gradual Heating and Quench Cooling

To obtain a boiling curve, two fundamentally different methods can be utilized: the gradual heating method and the quench cooling method.

#### *1.3.2.1 The Gradual Heating Method*

A variation of the gradual heating method is employed in this thesis. In this method, electric power is increased incrementally and held fixed while the temperature of the device stabilizes. The heat flux is measured at steady state by embedded temperature measurement devices (e.g. thermocouples, RTDs, etc.) located at disparate depths or can be deduced by having knowledge of power applied through the device. The heat flux through the exposed surface should be the largest contributor to heat removal. In other words, if the heated surface is oriented downwards, the dominant temperature gradient should be axial. If *y* is the axial co-ordinate, mathematically the heat flux, *q*, is related to the temperature gradient as:

$$q = k\frac{\partial T}{\partial y} \qquad \text{(Equation 1.1)}$$

The wall superheat, *ΔT*, is extrapolated from the existing temperature measurements or can be obtained by utilizing an Infra-Red camera. From a practical standpoint the gradual heating method can be used to construct the boiling curve from convective boiling to the CHF and can be used to observe the nucleate to film boiling transition. Many studies in the open literature do not rely on the power supply to infer the heat flux. In most of these studies, thermocouples are placed at 3 different depths in the centre of the heated element. Using equation 1.1, the heat

flux is calculated without relying on the power supply. An assumption is made here – that the measured heat flux at the centre of the device is approximately equal to the actual heat flux through the entire surface. An additional difficulty results when different boiling modes are present on the surface. For example, when the surface is inclined, the lowest portion maybe in a different mode of boiling than the highest portion (i.e. nucleate and film boiling may co-exist). Furthermore, the measured temperature differences between the thermocouples are small. This temperature difference is on the same order of magnitude as the relative accuracy of thermocouples. Physically this technique is representative of the Shield Tank Water and what is expected to occur under a severe accident. This statement is justified by noting that the Shield Tank Water is a passive heat sink that surrounds the Calandria Vessel at the time of the accident.

#### *1.3.2.2 The Quench Cooling Method*

Use of the quench cooling method allows one to construct the boiling curve from the minimum heat flux to single phase natural convective cooling (points D to A in Figure 1.2). This technique begins by raising the heated element temperature to a mean temperature much greater than the surface temperature believed to exist at the CHF and then plunging this device into a pool of subcooled or saturated liquid. In contrast to the gradual heating method, the quench cooling method is not steady state – i.e. it accounts for the thermal inertia of the heated element. The energy storage in the element is:

$$E_s = \rho V C T_{avg} \qquad \text{(Equation 1.2)}$$

Ideally only one side is losing energy to the bulk fluid, thus the energy loss is related to the surface heat flux as (Guo and El Genk (1992)):

$$q = -\frac{\frac{d}{dt}E_s}{A} = -L\rho C\frac{d}{dt}T_{avg} \qquad \text{(Equation 1.3)}$$

Physically this method is more applicable to the severe accident management strategy found in Light Water Reactors (LWR) where the exterior of the reactor vessel is flooded by water in an attempt to prevent external melt relocation. The surface temperature is determined in a similar technique to the one used in the gradual heating method.

The quench cooling method is elegant and capable, in theory, to produce a meaningful boiling curve. Large uncertainties are introduced due to the rapid temperature transients of the devices as well as differing response

times expected to be found in temperature measuring devices. Also, this method relies on knowledge of the average temperature in the heated element at all times. It is difficult to argue that the embedded temperature measurements and their locations are indeed representative of the average temperature at all times during the quench cooling process.

Both methods can be plagued by the presence of different boiling regimes on different locations of the heated surface. For example, nucleate boiling can co-exist on the same heated surface with film boiling which is all separated by a quenching front. This can be combated by good heated element design, i.e. one in which the wall temperature along the surface shows little variability.

### 1.3.3 Literature Review

A wealth of experimental and theoretical studies is available for an upwards facing plate in a pool boiling environment. Nucleate boiling curves and heat transfer coefficients have been studied extensively for the upwards facing surfaces as well as other industry relevant geometries, such as cylinders and spheres. The Stephan-Andelsalam (1984) study grouped much experimental data and developed a correlation for nucleate boiling heat transfer for varying surfaces and geometries using statistical regression techniques. Earlier, more deterministic approaches were pioneered by Mikic and Rohsenow (1969) in their derivation of a nucleate boiling correlation that related the heat flux to average frequency of bubble emission. For an upwards facing disk of similar diameter to the disk studied here, evaluating the Mikic-Rohsenow correlation for water at the saturation temperature results in (Petrovic (2004)):

$$q = 1870\sqrt{f}(T_w - T_\infty) \qquad \text{(Equation 1.4)}$$

Use of the above equation requires knowledge of the bubble release frequency, which will vary based on orientation and confinement. The bubble release frequency can potentially be calculated or measured. Indeed, the former approach was undertaken successfully by MacKenzie *et. al.* (1999).

There is still considerable debate on the dominant mechanisms in nucleate boiling, for instance the assumption that wall superheat is steady in time and space has been questioned (Theofanous *et. al.* 2002). A consensus still doesn't exist even in the light of all the available experimental data for an upwards facing surface. By extension, nucleate boiling under varying heater surface conditions and inclinations is also of considerable debate.

Nishikawa *et. al.* (1984) studied the effects of heater element orientation on nucleate boiling and concluded that at high heat fluxes, surface orientation minimally impacts the boiling curve. For strictly downwards facing surfaces the fundamental bubble dynamics are different as bubbles are found to more frequently coalesce and cover the majority of the heated surface before escaping into the bulk liquid (Guo and El-Genk (1992), Yang *et. al.* (1997)). From a practical standpoint, intricacies of the boiling curve are of little importance as the wall temperatures are low enough to permit reliable operation of the device. What is of importance is the CHF, as this point limits the safe and reliable operation of a device. Kutateladze (1952) used a semi-empirical approach to pool boiling and was successful in being the first to gain an understanding of burnout. Zuber (1959) argued that film boiling was instigated due to a Taylor-Helmholtz instability and assumed in his theory (with adequate justification) that a superheated liquid layer of approximate size ~0.1 mm exists immediately on the surface. Zuber's theory agreed very well with data obtained by Kutateladze (1952) and more recently by Dhir (1992). Recently, however, the hydrodynamic limit was violated in experimental data obtained by Theofanous *et. al.* (2002). In this study the researchers noted that the CHF is very sensitive to surface conditions, such as degree of aging due to oxidation. Thus, an accepted theory to CHF for an upwards facing surface is still not available.

There are a substantial number of published experimental studies on downwards facing surfaces that have applications in the severe accident management strategy of LWR. Some relevant studies and major findings are summarized in Table 1.1.

**Table 1.1: CHF Experiments for Downwards Facing Surfaces**

| **Researchers** | **Conditions** | **Findings** |
|---|---|---|
| Theofanous *et. al.* (1994) | Stainless Steel Curved Surface, Full Scale, Saturated Boiling, Confined, Gradual Heating | Measured CHF azimuthally |
| Yang. S.H. *et. al.* (1997) | Stainless Steel Flat Plate, Saturated Boiling, Unconfined, Gradual Heating | Measured CHF as function of inclination angle |
| Yang J. *et. al.* (2005) | Aluminum Hemispherical Surface, | Measured CHF azimuthally, for a |

| | | |
|---|---|---|
| | Saturated Boiling, Unconfined, Gradual Heating | plain and coated surface |
| Guo and El-Genk (1992) | Copper Disk, Saturated Boiling, Unconfined, Quench Cooling | Measured CHF as a function of inclination angle |

As can be seen from Table 1.1, a number of similar experiments have been performed. But the numerical results of CHF vary greatly, ranging from ~200 kW/m$^2$ (Guo and El-Genk (1992)) to ~700 kW/m$^2$ (Yang *et. al.* (2005)). Further study is warranted.

There is a lack of data for downwards facing orientations and even further deficiency in data for confined boiling. One such study that attempted to alleviate this was recently completed by Su *et. al.* (2008). The researchers derived a correlation for a downward facing heated surface in a pool boiling environment under confined conditions. In this paper, water was the working fluid and boiling curves were constructed for two differently sized stainless steel disks under varying gap or confinement conditions. The heated surface was oriented downwards and an unheated plate was placed beneath it. The methodology used in deriving the correlation is explained and involves the wall superheat and the Bond number. Interestingly, the derived correlation is based on the earlier works of Kutateladze and Zuber, who were, as discussed earlier, based on potentially very different physics. The experimental data fit optimally to the following powers for wall superheat and Bond number:

$$q \propto \Delta T^{0.71} \qquad \text{(Equation 1.5)}$$

$$q \propto Bo^{0.1} \qquad \text{(Equation 1.6)}$$

The Su *et. al.* (2008) study unfortunately did not measure the CHF, and focused instead on characterizing the boiling phenomenon. Part of the motivation in this thesis is to attempt a novel confinement strategy and report on the results.

# 2 Design and Construction

An Experimental Pool Boiling Facility (EPBF) has been designed, constructed and utilized to study boiling heat transfer in a pool boiling environment. This chapter is organized in a top down manner so as to clearly describe the facility.

The system level design requirements establish the requirements of the system as a whole (Section 2.1). The detailed design of the solution begins by further reducing the system into sub-systems (Section 2.2.x). The function of each sub-system is discussed and the sub-systems are further reduced into individual components (Section 2.2.x.y).

## 2.1 System Level Design Requirements

The EPBF is designed to meet the following requirements:

R-1. System shall be capable of supplying a directed heat flux

R-2. The available range of heat fluxes shall be such as to allow the study of boiling heat transfer from the onset of nucleate boiling to the instigation of film boiling

R-3. The temperature variability along the heater-coolant interface shall be minimized as much as practicable

R-4. The test section shall be designed to allow the study of confined/obstructed boiling heat transfer

R-5. The test section shall be designed to allow the study of unconfined boiling heat transfer

R-6. The inclination angle of the test section shall be adjustable from 0° to 20° relative to the downwards facing orientation

R-7. The system shall be capable of acquiring data that can be used to construct a nucleate boiling curve

R-8. Distilled water is to be the working fluid

R-9. The test section is cooled by the working fluid at atmospheric pressure under natural circulation

R-10. The bulk temperature of the working fluid shall be adjustable

R-11. Facility shall be structurally stand-alone

R-12. System must use the Regatron 96 kW DC Power Supply and associated distribution cables and connectors

## 2.2 Detailed Design

The design presented in this thesis meets all of the requirements listed in Section 2.1. Figure 2.1 presents the EPBF's constituent sub-systems. The requirement(s) that each sub-system meets are listed in Table 2.1.

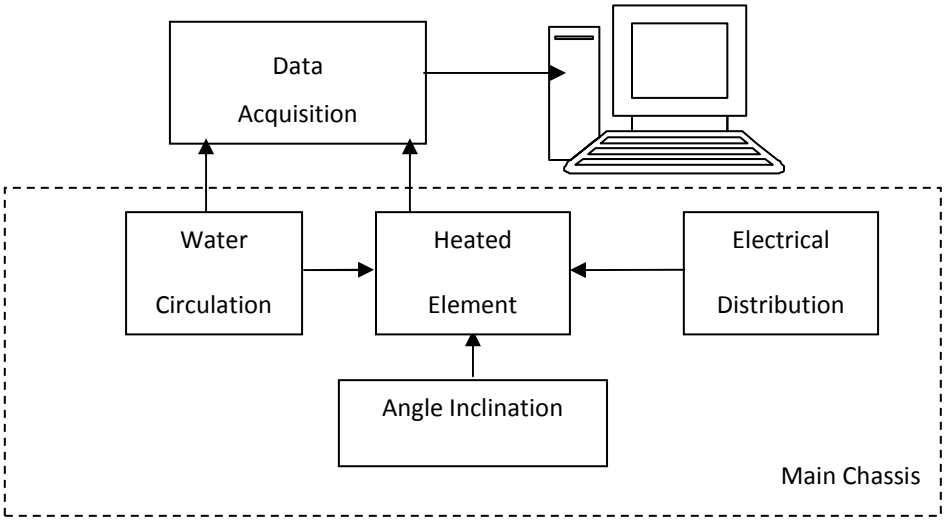


**Figure 2.1: EPBF Sub-Systems**

**Table 2.1: Sub-System Description**

| Sub-System | Description | Requirements Met |
|---|---|---|
| Heated Element | Brass rod electrically heated by vertically inserted cartridge heaters. Thermally insulated on all surfaces except the bottom surface. Contains thermocouples at two different depths. Two variations are presented (confined and unconfined). See Section 2.2.1 for detailed description. | R-1, R-2, R-3, R-4, R-5 |
| Angle Inclination | Two carbon steel rods that slide into holes located on the main chassis. The connection points determine angle of inclination. See Section 2.2.2 for detailed description. | R-6 |
| Electrical Distribution | Allows for control of supplied power to the cartridge heaters. Safely distributes power from the power supply to the cartridge heaters. See Section 2.2.3 for detailed description. | R-1, R-2, R-11, R-12 |
| Water Circulation | Allows for control of pool temperature and level. Circulates water | R-8, R-9, R-10 |

| | | |
|---|---|---|
| | between the test section tank and the auxiliary tank.<br>See Section 2.2.4 for detailed description. | |
| Main Chassis | Aluminum frame supporting the heated element, the electrical distribution and water circulation sub-systems.<br>See Section 2.2.5 for detailed description. | R-11 |
| Data Acquisition | Acquires temperature data from 13 thermocouples, plots the results in real-time and writes data to a file. See Data Collection section in Experimental Procedure chapter for further discussion. | R-7 |

### 2.2.1 Heated Element

The majority of difficulties and complexities in this experiment reside in the design and construction of the heated element.

There are two variations of the heated element and they are denoted as “confined” and “unconfined”. Mechanical drawings are presented in Figure 2.2 and Figure 2.3, respectively. The assigned names are based on the boiling behaviour that results. For example, the confined variation will demarcate bubble motion to the centre disk of the heated element. In the unconfined variation, once a bubble nucleates it will be free to move along the entire heated element in any direction.

The figures show the top view of the heated element in the centre along with three section views. The heated element is submerged in a pool of water to a depth so that the waves generated by boiling do not strongly influence the thermal-hydraulic behaviour at the heater-water interface. It was found that a 25 mm depth of submergence is suitable. For scaling purposes, the depth of submergence is approximately one-quarter the length of the Brass rod. The confined variation of the heated element is composed of a Brass rod, 28 cartridge heaters, 12 thermocouples, a Mullite tube, flexible Ceramic fibre blanket, and an Aluminum shell. Silicone is used as an adhesive and sealant between the Brass rod and Mullite tube and the Mullite tube and Aluminum shell.

In the unconfined variation, the Mullite tube is eliminated and the bottom of the Brass rod is made flush with the bottom of the Aluminum shell. Silicone is applied between the Brass rod and the Aluminum shell only.

Sections that follow discuss each component in detail.

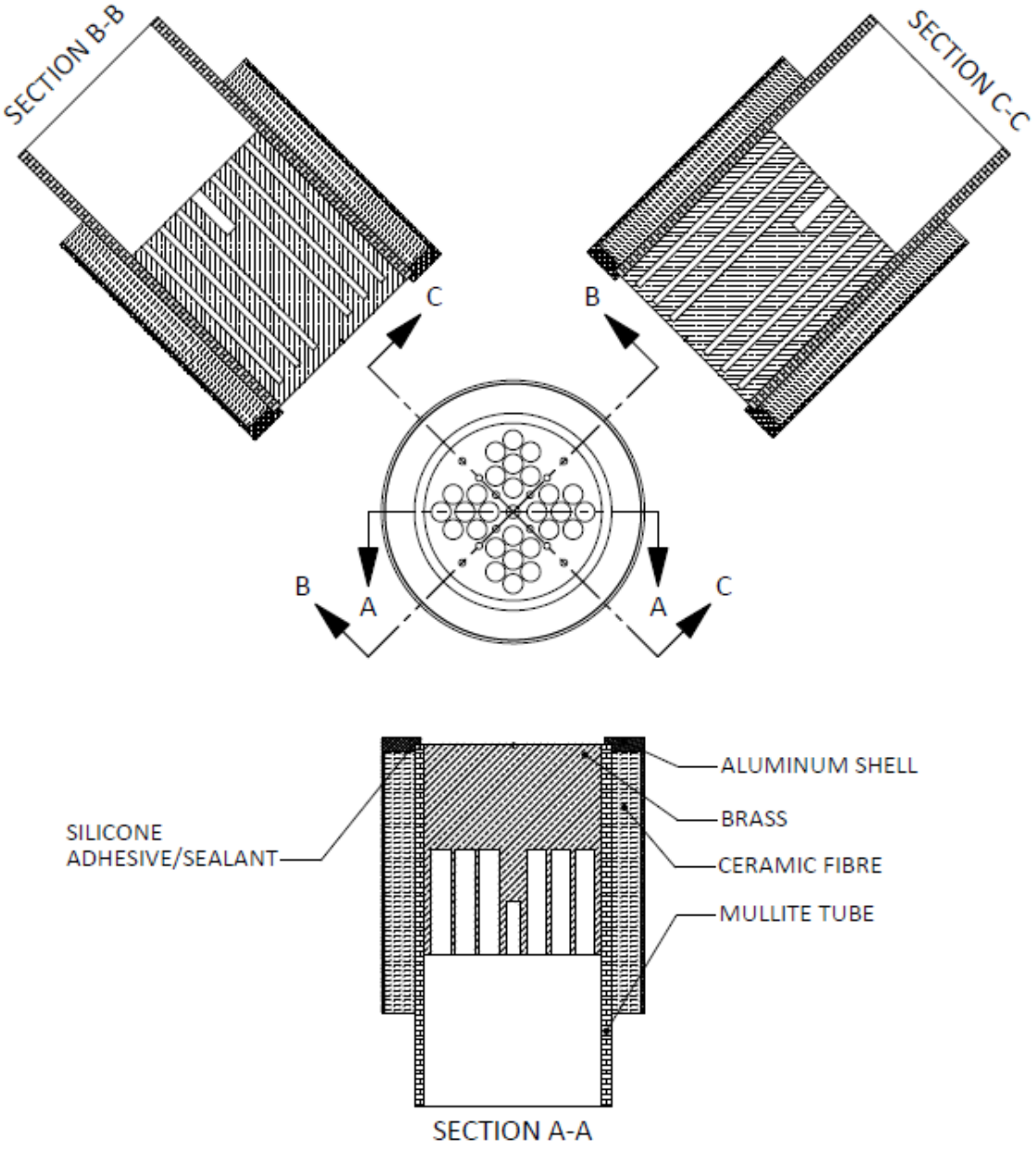


**Figure 2.2: Heated Element: Confined Variation**

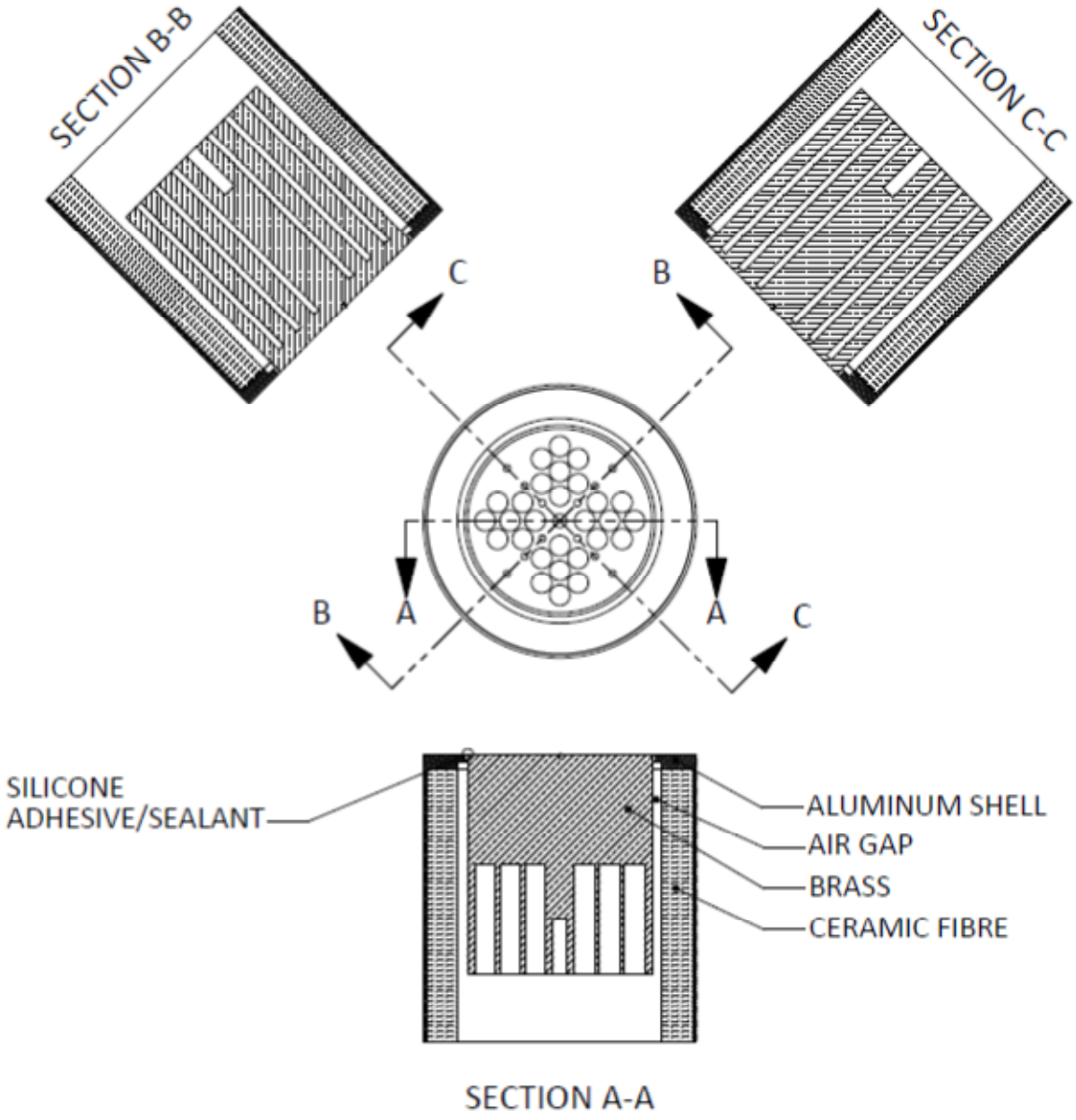


**Figure 2.3: Heated Element: Unconfined Variation**

#### *2.2.1.1 Brass Rod*

The Brass Rod has a diameter of 86.4 mm and length of 101.6 mm. The type of Brass used is Free Machining Brass (360 Brass). This material is selected for its very good thermal conduction properties, high resistance to corrosion

and ease of machining. The Brass Rod is precision machined to allow for the insertion of the cartridge heaters, thermocouples and a threaded rod.

There are four sets of seven cartridge heater holes arranged in a honeycomb pattern. The holes are first drilled and then reamed to a diameter of 9.525 mm. The depth of these holes is approximately 50.8 mm. Large tolerances in depth are permissible because the cartridge heaters have a significant no-heat length.

There are two sets of six thermocouple access holes arranged radially along the Brass rod. The thermocouple holes are drilled and then reamed to a diameter of 4 mm with tight tolerances placed on depth. The thermocouple access holes are made to two different depths (see Section Views B-B and C-C of Figure 2.2 or Figure 2.3).

The centre hole is drilled and tapped to allow for the insertion of a threaded rod. The hole diameter is 6.35 mm with an imperial thread (1/4-20). The depth of the hole is approximately 30 mm. A top view of the precision machined Brass rod is shown in Figure 2.4.

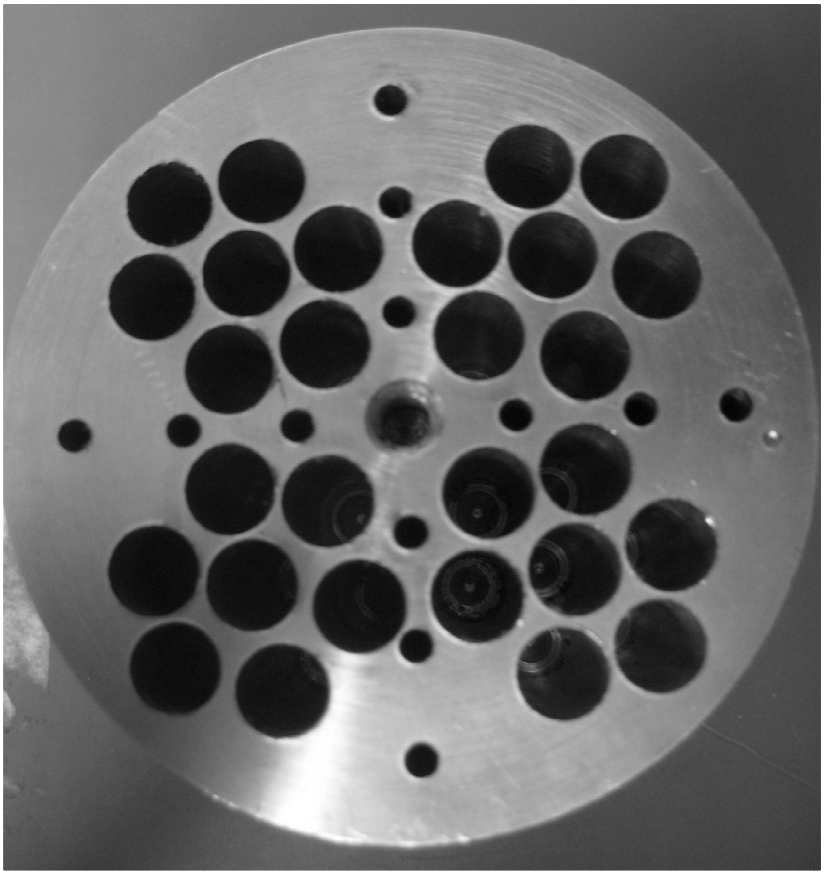

**Figure 2.4: Top View of Precision Machined Brass Rod**

#### *2.2.1.2 Cartridge Heaters*

Twenty eight cylindrical cartridge heaters are inserted vertically into the Brass rod in order to provide a suitable heat flux. The length of each cartridge heater is 50.8 mm with a diameter of 9.53 mm.

Heating is attained by supplying a voltage difference across the leads of the cartridge heater. In the presence of a voltage, current will flow through the Nickel Chromium wire in the cartridge heaters and dissipate heat. Nickel-Chromium wire is used because the resistivity of this material is fairly constant with changes in temperature. A thin layer of Magnesium Oxide surrounds the Nickel Chromium wire. Magnesium Oxide is an electrical insulator with a high dielectric strength and high melting temperature. The cartridge heater's external sheath is made of an Inconel alloy. The use of this alloy works to minimize the temperature drop across it and the Brass rod. To further optimize heat transfer from the heaters to the Brass a thermally conductive liquid is applied to the Inconel sheath before the cartridge heaters are inserted into their respective holes. The thermally conductive liquid is a proprietary material known commercially as WATLUBE.

Each cartridge heater can output a maximum power of 350 W at 100 VDC. The maximum instantaneous power that can be input into the heated element is therefore 9.8 kW.

#### *2.2.1.3 Thermocouples*

Type K thermocouples of 3.175 mm OD are inserted in the thermocouple access holes in the Brass rod. The thermocouples have a grounded junction; this means that thermocouple wires are co-joined to the sheath at the tip. This junction type offers good electrical insulation, is not susceptible to mechanical damage and yields a point temperature measurement at the precise location defined by the bottom of the thermocouple access hole centre (see Figure 2.2, Figure 2.3 Section B-B and Section C-C).

The thermocouples are 203 mm long as measured from the bottom of the sheath to the thermocouple connectors. The thermocouple connectors used are the miniature type. The thermocouple sheath is chosen to be Inconel. A large systematic uncertainty can be introduced if the thermocouple tips are not in good contact with the bottom of the thermocouple access holes. In order to ensure good tip contact, ceramic cement is applied to the sides of the thermocouple sheath before the thermocouples are inserted into their respective access holes.

Type K thermocouple extension wire is field run from the thermocouple connectors to the data acquisition system. Only temperature data is acquired in this experiment. A detailed explanation of how the data is acquired and manipulated is discussed in the Experimental Procedure section.

#### *2.2.1.4 Threaded Rod*

A threaded rod is inserted in the top centre of the heated element to provide structural support. The rod is made of galvanized carbon steel. It exhibits acceptable resistance to corrosion and good structural properties. For a metallic compound, galvanized carbon steel is not a good thermal conductor. This property is desirable for the uses of this experiment as it results in a small amount of heat conduction through the structural support.

#### *2.2.1.5 Ceramic Fibre Blanket*

A ceramic fibre blanket is used to thermally insulate the top and sides of the Brass rod. This material is inexpensive, flexible, and easily cut with standard scissors. It is non-hazardous to human health and can be used continuously to very high temperatures.

The ceramic fibre blanket is inserted as part of the assembly after the aluminum shell has been joined to the element by the silicone adhesive (see Sections 2.2.1.6 and 2.2.1.7). Note that ceramic fibre is also placed on the top of the Brass rod after the thermocouples and cartridge heaters have been installed. The presence of the ceramic fibre blanket is not shown on the top of the Brass rod in Figure 2.2 and Figure 2.3 because showing it would obscure the detailed hole arrangement of the Brass rod. The principle design feature of the heated element is that a directed heat flux is supplied through only one face with all other faces thermally insulated.

#### *2.2.1.6 Aluminum Shell*

An Aluminum shell is used to prevent the ceramic fibre blanket from absorbing water. The Aluminum shell is joined to the Brass rod by a Silicone adhesive. In the confined variation, it is also bonded to the Mullite tube.

The Aluminum shell is one solid piece and is constructed by boring through 127 mm diameter

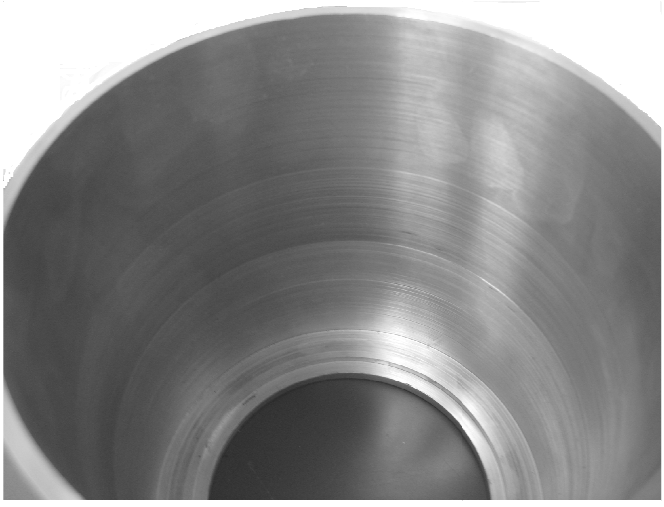

II

aluminum rod to a wall thickness of 3.175 mm at the sides. The bottom wall is made to 6.35 mm wall thickness with a step reduction in thickness to 3.175 mm at the innermost diameter. Aluminum was selected for its ease of machining.

#### *2.2.1.7 Silicone Adhesive/Sealant*

Silicone is used to form water tight seals between the Brass rod, Aluminum shell and the Mullite tube. Silicone has good thermal stability to 250 ˚C, and is able to accommodate for differing rates of thermal expansion in the neighboring materials.

#### *2.2.1.8 Mullite Tube*

A Mullite tube is used only in the confined heated element variation. It is a rigid tube with nearly zero porosity. Other desirable properties are that it can be used continuously at very high temperatures and is also a good thermal insulator.

Mullite is a ceramic zero porosity brick like material that is prone to cracking. Cracking can be caused by too rapid a change in the temperature of the material or by thermal stresses in the heated element. Thermal stresses are imposed by differing rates of thermal expansion in neighboring materials. For example, Brass will expand at a much greater rate than Mullite. If not accommodated for, the Brass rod in this design can come into contact with the Mullite tube and lead to mechanical damage of the Mullite tube. The Brass rod is made undersized relative to the Mullite tube to minimize thermal stresses and also allow for manufacturing tolerances. The Mullite tube has an ID of 86.87 mm with a wall thickness of 9.525 mm. Note that large manufacturing tolerances were observed in the Mullite tube. In particular, it was found not to be perfectly round as well as having an ID that was 1.15 mm larger than expected.

The Mullite tube is also used as a secondary means of structural support (See Section 2.2.2.1).

#### *2.2.1.9 Aluminum Tape*

The last step in the construction of the heated element is to place Aluminum tape on the exposed surfaces of the ceramic fibre blanket. This is done to eliminate water uptake in the ceramic fibre blanket. Aluminum tape is stable to high temperatures and requires minimal effort to apply.

### 2.2.2 Angle Inclination

The threaded rod provides structural support in both the confined and unconfined heated element variations. The threaded rod is inserted in the top centre of the heated element with the opposite end in the centre of an aluminum disk. This threaded rod is the primary structural support of the heated element. At high powers or at sustained film boiling conditions the primary structural support can fail due to thermal creep deformation of the Brass rod.

The heated assembly is attached to the main chassis by a stainless steel block and two carbon steel rods as follows: the stainless steel block is bolted onto the aluminum disk where horizontally placed holes allow for the insertion of two carbon steel rods. The carbon steel rods are attached to the end of the main chassis. A pair of set screws is placed through the stainless steel block and contacts the carbon steel rods so as to fix the location. Shaft collars are placed at the ends of the carbon steel rods so as to eliminate the possibility of the carbon steel rods detaching from the main chassis.

Adjustment of the angle inclination is achieved by changing the holes that the carbon steel rods penetrate through on the main chassis. An isometric assembly of the components needed for angle adjustment is shown in Figure 2.6.

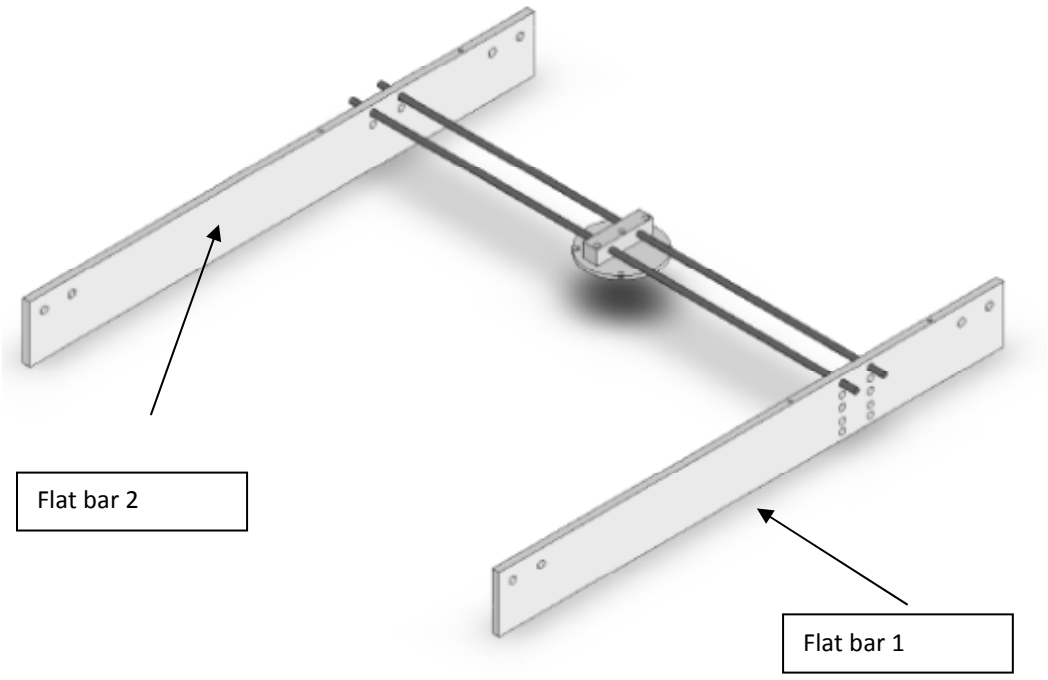


**Figure 2.6: Angle Adjustment (Showing 0˚ Inclination)**

The carbon steel rods are slotted through oversized holes in the main chassis. The carbon steel rods are therefore forced to flex for all angle inclinations except for the 0° inclination. Note that not all components in the heated element structural support are shown in Figure 2.6. The threaded straight bar attaching the Brass rod to the stainless steel block is not shown, neither are the shaft collars or the attachments to the Mullite tube. For the latter see Figure 2.7.

#### *2.2.2.1 Mullite Tube Attachment*

In the confined heated element variation, a secondary structural support device is provided. The aluminum disk mentioned earlier has four grooves that allow for the insertion of bolts. A clamp is tightened onto the Mullite tube and bolts are secured onto the aluminum disk by tightening of wing nuts. See Figure 2.7. This secondary structural support does not provide angle adjustment and is only relied upon in the event of the primary support failing. Its presence also reduces the amount of steam/water ingress into the heated element.

**Figure 2.7: Mullite Tube Attachment (McDanel Advanced Ceramic Technologies, 2009)**

#### *2.2.2.2 Final Assembly*

Photographs of the final completed assembly as used in the confined orientation experiments are documented in Figure 2.8 and Figure 2.9. Note that pictures were taken after all experiments were completed. As a result some components have oxidized. The pictures are useful if one needs to reconstruct this experimental facility.


**Figure 2.8: Fully Instrumented Heated Element, Confined Variation**

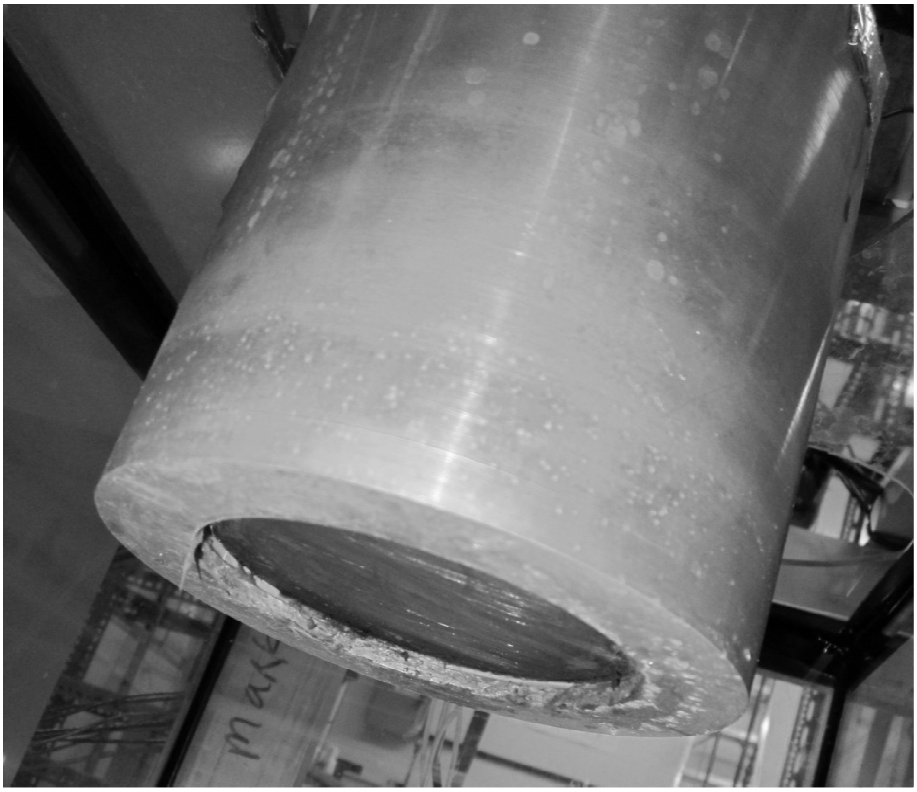

**Figure 2.9: Heated Element, Confined Variation End View**

### 2.2.3 Electrical Distribution

A resistive circuit is used to generate heat in the heated element. The circuit is very simple: voltage is adjusted at the power supply and, as a consequence, a known amount of current will flow through cartridge heaters and heat the device. The requirements for safety, reliability and adherence to the electrical code introduce some complications to the final circuit design and construction.

Note that each cartridge heater is treated as a resistive device with a nominal resistance of 28.8 Ω and that the circuit is powered by a DC power supply with a power range adjustable from 200 W to 96 kW. The circuit schematic is shown in Figure 2.10:

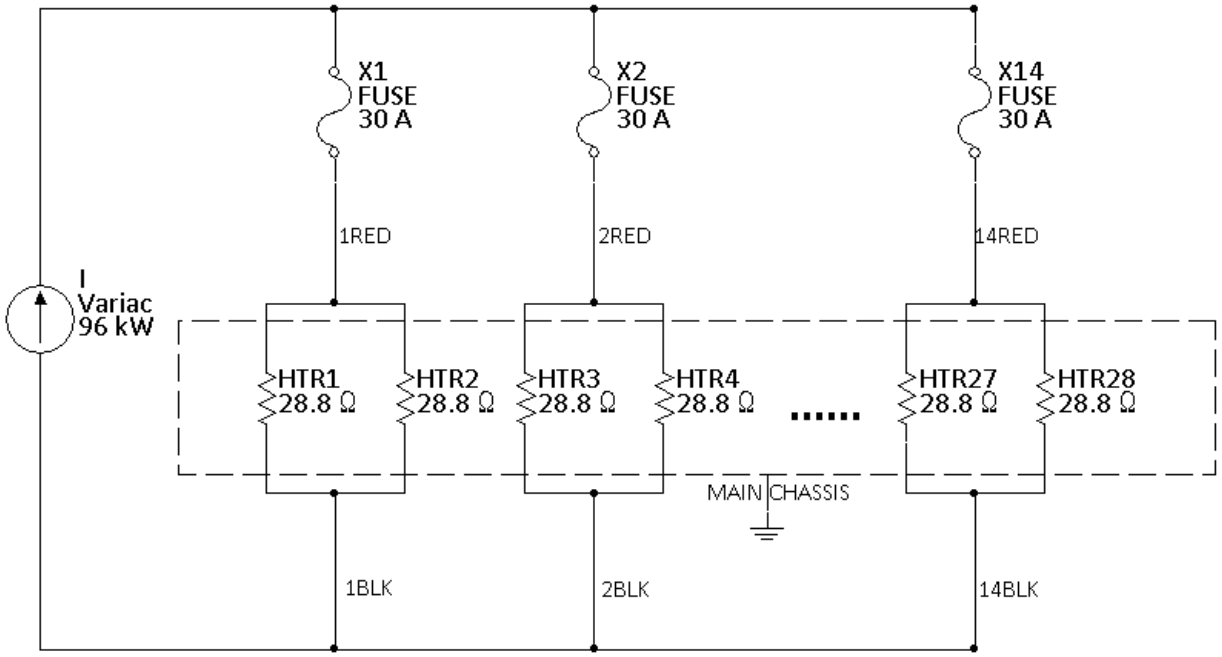


**Figure 2.10: Resistive Circuit Schematic**

The following section discusses the electrical components used and the last section shows the final arrangement with accompanying photographs.

#### *2.2.3.1 Electrical Components*

All circuit components are obtained as “off the shelf” solutions with the exception of the high amperage distribution bars. The electrical devices and wires are all terminated in either the Electrical Cabinet (EC) or a

Junction Box (JB). The EC is mounted onto the main chassis and contains the major electrical components. The JB is mounted directly above the heated element and is where the individual cartridge heater terminations are. The JB is required due to the excessive lead time encountered in obtaining cartridge heaters with customized lead lengths. Wires are run from the EC to the JB along L-profile aluminum pieces mounted onto the frame. The wires are tied down using tie-wraps. Unused wires are covered by variable size wire caps and are secured to the frame. The following is a list of "off the shelf" electrical components, their location and purpose:

**Table 2.2: Electrical Components**

| **Component (Label)** | **Location** | **Purpose** |
|---|---|---|
| 30 A Fuse (N/A) | EC | In the event of heater failure, the fuse will blow and electrically disconnect the damaged heater(s) from the main circuit. Fourteen fuses are used to allow for easier troubleshooting. Fuses are of the cartridge type. |
| Fuse Holder (F##) | EC | Holds fuse. Allows for easy troubleshooting. |
| Large Terminal Block (T##) | EC | Used to terminate wires from the high amperage distribution bars to the fuse holders and from the small terminal blocks. |
| Small Terminal Block (N/A) | JB | Terminates wires from the heated element and large terminal blocks. |
| Ring Terminals (N/A) | EC | Wires are crimped onto ring terminals and ring terminals are placed in contact with the distribution bar. |

All components are DIN rail mounted. Note that wireways are used in the EC. They are used to retard cable fires in the unlikely event that one occurs and they also encourage orderly arrangement of wires and components inside the cabinet.

The main chassis is connected to earth ground and is electrically separated from the resistive circuit. This connection is achieved by securing a green wire to the frame and an unused water tap. Since the grounding wire is made of copper and the frame is aluminum a liquid anti-oxidation compound is used at the contact. It is important to note that the resistive circuit is electrically separate from the heated element and the main chassis. In this way, thermocouple temperature measurements are not susceptible to electrical noise.

Two Distribution Bars (DB1 and DB2) are used to connect the power supply to the circuit and distribute current to the heaters. They are composed of a Brass plate, plastic backing and necessary holes for connection to power supply leads and ring terminal connectors. Note that wires are crimped onto ring terminals in order to form a reliable connection. A 3D isometric representation of a distribution bar is shown in Figure 2.11. All electrical components used in achieving reliable and safe power distribution have been discussed.

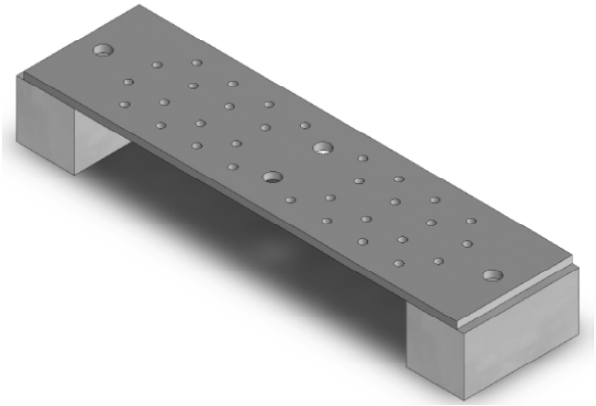

**Figure 2.11: Isometric View of DB Assembly**

### *2.2.3.2 Final Layout and Assembly*

The EC layout along with the labeling convention is shown:

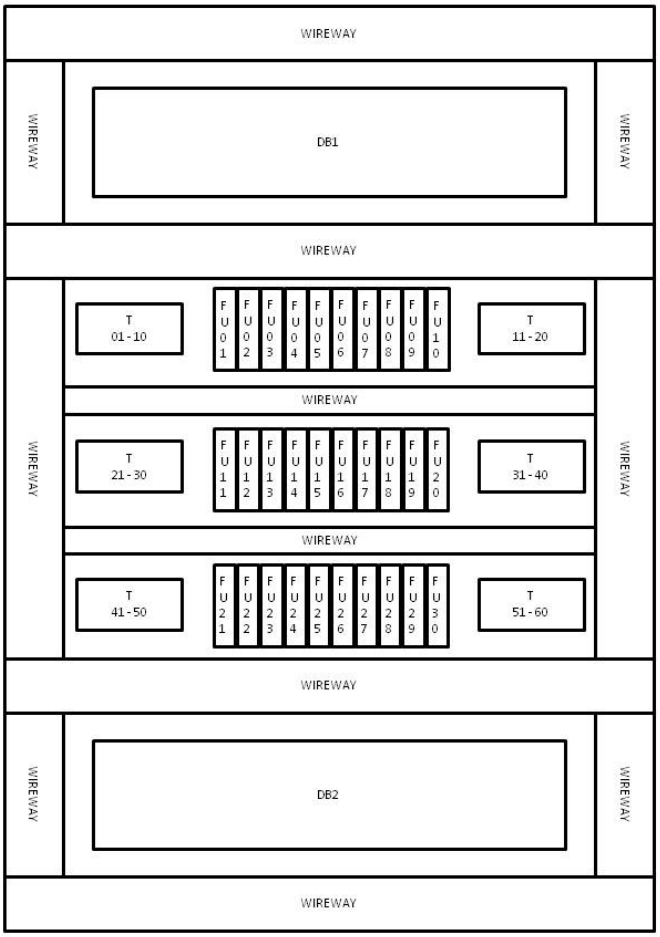


**Figure 2.12: EC Layout**

A photograph of the EC internals is shown on the following page. Information presented in Figure 2.12 can be linked with the system as it is in the field. Note that the distribution cables from the power supply enter the EC from top and bottom penetrations. Wires that distribute current to the cartridge heaters depart the EC from side penetrations.

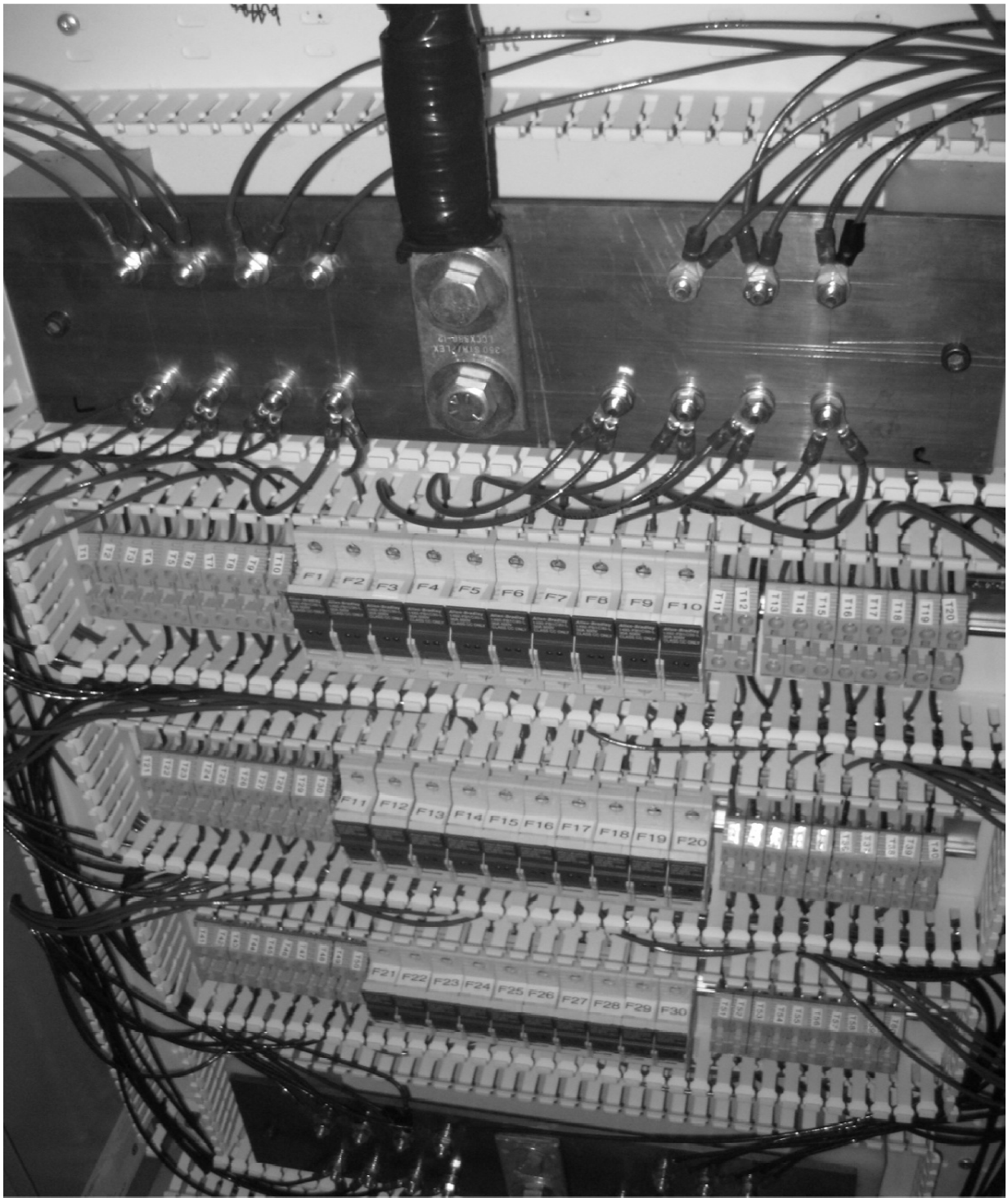


**Figure 2.13: Photograph of EC Internals**

Wires departing the EC are terminated in the JB. A photograph of the JB internals with the system wired is shown in Figure 2.14:

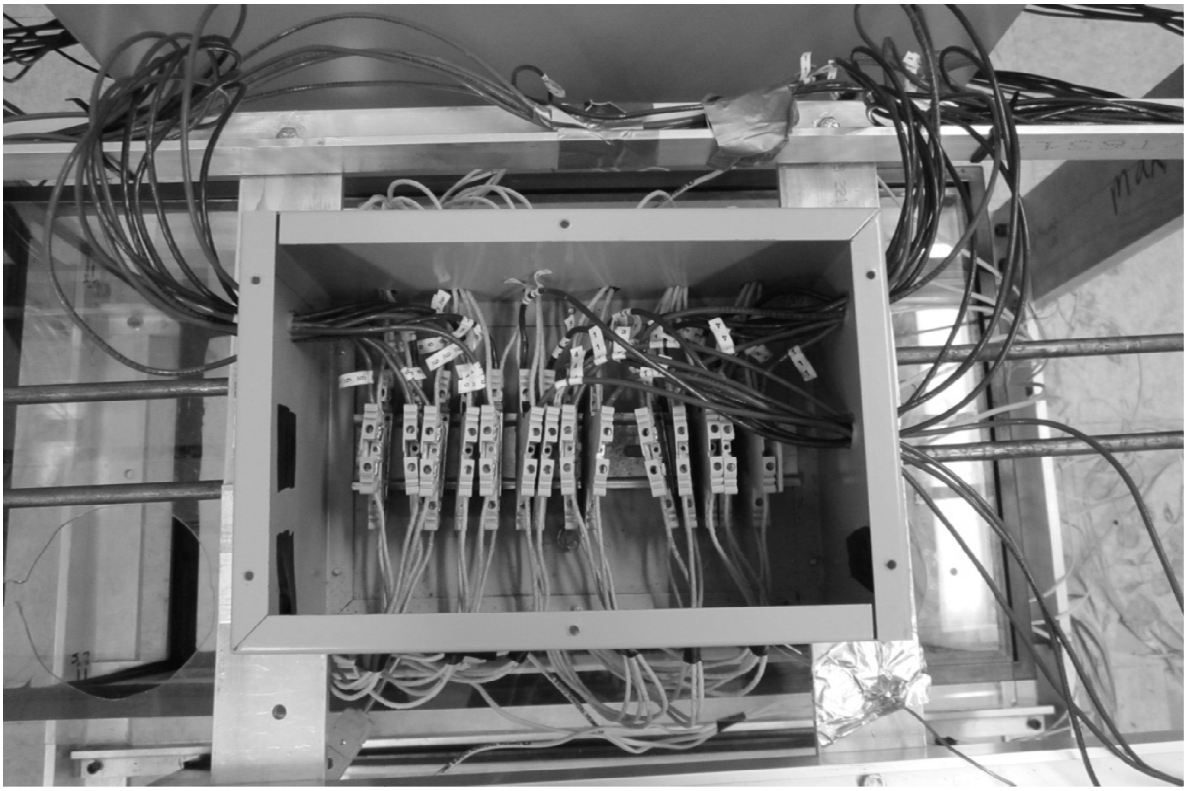

**Figure 2.14: JB Wiring**

Note that wires departing the EC are marked with wire markers. The numbers on the wires are associated with matching numbers on the fuse holders. Single wires inside the EC are terminated individually in each screw terminal. In the JB, heater wires can be terminated individually or are partnered with wires departing the EC. From Figure 2.14, heater wires located in the upper part of the JB are terminated with partnering distribution wires for every individual screw terminal.

### 2.2.4 Water Circulation

A separate heating/cooling and water circulation system is needed independent of the heated element if one is to study subcooled pool boiling. The design utilized in this thesis consists of two immersion pumps with accompanying manually adjustable valves, a coil type heat exchanger connected to water mains, a test section

tank, an auxiliary tank and a thermocouple. The Process and Instrumentation Diagram (P&ID) is shown in Figure 2.15.

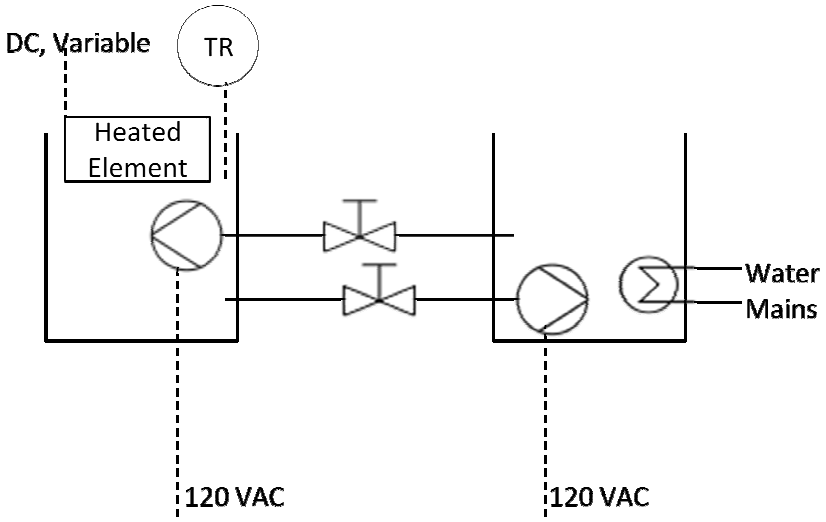


**Figure 2.15: P&ID of Water Circulation System**

A coil type heat exchanger is connected to water mains and is used to both heat and cool the pool of water in the auxiliary tank. The heat exchanger is copper tubing bent into a helical pattern. The heat is exchanged by adjusting the temperature and flow through the coil.

The working fluid is circulated between the test section tank and the auxiliary tank by two separate fluid circuits. The circuits are each composed of a pump, a manual valve, and flexible plastic tubing with the pumps being line powered. The valves are adjusted so that the flow rate in each circuit is approximately the same. If the flows are not matched then the water levels in the tank will not be equal. When raising/lowering the pool temperature, more operator intervention is required as water density differences will influence the mass flow rates through the circuits. Once equilibrium is reached, however, minimal operator intervention is required. The preferred method of operator intervention is by removing line power from the pump that is transferring more mass.

A thermocouple is placed approximately 25.4 mm to the side and 25.4 mm below the heated element in the test section tank. The temperature reading from this thermocouple is used to determine the bulk pool temperature. Note that this thermocouple is strategically placed such that it is not in the path of a venting vapour slug. Minimal temperature fluctuations are recorded by this thermocouple during experimentation.

A polycarbonate cover is placed on top of the test section tank to minimize steam loss to the environment.

### 2.2.5 Main Chassis

The main chassis provides strucutral support for all components used in the experiment. The majority of the weight is attributed to the water in the tanks (weight of ~100 kg), to the electrical cabinet (weight of ~50 kg), and the heated element assembly (weight of ~15 kg). The frame is all aluminum and is composed of a combination of flat bar and L profile pieces. An isometric of the frame is shown in Figure 2.16. Note that the electrical cabinet is shown in the bottom right hand corner without a door. This is done to indicate mounting locations.

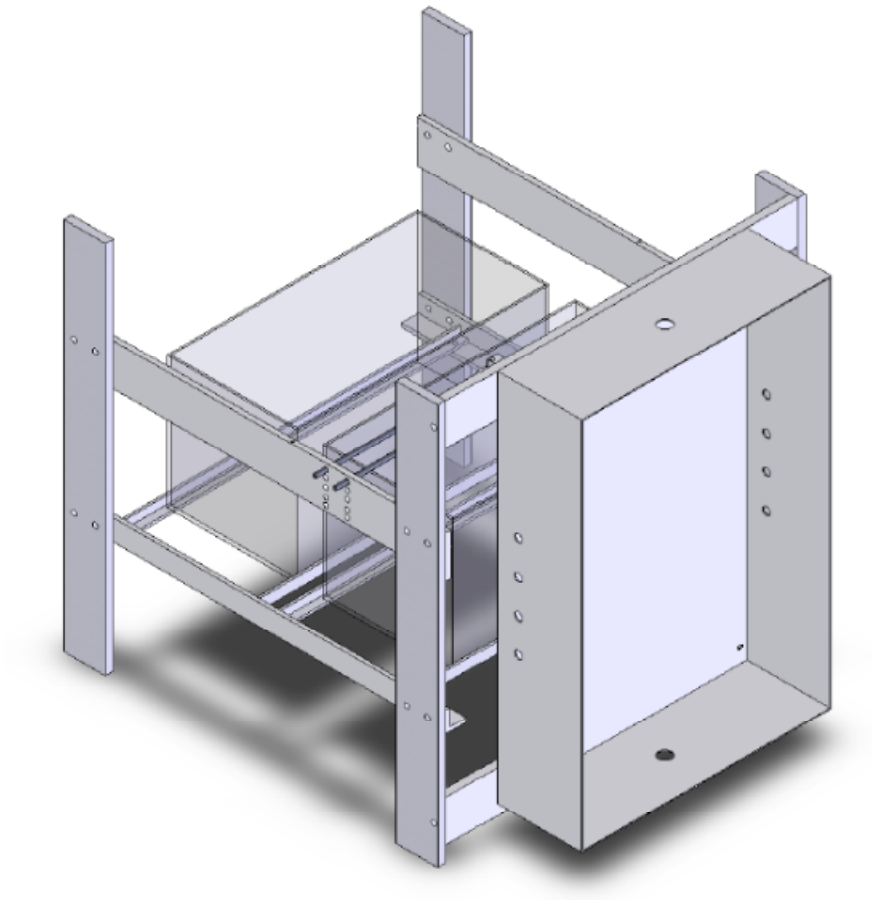

**Figure 2.16: Main Chassis Isometric View**

The location of the heated assembly and tanks is better seen in a top view of the frame, which is shown in Figure 2.17.

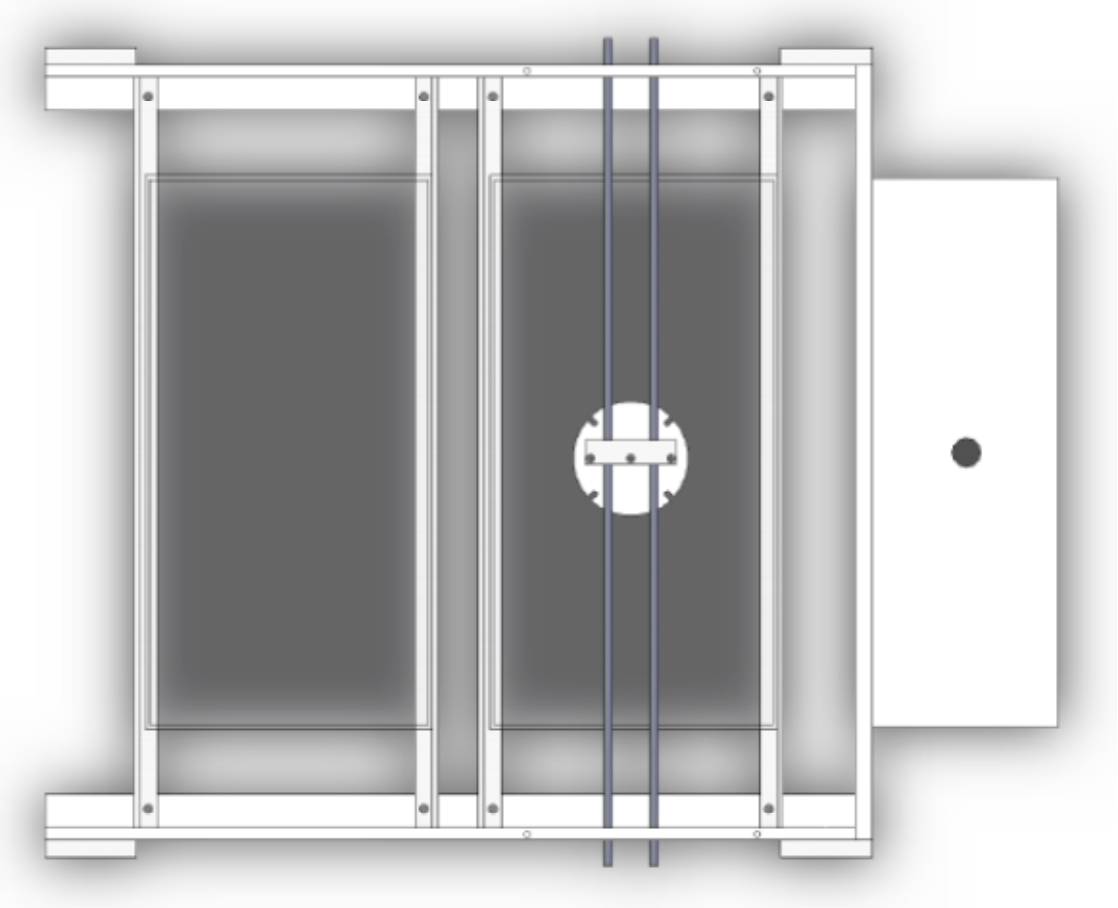

**Figure 2.17: Main Chassis Top View**

Holes are drilled and tapped and individual pieces are secured by stainless steel bolts.

## 2.3 Design Calculation of the Heated Element

The heated element needs to meet requirements R-1, R-2 and R-3 discussed earlier. Calculations are presented in this section that show the heated element design ranges and therefore objectively state how the requirements are practically met. Each subsection discusses how the individual requirements are met.

### 2.3.1 Directed Heat Flux

A directed heat flux is obtained by insulating all sides except the bottom surface. There are losses through the sides and this can be quantified by either constructing a detailed model of the device or by using available data. The latter method is chosen here.

The efficiency of the device as a function of power level is shown in Figure 2.18. The efficiency doesn't vary strongly with power level and appears to be constant at approximately 90%.

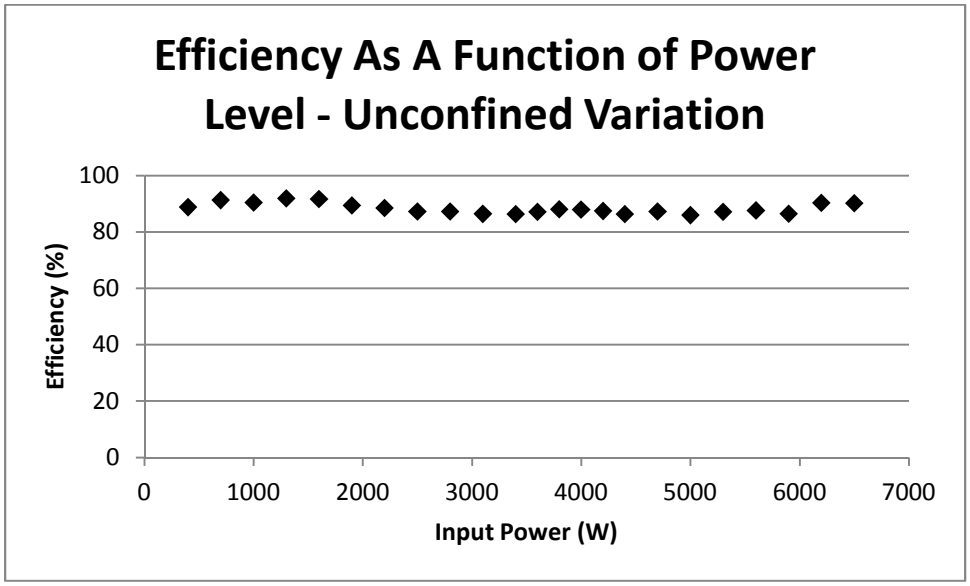


**Figure 2.18: Heated Element Efficiency Unconfined**

The efficiency has been found by taking the measured heat flux and dividing it by the theoretical maximum heat flux. Mathematically stated,

$$Efficiency = \frac{Measured\ Heat\ Flux}{Input\ Power / Exposed\ Area}$$

The method in determining the measured heat flux is discussed in the Experimental Procedure chapter.

Power losses occur due to heat escaping through the top and side of the heated element through all heat transfer mechanisms and through dissipation in the electrical wiring.

For the unconfined variation, the convective heat transfer coefficient at the surface is much greater than the convective heat transfer coefficient of air or of water around the heated element shell and as such the resulting efficiency is high.

For the confined variation, the convective heat transfer coefficient at the surface is lower than in the unconfined variation. Predictably, the resulting efficiency is lower (see Figure 2.19)

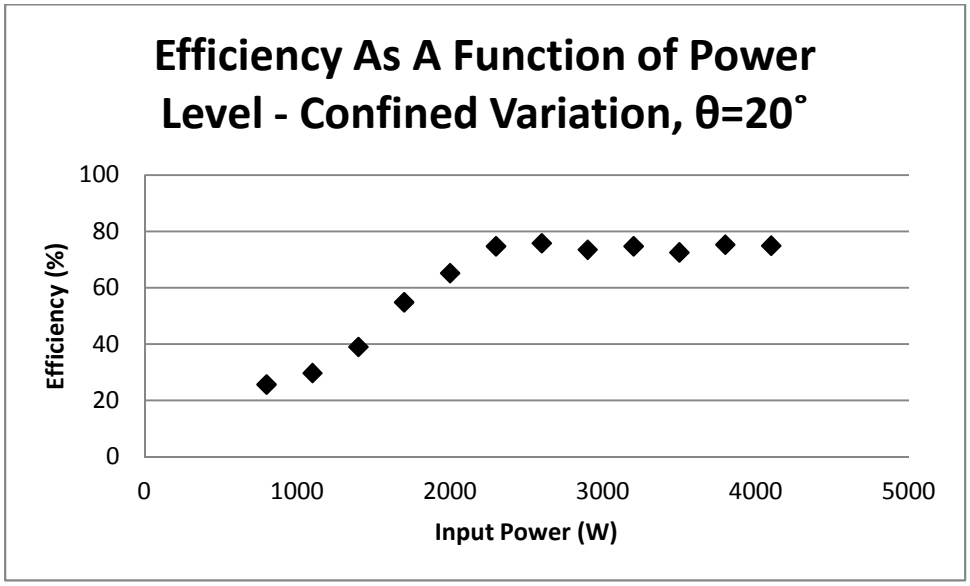


**Figure 2.19: Heated Element Efficiency Confined**

The efficiency measure shows that the design is effective and efficient in directing the heat through the downwards facing surface. Note that the knowledge of power input through the power supply reading is not relied upon in determining the heat flux through the exposed surface. It is used as a rationality check and instigation of CHF is noted for each power level, but it has not been used at all to construct the Boiling Curves.

### 2.3.2 Axial Temperature Distribution

The maximum temperatures in the device are required to be estimated in order to ensure that the selected materials are not taken beyond their limits. Simplifications are made in order to obtain a temperature profile along the axial direction of the heated element. The heated element is modeled as shown in Figure 2.20:

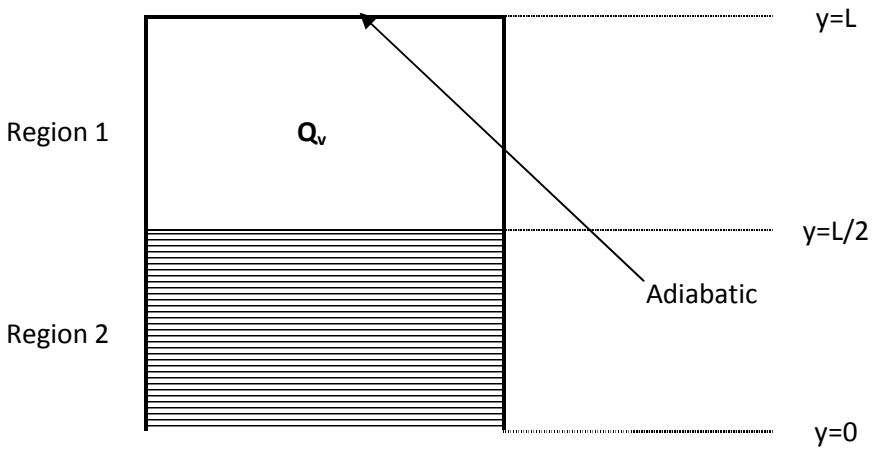


**Figure 2.20: Geometry of Simplified Heated Element**

Region 1 is intended to represent the top part of the Brass rod in which electrical heaters are inserted. The geometry here is simplified so that an analytical solution can be arrived at. There is a volumetric heat generation rate, $Q_v$, in Region 1. The general solution to the steady state heat equation is:

$$T(y) = -\frac{Q_v}{2k}y^2 + C_1 y + C_2 \qquad \text{(Equation 2.1)}$$

Region 2 is intended to represent the bottom part of the heated element where there is no heat generation. By Fourier's law,

$$k\frac{T(y)-T_W}{y} = Q_v(\frac{L}{2}) \qquad \text{(Equation 2.2)}$$

Where $T_w$ is the temperature of bottom surface. To arrive at a numerical solution, the following boundary conditions are physical and sufficient: 1) Adiabatic on the top surface, 2) Continuity of temperature between Regions 1 and 2, 3) Specified Temperature on the Bottom Surface. The result is plotted for both regions in Figure 2.21.

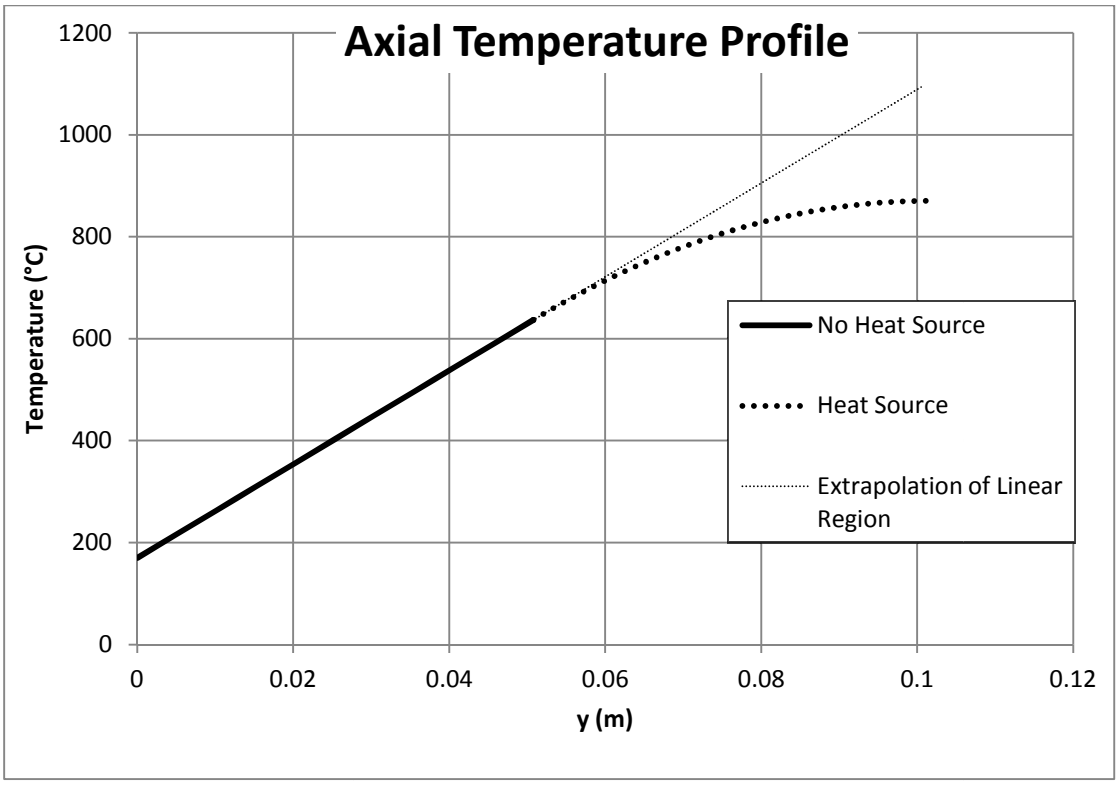


**Figure 2.21: Plot of Axial Temperature Distribution**

The specified bottom temperature is conservatively set to 170 ˚C as instigation of film boiling is expected to occur at a lower temperature. The thermal conductivity, *k*, is assumed to be constant at 120 W/mK.

At this power rate the volumetric heating rate is set to 67% of the total available power. The peak temperature is at the top of the Brass rod is approaching 900 ˚C. The demanded power should not exceed 67% of the total available power in steady state conduction since the melting point of Brass is ~900 ˚C. The calculation presented defines the power limit for this heated element design as being 6.5 kW. Operation above this power level is unsafe and unreliable.

### 2.3.3 Radial Temperature Variability

The cartridge heaters are arranged in a way to minimize the variability in temperature along the exposed surface. The goal is to have a temperature distribution that peaks not at the geometric centre line of the Brass rod but instead somewhere between the geometric centre line and edge.

Thermocouples offer point temperature measurement at fixed locations. A representative data set is graphed in Figure 2.22.

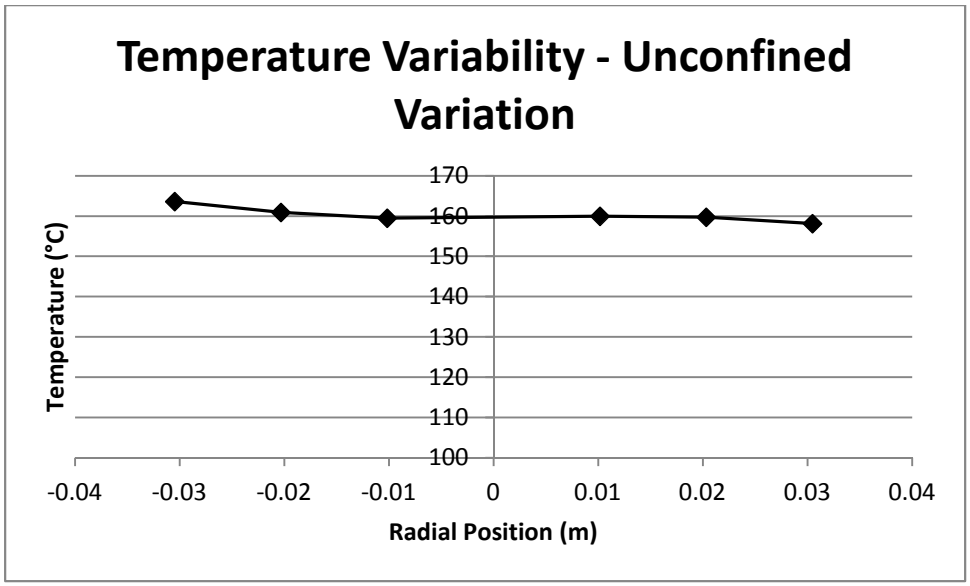


**Figure 2.22: Radial Temperature Variability**

The thermal conductivity of the element is the strongest parameter affecting the temperature gradient along the surface and axially. For data graphed in Figure 2.22, the maximum variation from the mean is approximately 2 ˚C. The objective of obtaining a flat temperature profile is met as the maximum variation shown is within the measurement uncertainty.

It is still noteworthy to discuss how positive this result is, as such a temperature profile is very difficult to obtain. Consider that the temperature variability in Copper based heated elements is approximately 1% (Hohl *et. al.* 2001). Since Copper conducts heat approximately 4 times better than Brass, a 1.5% variability is an excellent result.

## 2.4 System Limits and Range of Capability

The EPBF has a number of different constraints that limit the range of experiments that can be performed. The constraints in the heated element are discussed first, followed by the available ranges in pool temperature, angle inclination and electrical output. The last section discusses how the range of capability of the facility can be expanded.

### 2.4.1 Heated Element Constraints

The greatest difficulty is in the heated element, where a large amount of power is input and is directed in a relatively small space. Large temperature gradients result in thermal stresses, both transient and steady state, that can negatively impact the reliability of the device.

In both the confined and unconfined variations the power demanded from the power supply shall not exceed 2 kW from initially cold conditions (initially cold conditions is defined as the heated element being in thermal equilibrium with the pool of water).

In the unconfined variation, the maximum power that shall be demanded from the power supply is 6.5 kW. A power higher than this will result in melting of the Brass at the top of the rod. See Section 2.3.2.

In the confined variation, the maximum power that shall be demanded from the power supply depends on the angle of inclination. The power at which CHF was reached for each angle of inclination is stated in Table 2.3. In future experiments the demanded power shall not greatly exceed the required power to instigate film boiling.

**Table 2.3: Maximum Power for Confined Orientation**

| Angle | Power at CHF (kW) | Water Level from Tank Bottom (mm) |
|---|---|---|
| 0 | 1.6 | 203.2 |
| 2.5 | 1.8 | 190.5 |
| 5 | 2.2 | 190.5 |
| 6 | 3.4 | 190.5 |
| 20 | 4.7* | 203.2 |

*Extrapolated

If the demanded power is significantly higher than the power at CHF and the system is allowed to reach steady state then the heated element will fail catastrophically (i.e. fail to such an extent that it cannot be repaired).

The power demanded can be varied in a step fashion by as little as 100 W. The minimum power that can be output by the power supply is 200 W.

Note that the water level is labelled on the test section tank as N1 and N2 (203.2 mm and 190.5 mm). The water level is set so that approximately 25.4 mm of the heated element is submerged.

### 2.4.2 Range of Pool Temperatures

The pool temperature is adjusted by changing the temperature and flow rate of the water going through the Copper tubing. The water mains temperature can be as low at 8 ˚C and as high as 38 ˚C. Experiments presented here were conducted at temperatures ranging from 25-40 ˚C. It is anticipated that one could conduct an

experiment with a pool temperature as low as 15 ˚C with little difficulty. The pool temperatures can be varied in a continuous fashion.

### 2.4.3 Range of Angle Inclinations

The heated element can be positioned to be in 6 different angles relative to the water surface. The angles are calculated using a centre to centre distance between the support rods with the downwards facing orientation being defined as zero (i.e. disk is parallel with water surface). In the angle calculation sagging and flexing of the support rods is assumed to be negligible.

**Table 2.4: Available Angles**

| Angle (°) | Rod 1 Position (Flat Bar 1) | Rod 2 Position (Flat Bar 2) |
|---|---|---|
| 0 | Top, Top | Top, Top |
| 1.3 | 2nd from Top, 2nd from Top | Top, Top |
| 2.5 | 3rd from Top, 3rd from Top | Top, Top |
| 5 | 4th from Top, 4th from Top | Top, Top |
| 6 | 5th from Top, 5th from Top | Top, Top |
| 20 | Top, 2nd from Top | Top, 2nd from Top |

Angles shown in Table 2.4 are available regardless of the heated element variation.

### 2.4.4 Electrical Output

The electrical system limit was not reached for the experiments conducted in this thesis. There is only one path for current to flow from the power supply to the distribution bars in the electrical cabinet. The cable used is a power cable Type RHH or RHW-2. The cable has an ampacity of 230 A at 90 °C. Since the maximum voltage of the power supply is 100 V, it means that the maximum power that can be delivered through the cable is 23 kW. This power should not be exceeded or failure of the cable and a very hazardous environment may result.

### 2.4.5 System Range of Expansion

If one is interested in studying the effect disk size has on CHF then the heated element can be made larger or smaller with the accompanying change in the addition or reduction of cartridge heaters. There are 30 parallel

paths with the maximum allowable current being limited by the fuse as 15 A per path. Assuming that one is using identical cartridge heaters (same make and model) as used in this thesis the maximum number of cartridge heaters that can be used is 60. If 60 cartridge heaters are used then the maximum power that can be sent to the heated element is 21 kW. The power limit with 28 cartridge heaters is 9.8 kW. Note that these values are calculated on a purely resistive basis and do not factor in material limitations due to excessive temperatures. Design calculations as well as simple calculations while running the experiment must be performed to ensure that the components do not exceed their maximum continuous use temperature.

The range of pool temperatures can be increased with the addition of a high power immersion heater. This may or may not be practical depending on lab constraints.

The range of angle inclinations can be increased with a significant design change. A mechanical system consisting of a set of gears with a crank on both sides of the support rods can allow for careful adjustment of the angle and can likely accommodate angles from 0-45˚. It may not be desirable to have an inclination angle past 20˚ as this will increase the temperature gradient along the bottom surface and can result in different boiling modes in different areas of the heated element.

# 3 Experimental Procedure

This chapter contains a step by step procedure on how to carry out an experiment using the EPBF. The experiments performed in this thesis are stated in the test matrix section that follows the step-by-step procedure. A detailed discussion on how data is collected and analyzed is discussed afterward and the last section of this chapter discusses sources of uncertainties and attempts to quantify them.

## 3.1 Step-by-Step Experimental Procedure

The experimental procedure is as follows:

1. TURN ON Data Acquisition system and MONITOR $T_\infty$.
2. TURN ON Recirculation Pumps and MONITOR tank water levels.
3. ADJUST valves to match flow rates between tanks.
4. ADD/REMOVE water until desired water level is reached.
5. OPEN water mains to run hot/cold water through the heating/cooling coil.
6. ADJUST temperature and flow rate through coil depending until desired $T_\infty$ is reached.
7. TURN ON Regatron Power Supply as follows:
    a. MOVE breaker to ON position
    b. MOVE Power Supply handswitch to ON position.
    c. Scroll through menu viewed on the power supply window to Limit Settings and ADJUST limit settings to V = 70 V and I = 70 A.
    d. Go back to main menu and SET controlled values to I = 0 A, V = 0 V, P = 0 kW.
    e. PRESS ON/OFF power supply button located beside the window. Green light will illuminate, indicating that current can now flow through the distribution cables.

 DANGER OF ELECTRIC SHOCK EXISTS 

8. On main menu SET I = 20 A, V = 20 V and P = 1 kW. Power supply will indicate that it is in the power controlled mode of operation.

9. CHECK that temperature data is being recorded with an appropriate hard disk location and name.
10. MONITOR heated element temperatures and allow them to reach steady state.
11. ADJUST temperature and flow rate through heating/cooling coil to maintain desired $T_\infty$.
12. RAISE power level by 100, 200, or 300 W as conditions dictate.
13. If display indicates that power supply is no longer in power controlled mode of operation, then RAISE the setting of current and voltage to an appropriate value.
14. CREATE new file and record data with new power level.
15. WAIT for heated element temperatures to reach steady state (minimum 10 minutes) while continuing to:
    a. ADJUST temperature and flow rate through heating/cooling coil to maintain desired $T_\infty$.
    b. If needed, ADD water until desired water level is reached.
    c. If water levels in the tanks are different, TURN OFF the recirculation pump in which the water level is lower. WAIT for levels to equalize and then TURN ON the same recirculation pump.
16. If heated element temperatures do not fluctuate or rise appreciably for a period of 5 minutes, then steady state is reached. CHECK that data has been recording.
17. If everything is behaving as expected for this power level, REPEAT steps 12 through 16 until CHF is reached.
18. At CHF the temperatures in the heated element rise quickly to ~200 ˚C and will continue to rise unless the operator intervenes. Remove electrical power to the heated element by depressing the ON/OFF button. The green LED will no longer be illuminated once power is removed.
19. TURN OFF power supply by placing the hand switch in the OFF position and by opening and locking out the breaker in the OFF position. Electrical shock danger has now been removed.
20. WAIT for heated element to cool down to temperatures that allow for polishing of the surface.
21. REMOVE water from the tanks such that the surface can be polished.
22. Polish the surface in a circular pattern using emery sandpaper P80.

Note that the operator is required to continually monitor the water levels in the tanks, heated element temperatures and the bulk fluid temperature. The operator is to take corrective action if any parameter deviates from the desired value or changes unexpectedly.

## 3.2 Data Collection

Note that the hardware and software used in obtaining temperature measurements was purchased and developed by B. A. Statham as part of his research. It was modified by B. A. Statham for use in this experiment. The data acquisition system is discussed here for clarity, completeness and to ensure that future experiments can be reproduced without great difficulty.

Data is acquired and plotted in real time using a National Instruments (NI) Data Acquisition system. The hardware used is NI cDAQ-9178 8-Slot USB Chassis with a NI 9213 16-Channel Thermocouple Input Module. The temperature data is plotted on the LabView Front Panel of the program (see Figure 3.1) as data is acquired. The operator has temperature information at all times while running the experiment. The temperature is recorded in a text file along with a time stamp.

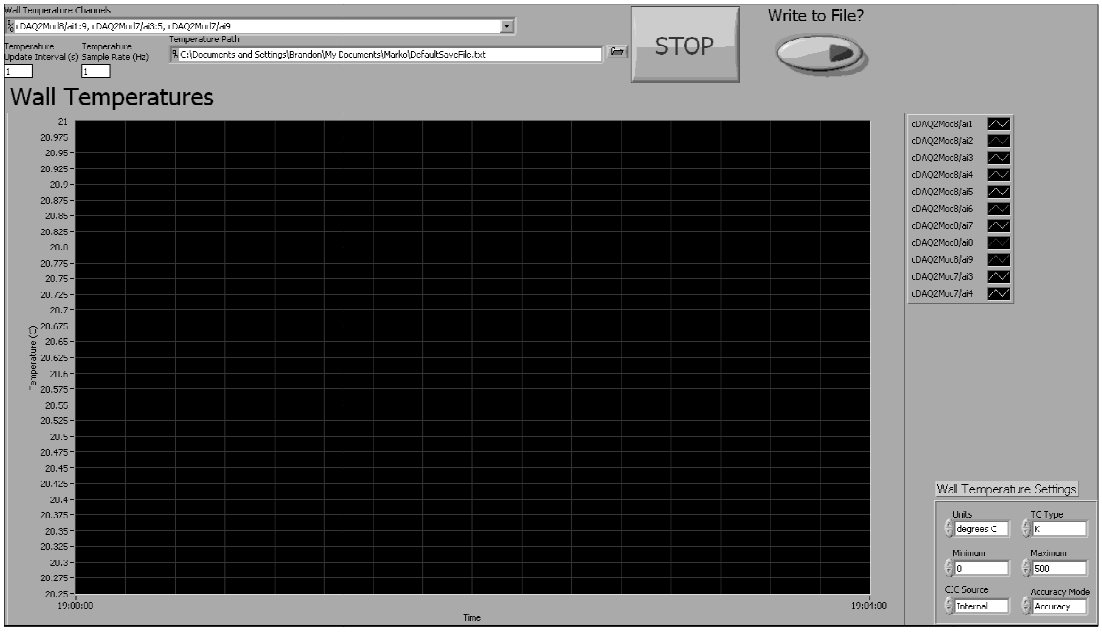


**Figure 3.1: Temperature Recording Front Panel**

The temperature data is acquired in high-accuracy mode with a reference given by utilizing the internal cold-junction compensation feature of NI 9213. High-accuracy mode is a time-average measurement of temperature over the span of 1.359 s.

The LabView Block Diagram of the program is shown in Figure 3.2:

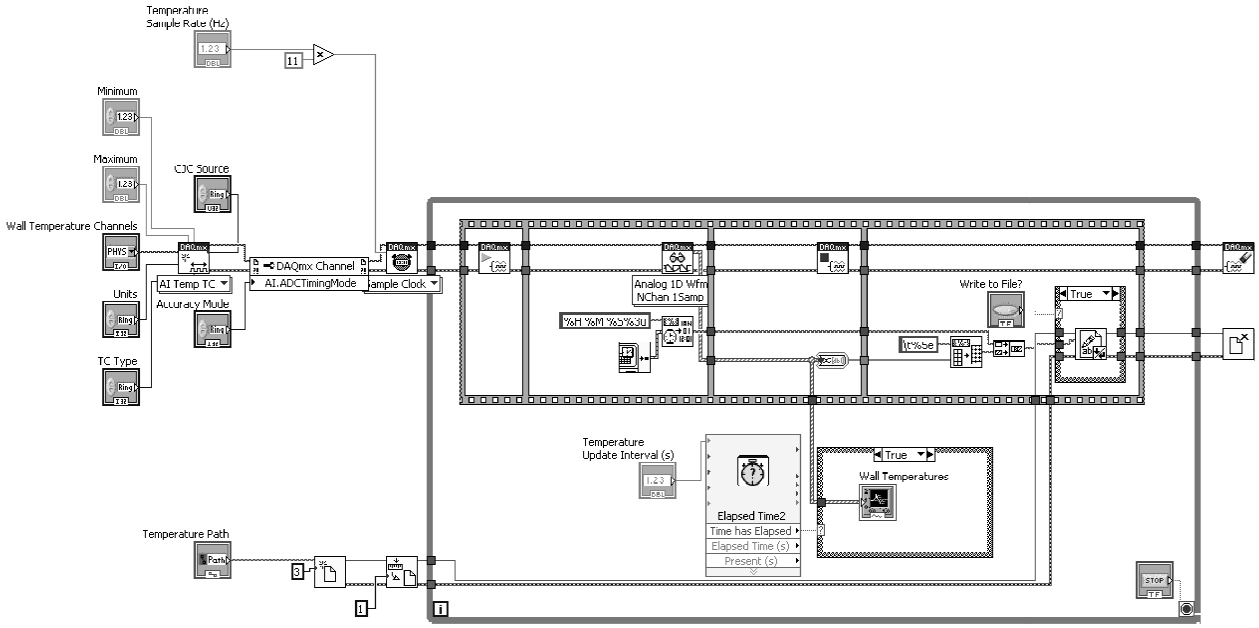


**Figure 3.2: Temperature Recording Block Diagram**

The Block Diagram is an application developed by LabView to aid in rapid development of the Front Panel. The temperature data collected is then imported into MS Excel for analysis.

## 3.3 Test Matrix

For the unconfined heated element variation only one experiment is performed. The device is oriented downwards with a 0˚ inclination and the temperature of the bulk is maintained at nominally 35 ˚C.

The confined variation was studied in 15 different experiments. The angle of inclination and bulk fluid temperature is varied between the allowable ranges afforded by the EPBF. The test matrix is presented in Table 3.1.

**Table 3.1: Test Matrix for Confined Variation**

| $T_\infty$ \ Θ | 0° | 2.5° | 5° | 6° | 20° |
|---|---|---|---|---|---|
| 25°C | X | X | | | |
| 30°C | X | X | X | X | X |
| 35°C | X | X | X | X | X |
| 40°C | | | X | X | X |

An 'X' indicates that the test was performed successfully for the conditions shown. For the 0˚ and 2.5˚ inclination it was not possible to maintain $T_\infty$ at 40 ˚C. For 5˚, 6˚, and 20˚ an experiment with $T_\infty$ at 25 ˚C was not attempted.

## 3.4 Data Analysis

Once good temperature data is obtained the next step is to analyze the data so as to construct a boiling curve and numerically determine the CHF. The following sections discuss how the temperature data is manipulated to construct a boiling curve and calculate the CHF.

### 3.4.1 Heat Flux Determination

The heat flux through the exposed surface is calculated from the measured temperature values. The heat flux through the unheated portion of the Brass rod is linear axially. To determine the downwards heat flux:

$$q = k\frac{T_2 - T_1}{\Delta y} \qquad \text{(Equation 3.1)}$$

Where:

$T_2$ is the average of the temperature values given by thermocouples located high in the heated element (see Figure 2.2 Section B-B),

$T_1$ is the average of the temperature values given by thermocouples located low in the heated element (see Figure 2.2 Section C-C),

$\Delta y$ is the difference in depth between the two thermocouple levels,

and *k* is the thermal conductivity of the Brass rod.

In the calculation of the heat flux, no temperature values were discarded as outliers. All temperature values are used.

The separation distance, *Δy*, is fixed and is set by the differing hole depths.

The thermal conductivity, *k*, is a function of temperature and is evaluated at the mean temperature of all heated element temperature recordings. The thermal conductivity is evaluated with only one input: $T_{1,2} = \langle T_2, T_1 \rangle$, where *T* is in Kelvin. The expression for *k* is:

$$k(T_{1,2}) = a + b(T_{1,2} - 273) \qquad \text{(Equation 3.2)}$$

Where *a* and *b* are calculated as 75.82 $Wm^{-1}K^{-2}$ and 0.1183 $Wm^{-1}K^{-2}$ from data provided by from Touloukian and Ho (1972).

The heat flux is calculated using Equation 3.1 for all available data. However, in construction of the boiling curve only steady state data is used. The approach used in this thesis calculates an average heat flux from the last 50 data points. An alternative approach would be to calculate the heat flux at the very last available data point. Both approaches yield similar results, but the former approach encourages a statistical study of the data (i.e. a low standard deviation in the data implies the values are precise).

The following table summarizes the individual values in Equation 3.1 for a heat flux of ~500 $kW/m^2$:

**Table 3.2: Item Values in Equation 3.1**

| Attribute in Equation 3.1 | Numerical Value |
|---|---|
| *k* | 127 W/mK |
| *ΔT* | 20 ˚C |
| *Δy* | 5.08 mm |

Note that unreduced data for representative conditions is shown in Appendix A. All utilized data has been attached as a series of MS Excel spreadsheets in the CD that accompanies this thesis.

### 3.4.2 Surface Temperature Determination

The surface temperature is not directly measured in this experiment. It is found by linear extrapolation from the measured temperature values. The following expression is used to find the surface temperature:

$$T_w = T_1 - \frac{1}{2}(T_2 - T_1) \qquad \text{(Equation 3.3)}$$

The above expression is a special case of linear extrapolation and is valid because the distance between the surface and the first set of thermocouples is 2.54 mm, which is precisely half of the separation distance.

To be consistent with the approach in Section 3.4.1 the average of the last 50 data points is used to determine the surface temperature.

### 3.4.3 Construction of a Boiling Curve

A boiling curve is constructed for each experiment. It is useful to construct a boiling curve because its linearity is a good indication of how well controlled the experiment is. The boiling curves are constructed by plotting the steady state heat flux as a function of wall superheat. The wall superheat is the surface temperature minus the temperature at saturation. For water at atmospheric pressure $T_{sat}$ = 100 ˚C.

### 3.4.4 Critical Heat Flux Calculation

Upon departure from nucleate boiling the temperature of the heated element rises rapidly and in some cases non-uniformly. Calculating the CHF as the temperature of the heated element is rapidly increasing is not practical and is prone to large errors (see Section 4.1.3).

The approach taken here is to determine the CHF by linear extrapolation from the known nucleate boiling data point. The extrapolation is based on the new power level that resulted in film boiling. Mathematically,

$$q_{CHF} = \frac{P_{CHF}}{P_{NB}} q_{NB} \qquad \text{(Equation 3.4)}$$

Where the subscript NB refers to the last known Nucleate Boiling data point.

Once the power level is increased the temperatures can exist in a quasi-steady state for a significant period of time before film boiling is instigated. For these cases it is possible to compare the result calculated by equation 3.4 with the measured heat flux just before the temperature excursion occurred. The values are found to match almost exactly.

### 3.4.5 Estimation of Uncertainties

Every measurement has sources of systematic and random error. In this experiment the following systematic errors are identified in the heated element:

1. Thermocouple accuracy
2. Manufacturing tolerances in hole depth
3. Differing rates of thermal expansion
4. Recirculation system impact on thermal-hydraulic behaviour
5. Pool temperature thermocouple impact on thermal-hydraulic behaviour
6. Wear and aging of the heated element
7. Level fluctuation in test section tank
8. Thermocouple drift or fouling
9. Quantization error

Sources of random error are due to electrical noise and vibrations brought on through the vigorous boiling process. There are further uncertainties in the controlled parameters of pool boiling temperature and angle inclination. The measurement uncertainties are quantified as discussed in the following sections.

#### *3.4.5.1 Heated Element Systematic Errors Included in the Combined Measurement Error*

Thermocouple accuracy impacts the heat flux and wall superheat calculation. From the manufacturer data sheet (Omega, (2011)), the limits of error are 2.2 ˚C or 0.75% of the measured value, whichever is greater, for measured temperatures above 0 ˚C. Since temperature data used in constructing the boiling curve is always less than 290 ˚C, the limits of error are calculated using the 2.2 ˚C value given by the manufacturer. The error in the temperature difference is calculated by:

$$e_{\sigma T} = \sqrt{\sigma T_2^2 + \sigma T_1^2} \qquad \text{(Equation 3.5)}$$

Where $\sigma T$ is:

$$\sigma T(\%) = \frac{2.2}{T} \qquad \text{(Equation 3.6)}$$

Note that the limits of error are derived from a maximum and minimum range and thus can be assumed to correspond to *2σ*. The error in temperature varies as a function of the measured value. For purposes of illustration, assuming that *T* = 150 ˚C results in an error in the temperature difference of ~2%.

Manufacturing tolerances in the thermocouple access holes depth are 0.8 mm. This value includes machining tolerance and tool tolerance. The error in the separation distance, $e_{\sigma y}$, is calculated to be ~4% and is assumed fixed.

In calculating the heat flux, the thermal conductivity is assumed to be known to infinite precision. The value of thermal conductivity is evaluated at the average temperature stated by the heated element thermocouples. This simplification is also assumed to result in a negligible error since the thermal conductivity is not a very sensitive function of temperature. Also, the temperature difference in this experiment is relatively small compared to the dataset used to calculate the sensitivity of thermal conductivity to temperature. Thus, the systematic error contribution to heat flux is found from:

$$e_q = \sqrt{e_{\sigma T}^2 + e_{\sigma y}^2} \qquad \text{(Equation 3.7)}$$

Since the errors in temperature are themselves not fixed values (i.e. the error is a function of temperature) the error value is not fixed either. Assuming *T* = 150 ˚C, as before, the total systematic error in the heat flux measurement is ~5%.

A linear extrapolation is performed to calculate the wall superheat, which means that an additional error due to extrapolation is introduced. Unfortunately, since only two points are used to draw the line an extrapolation error cannot be calculated. If three points were available and a linear least squares fit was performed then the extrapolation error can be calculated. The systematic error in surface temperature is therefore assumed to be 2.2 ˚C as defined by thermocouple accuracy. Note that the true value of surface temperature error is known to be greater than the assumed value of 2.2 ˚C.

#### *3.4.5.2 Heated Element Systematic Errors Not Included in the Combined Measurement Error*

Good instrument and experimental design minimizes systematic errors. This section discusses items 3 to 9 mentioned in Section 3.4.5.

In this experiment the biggest systematic error that can potentially arise is due to poor mechanical contact between the thermocouple tip and the heated piece. Upon losing good contact, air will exist between the piece and the thermocouple. Since air is an insulator, a large bias will be introduced in the resulting temperature measurement. This bias can be different for all thermocouples and can potentially corrupt data to the point that nothing can be inferred. Similarly, debris collected between the thermocouple tip and the heated piece can result in a negative bias. Also, there is a finite temperature drop between the heated piece and the thermocouple tip contact. The design presented here combats this potential problem by implanting thermocouples and surrounding the thermocouple sheath with a high temperature, high rate of thermal expansion ceramic adhesive. Also, the thermocouple sheath's rate of thermal expansion is similar to the rate of expansion for Brass and the thermocouples tips are cleaned free of debris prior to insertion. During experimentation it is expected that if this systematic error exists it would manifest itself by introducing a large temperature fluctuation and an under prediction of the true value of temperature at the point of measurement. Fortunately, the former behaviour was not experienced and this systematic error is believed to be negligible on the basis of good instrument design. The latter is manifest in a small negative bias. Through visual inspection boiling was observed and is known to occur at 100 ˚C. The surface temperature data for some experiments stated that the surface temperature was slightly below 100 ˚C. For illustrative purposes, the negative bias is at most 4 ˚C and at times does not exist. The boiling curves plotted in the Experimental Results section all begin with data at which vapour bubbles were first observed. Therefore, the boiling curve graphs can be used to infer what the negative bias is.

If one is to study subcooled pool boiling, some sort of recirculation system or a cooling coil must be used to control the pool temperature as the heated element heats the pool. This experiment uses a recirculation system with a cooling coil. This sub-system modifies the very behaviour that is intended to be studied. The effect, however, is believed to be negligible. To investigate, the recirculation system was turned off and the boiling behaviour was seen not to be altered by visual inspection.

A thermocouple is placed in the pool of water to measure the pool temperature. This device also modifies the very behaviour that is intended for study, but the impact is extremely small. The size of the thermocouple is small and it is placed in an area of the pool that does not interfere with the boiling process.

The heated element is subject to large temperature transients, which lead to mechanical deformation of the device. In terms of measurement problems, this could cause a large systematic error in the temperature measurements. Over the course of experimentation, however, this problem was not manifest. Another practical issue that arises is aging of the cartridge heaters. The resistance of the cartridge heaters is found to stay constant and the resulting heat flux from known power levels was not found to change with age. Mechanical deformation does result in cartridge heaters that cannot be removed from the Brass rod without significant difficulties.

Even if flow rates between tanks are matched, the level can fluctuate in the test tank due to steam escape into the environment. This will introduce a transient effect to an experiment that is believed to be steady state. A decreasing water level will mean that the downwards heat flux is increasing and vice versa. This is because the heated element in reality is not ideal and does transfer heat through the insulated sides. The level is found to fluctuate by approximately 0.1 mm/min for most experiments and even approaches zero for some experiments that were conducted. The observed change in downwards heat flux is also small. Unfortunately, level data was not obtained and the sensitivity of heat flux with respect to level for practically relevant values was not acquired. The sensitivity is expected to be small and is combated by operator intervention. The water level is maintained to a mean value within ± 1 mm.

Differing rates of thermal expansion in the thermocouple wires and resulting hysteresis can result in measurement drift. Since the experiments were conducted within a one month time frame, drift is expected to be negligible and was not observed in the data.

Going from an analogue signal to a digital value available for manipulation in a text file introduces quantization error. According to NI 9213 specifications, the ADC used is 24-bit and results in a measurement sensitivity of 0.02˚ C. Since the measured value is approximately 4 orders of magnitude greater than the sensitivity, the error is thought to be negligible.

#### *3.4.5.3 Heated Element Quantification of Random Errors*

Random errors due to environmental disturbances such as electrical noise or vibrations in the heated element are assumed to be normally distributed. Steady state data over the last 50 data points is used to calculate the standard deviation in both heat flux and surface temperature.

The numerical results vary on a case by case basis from as low as 0.25% to as much as 5%. From the data available a good representative value of one standard deviation is $\sigma_{rq}$(%)=2%. Further calculations are performed in this section using this assumed value for the purposes of illustration.

The variability in surface temperature due to random fluctuations is lower than that in the heat flux. Note that the difference in temperature measurements is used to calculate the heat flux with any fluctuations being amplified. Thus, the variability in temperature is expected to be much smaller than the variability in heat flux. An upper bound is $\sigma_{rT}$(%)=0.1 %.

#### *3.4.5.4 Heated Element Combined Measurement Error*

The systematic and random errors are all independent of each other and the total measurement error can be combined in a root mean squared sense. The combined measurement error in the heat flux calculation is given by using the following expression:

$$e_{q,combined} = \sqrt{e_{\sigma T}^2 + e_{\sigma y}^2 + (2\sigma_{rq})^2} \qquad \text{(Equation 2.8)}$$

With the values stated earlier the measurement error in heat flux is ~6%.

The combined measurement error in the surface temperature calculation is given by the following expression:

$$e_{T,combined} = \sqrt{e_{\sigma T}^2 + (2\sigma_{rT})^2} \qquad \text{(Equation 2.9)}$$

With the values stated earlier the measurement error in surface temperature is ~2%.

Note that measurement errors are calculated on a case-by-case basis for the boiling curves and CHFs presented later in the thesis. Therefore, the values used here are for illustrative purposes only.

#### *3.4.5.5 Critical Heat Flux Extrapolation Error*

Calculating the CHF when the temperature excursion is occurring is not practical due to temperature fluctuations, time lag errors and the non-uniform instigation of film boiling. The heat flux at the departure from nucleate boiling is not directly measured but is extrapolated from the last known data point, as discussed previously. This introduces an additional error that is assumed to be pro-rated. For example, if film boiling occurs at 2.2 kW and data is available is at power level 2.1 kW with corresponding heat flux $q_{NB}$ = 250 kW/m$^2$ the CHF is found by using Equation 2.4:

$$q_{CHF} = \frac{2.2}{2.1} \times 250 = 295 \text{ kW/m}^2$$

Using the same reasoning, the error in the CHF is:

$$e_{q,CHF} = \frac{P_{CHF}}{P_{NB}} e_{q,combined} \qquad \text{(Equation 3.11)}$$

Inserting the values given earlier, the error in the CHF is ~7%.

#### *3.4.5.6 Pool Temperature and Angle Inclination Uncertainty*

The single thermocouple that is used to determine the pool temperature has a combined measurement uncertainty of ~8%. This value includes random errors and the systematic error of reference accuracy. This is a large error.

The angle uncertainty is calculated to be ±0.3˚ for inclination of 0˚, 2.5˚, 5˚ and 6˚. For these inclinations the angle is calculated by using the following expression:

$$\theta = \arctan\left(\frac{\Delta_{c-c}}{L_{c-c}}\right) \qquad \text{(Equation 3.12)}$$

Where $\Delta_{c\text{-}c}$ is the vertical separation distance between the set of holes from centre to centre and $L_{c\text{-}c}$ is the length of the support bar from the main chassis holes centre to centre. Both inputs used to calculate the angle are well known. The assigned tolerances are $2\sigma\Delta_{c\text{-}c}$=2.54 mm and $2\sigma L_{c\text{-}c}$=6.35 mm. These values include uncertainties in the locations of the rod after flexing and machining tolerances. A maximum and minimum is calculated for the angle $\Theta$ using the assigned tolerances and the corresponding uncertainty in angle is found to be ±0.2˚. This uncertainty is combined with the uncertainty in assembly tolerances of the heated element and the angle tolerance of the main chassis in a root mean squared sense with the tolerances in assembly and main chassis both assigned an uncertainty of ±0.1˚.

A similar calculation is performed for the 20˚ angle with the denominator in Equation 3.12 being changed to the separation distance between adjacent holes on the main chassis. The tolerance in hole separation is taken to be 0.254 mm and uncertainty in centre to centre hole separation is reduced to 1.27 mm due to the reduced amount of bending and flexing. The resulting uncertainty in angle is ±1˚.

# 4 Experimental Results

This chapter provides plots and tabular data of the experimental results. Data obtained pertaining to the confined variation is presented first and is followed by the unconfined variation.

## 4.1 Confined Study

### 4.1.1 Boiling Curve

The heat flux through the exposed surface is plotted as a function of wall superheat, $\Delta T$, for the confined variation in Figure 4.1 to Figure 4.5.

The confined variation of the heated element is defined in Section 2.2.1. How the boiling curves are constructed is discussed in the Data Analysis sections 3.4.1, 3.4.2, 3.4.3, and 3.4.5. The pool temperature was well controlled in this experiment, with an uncertainty of ~±2.3 ˚C with 95% level of confidence.

The inclination angles were also well controlled in this set of experiments. For inclination angles less than or equal to 6˚ the uncertainty is ±0.3˚. For the 20˚ inclination angle the uncertainty is ±1˚.

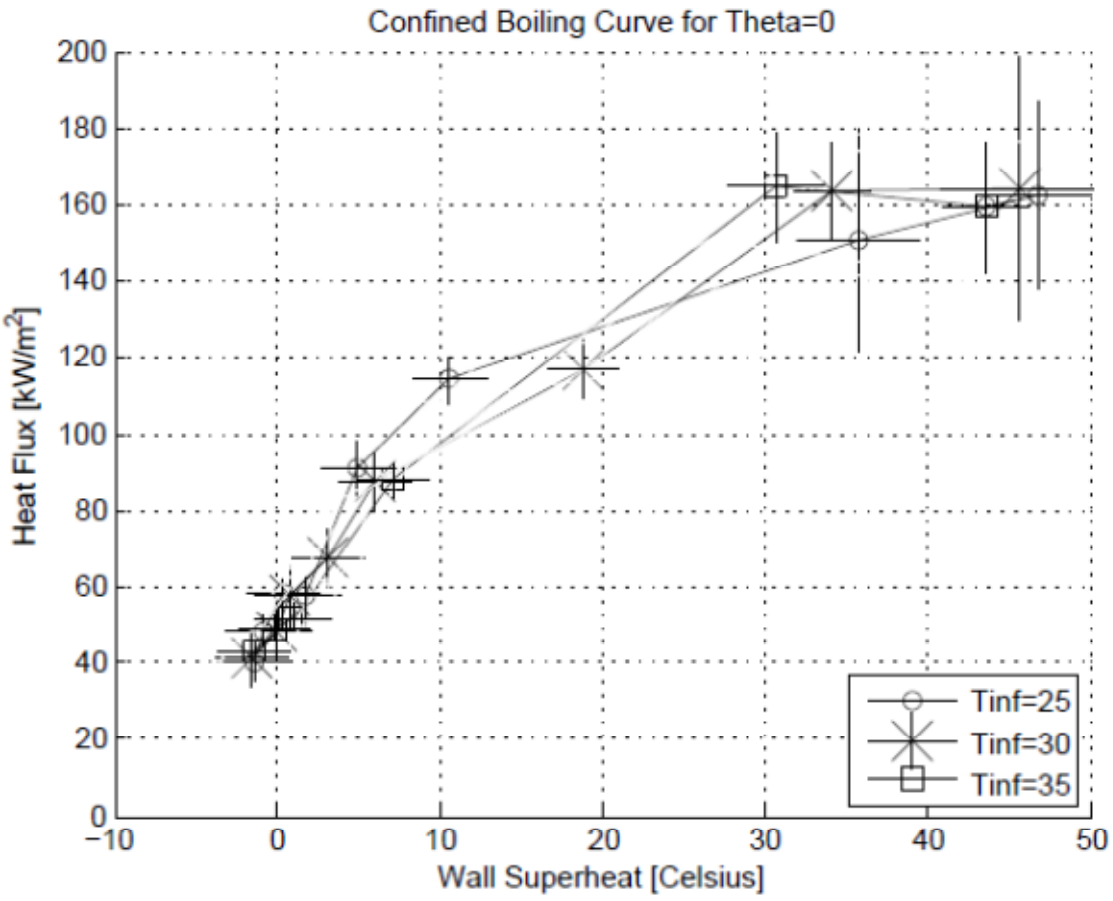


**Figure 4.1: Boiling Curve, Confined Variation, θ=0˚**

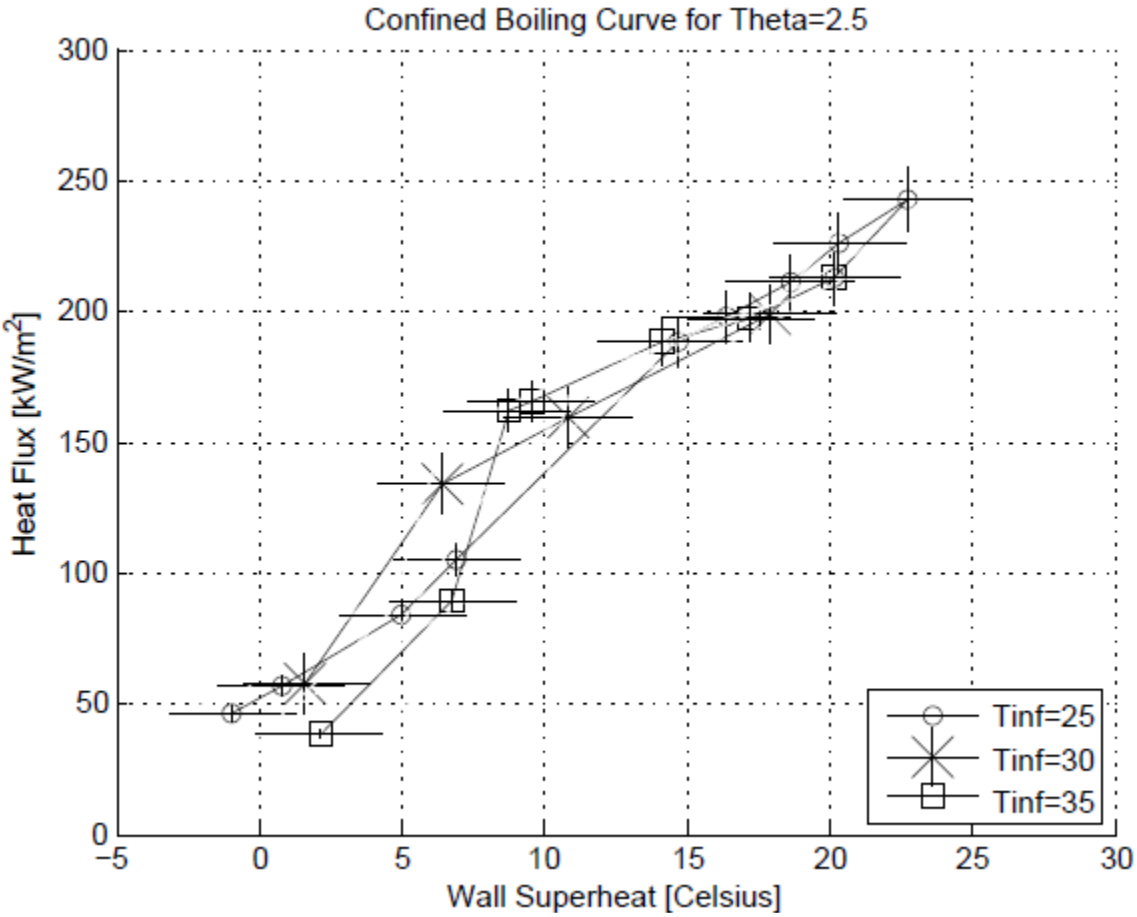


**Figure 4.2: Boiling Curve, Confined Variation, θ=2.5˚**

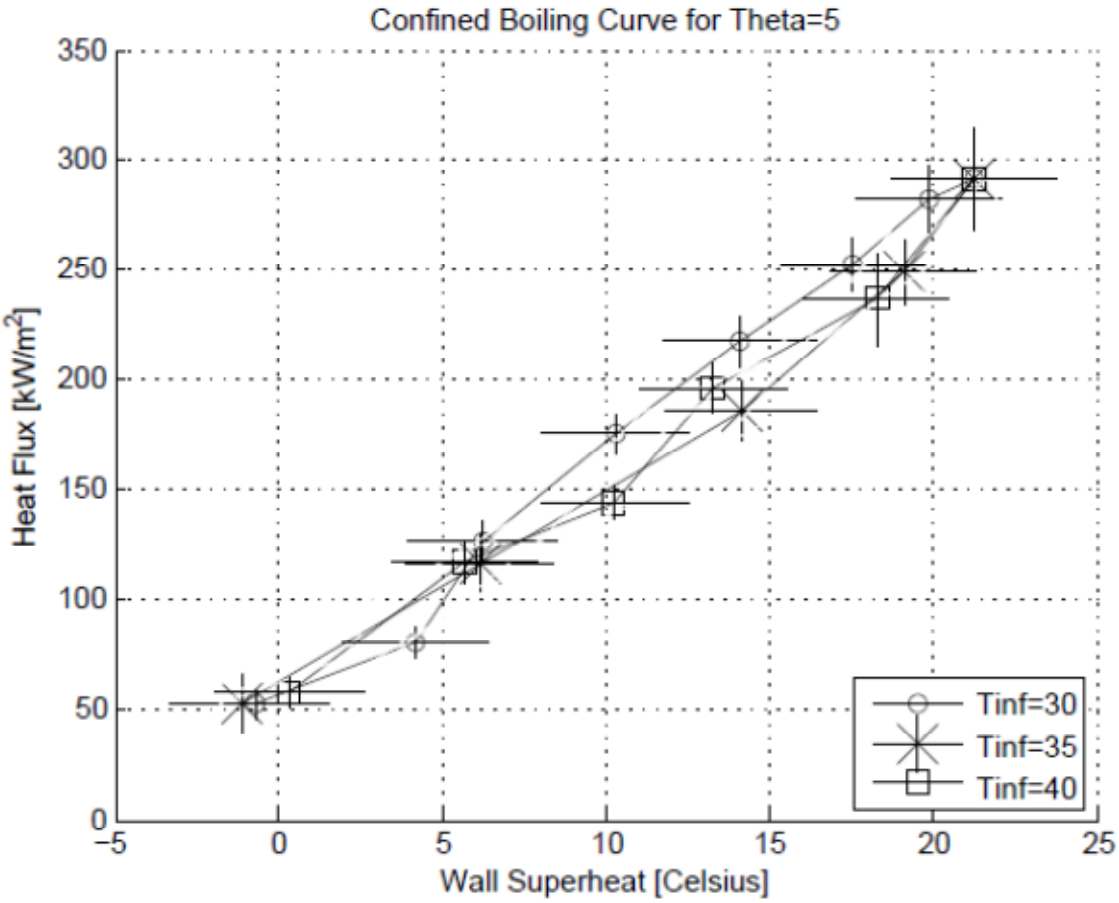


**Figure 4.3: Boiling Curve, Confined Variation, θ=5˚**

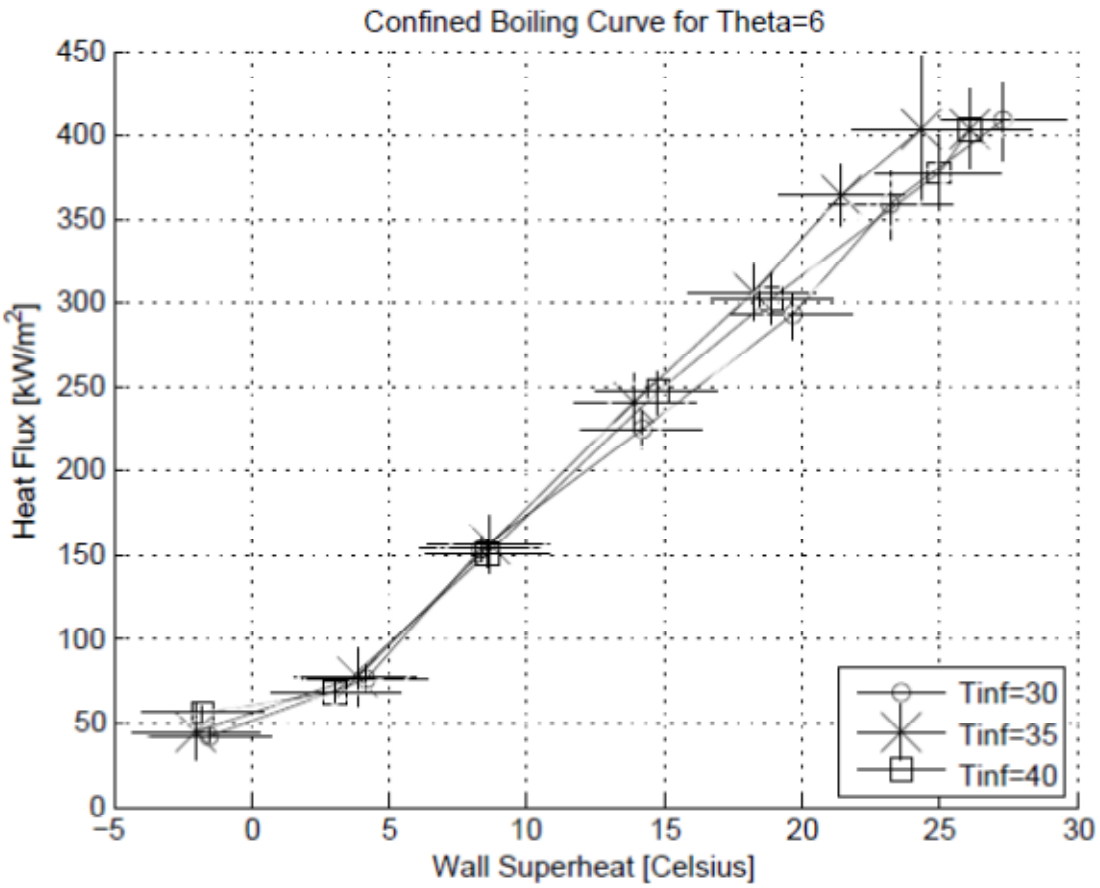


**Figure 4.4: Boiling Curve, Confined Variation, θ=6˚**

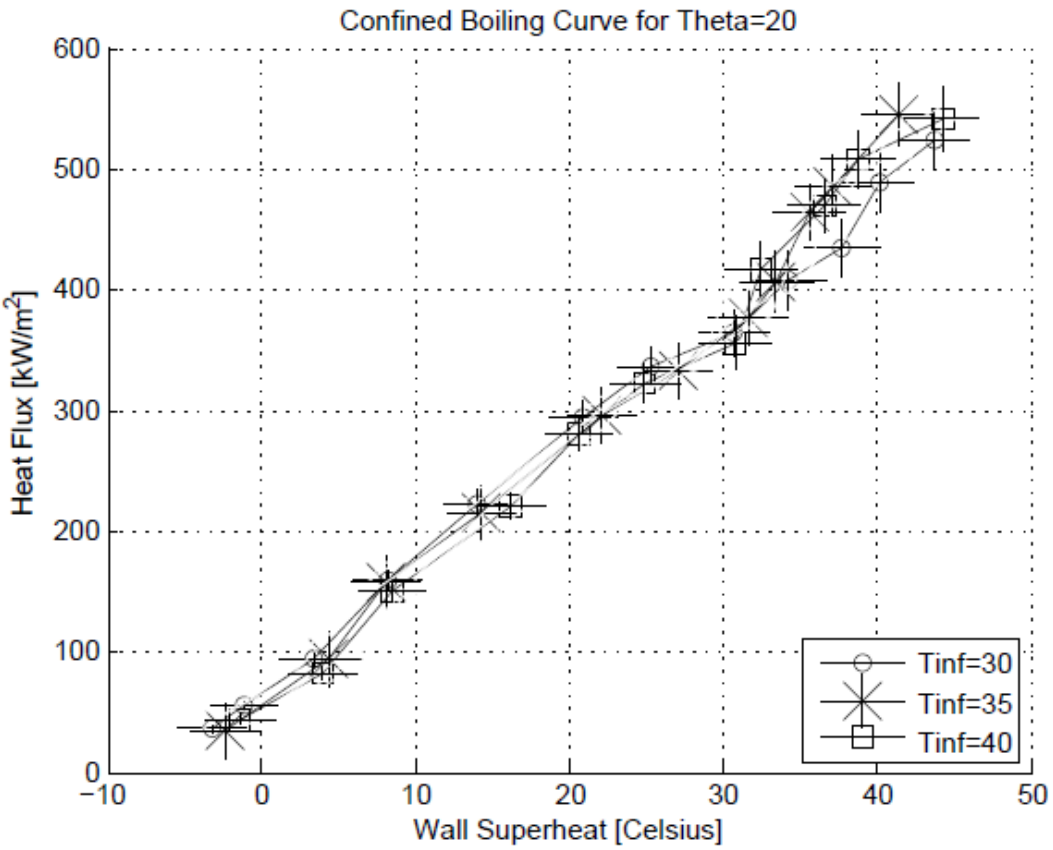


**Figure 4.5: Boiling Curve, Confined Variation, θ=20˚**

### 4.1.2 Polished Versus Aged Surface

An experiment is also performed with the heated element polished and with it "aged". The condition of the "aged" heated element is that it was not polished after one successful CHF experiment. The two boiling curves are shown in Figure 4.6.

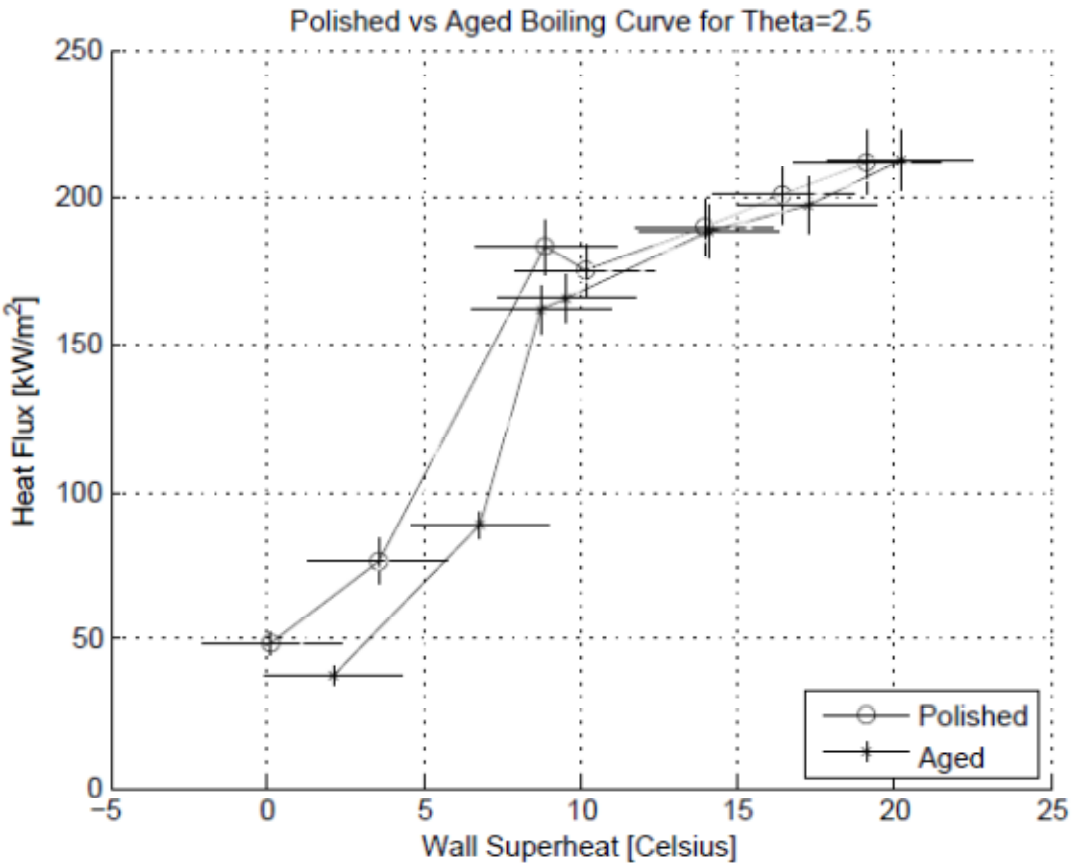


**Figure 4.6: Boiling Curve for Aged and Polished Surface, $T_\infty$=35 ˚C**

### 4.1.3 Transition from Nucleate to Film Boiling

An abrupt transition from nucleate boiling to film boiling was observed in the confined variation. The resulting temperature excursion would lead to temperature measurements in excess of 200 ˚C. Also, the individual temperature measurements would increase by 50 ˚C or more compared to the nucleate boiling value. Power is removed as soon as the temperature recording approaches 200 ˚C. Figure 4.7 is a representative plot of the observed temperature response to a transition from nucleate to film boiling.

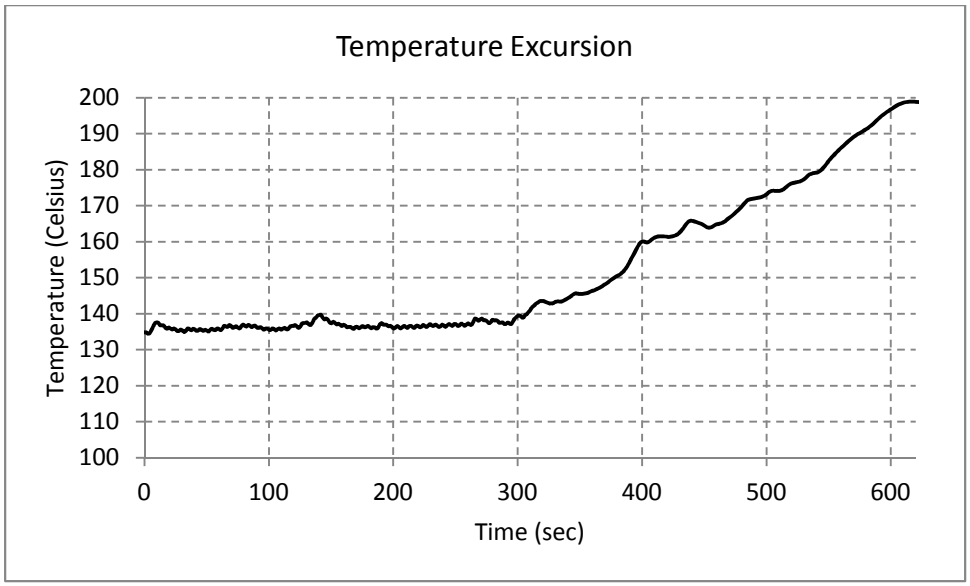


**Figure 4.7: Temperature Excursion at θ = 2.5˚**

The CHF was not reached for the 20˚ inclination due to fear of damaging the heated element. The CHF value for this angle of inclination is extrapolated from the boiling curve data as follows: 200 ˚C is divided by the peak temperature observed and is used to multiply the heat flux at the peak power. Thus, this calculation is intended to show that the CHF is monotonically increasing as inclination angle is increased.

### 4.1.4 CHF as a Function of Inclination Angle

The measured CHF as a function of inclination angle is plotted in Figure 4.8. The figure shows all determined CHF values for all experimental conditions. The methodology used to determine the CHF values is discussed in Section 3.4.4. Note that the data shows little spread in CHF values for different pool temperatures.

Table 4.1 states the numerical values of the CHF for a pool temperature of 30 ˚C.

**Table 4.1: CHF Table of Values for $T_\infty$=30 ˚C**

| Theta | CHF (kW/m$^2$) |
|---|---|
| 20 | 596 |
| 6 | 495 |
| 5 | 295 |
| 2.5 | 223 |
| 0 | 187 |

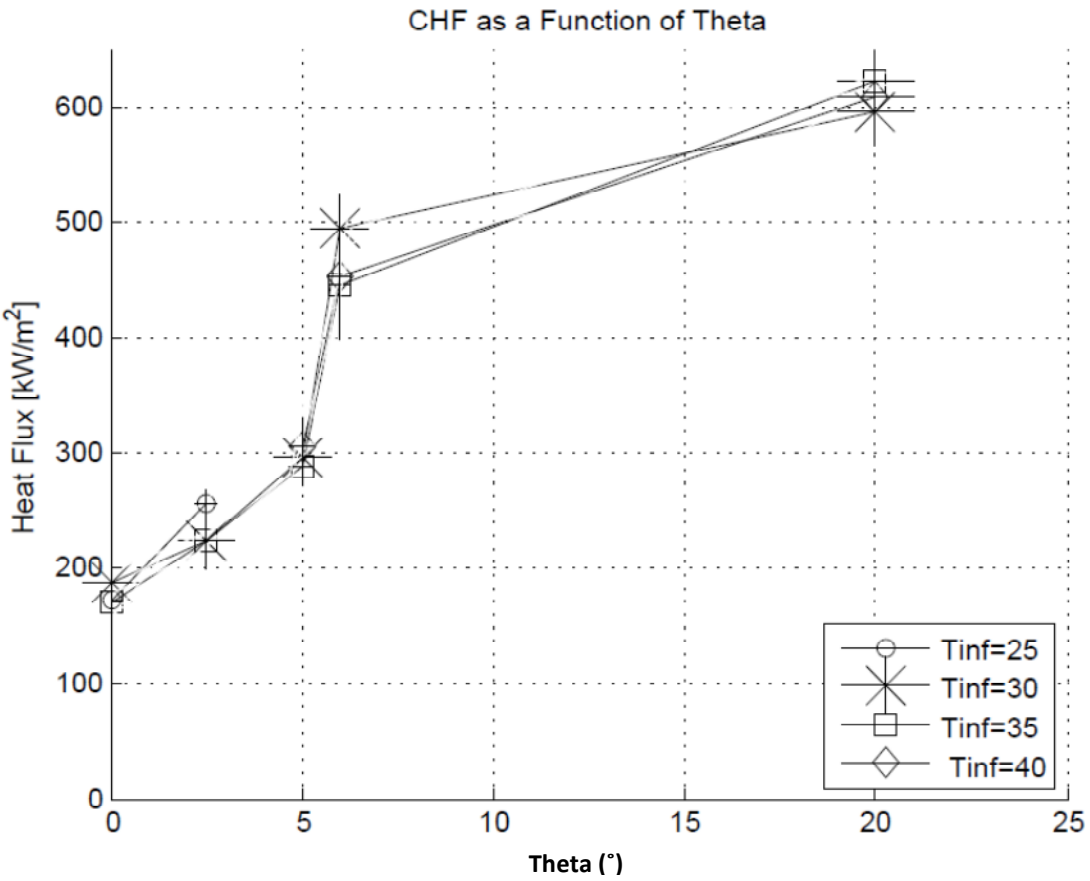


**Figure 4.8: CHF as a Function of *Θ***

## 4.2 Unconfined Study

### 4.2.1 Boiling Curve

The heat flux through the exposed surface is plotted as a function of wall superheat, Δ*T*, for the unconfined

variation in Figure 4.9.

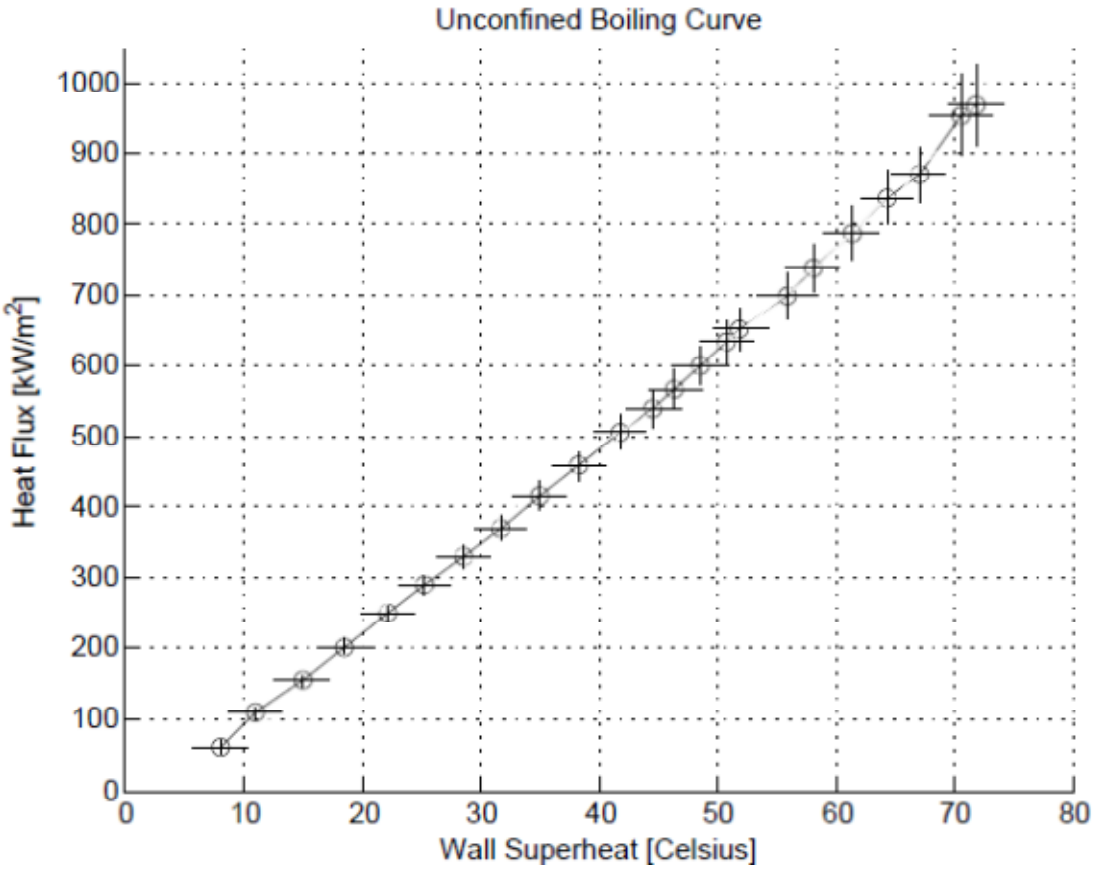


**Figure 4.9: Boiling Curve, Unconfined Variation**

The unconfined variation of the heated element is defined in Section 2.2.1. How the boiling curve is constructed is discussed in the Data Analysis sections 3.4.1, 3.4.2, 3.4.3, and 3.4.5. The pool temperature was difficult to control in this experiment due to the large input power, but it was maintained below 50 ˚C with the highest level of confidence. The best estimate of pool temperature was 35 ± 7 ˚C.

### 4.2.2 Transition from Nucleate Boiling to Film Boiling

The lowest power occurrence of when the transition from nucleate boiling to film boiling occurs is defined as the CHF. For the unconfined variation, it is expected that a temperature excursion would result or that the wall temperature would rise above 200 ˚C. This transition was not observed experimentally in the EPBF for this variation of the heated element. It can be said with a high degree of confidence, therefore, that the CHF for this geometry in this environment is greater than ~1 MW/m$^2$.

# 5 Discussion

This chapter opens by discussing the various heat transfer mechanisms found in nucleate pool boiling and then discusses qualitatively the important physics for the confined and unconfined variations applicable in the medium to high heat flux region. Following the discussion of the major mechanisms involved, obtained experimental data is compared with those obtained independently by other researchers. Important experimental observations are noted, the role of subcooling is discussed and finally a correlation relating the CHF to confinement is stated.

## 5.1 Heat Transfer Mechanisms

In nucleate pool boiling there are at least 6 mechanisms that are thought to strongly impact heat transfer. They are:

Natural Convection: In addition to density differences in the liquid phases, which result in movement, density differences between the liquid and vapour phases cause further motion. These statements are valid in the presence of a gravitational field. Figure 5.1 shows natural convection and two phase enhanced natural convection for an upwards facing surface.

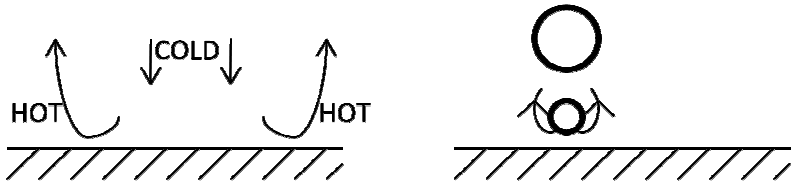


**Figure 5.1: Natural Convection in Single Phase and Two-Phase Flow**

The process of a vapour slug departing the heated surface, joining the bulk fluid then escaping to the surroundings is termed venting. It is a consequence of the density differences between the two phases and is an important mode of heat removal. Heat is transferred in the mode of latent heat found in the bubble as well as sensible heat found in the liquid surrounding the bubble.

Bubble Agitation: The nucleation of a bubble and subsequent motion alters the flow field in the surrounding liquid thus modifying the liquid phase natural convection process. The flow field varies circumferentially and in time, but simplistically it is similar to localized forced flow.

Bubbles coalesce and form a vapour slug (pancake-like larger bubble). This phenomenon causes motion in the liquid that surrounded the vapour bubbles prior to coalescence. Coalescences occurs frequently in downwards

facing orientations and is therefore thought to be important. In upwards orientations, bubbles coalescence and form vapour jets, but relative to downwards facing studies the impact is small.

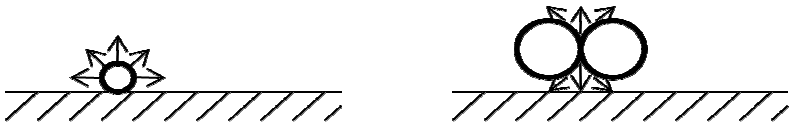

**Figure 5.2: Bubble Agitation Due to Nucleation (L) and Coalescence (R)**

Heat is transferred in the form of sensible heat. This mechanism is relevant for both downward facing and upward facing orientations.

Thermal Layer Stripping: As the bubble departs, a superheated liquid layer surrounding the bubble departs with it, thereby removing heat from the surface and in the vicinity of the heater. As the bubble or vapour moves the hydrodynamic drag causes mixing of the superheated liquid layer with the bulk fluid. Heat transfer is in the form of sensible heat. This mechanism is thought to be important for an upwards facing orientation, but is of reduced importance in inclined downwards facing studies because the superheated layer adjacent to the surface will not depart with the bubble or vapour slug. For a downwards facing plate, $\theta=0°$, this mechanism is of no importance.

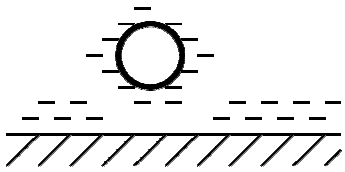

**Figure 5.3: Thermal Layer Stripping Following Bubble Departure**

Boiling: The surrounding liquid heats the vapour bubble and causes it to grow. Heat is transferred in the form of latent heat.

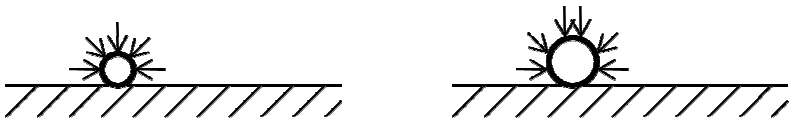

**Figure 5.4: Evaporation, Time Evolution of a Bubble**

Condensation: The bubble or vapour slug can collapse into the pool of water, shrink or reach some equilibrium size. This is of importance for subcooled pool boiling.

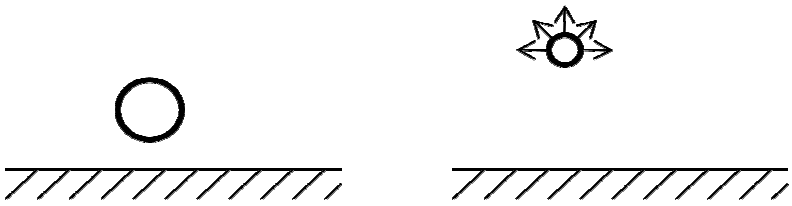

**Figure 5.5: Condensation Heat Transfer into the Pool, Time Evolution of a Bubble**

## 5.2 Confinement Level and Application of the Bond Number

The Bond number is a dimensionless number used to quantify the relative strengths of the buoyancy force to adhesive force. It is given by:

(Equation 5.1)

Where *s* is a characteristic dimension expressing the confinement level and *L* is the capillary length:

(Equation 5.2)

In LWR experiments, the Bond number is frequently used to describe the level of confinement. In these experiments *s* is assigned the gap size or separation distance between a heated and an unheated wall.

For the geometry studied in this thesis the confinement level is given by:

(Equation 5.3)

Where *D* is the diameter of the heated plate and $\Theta$ is the inclination angle.

The characteristic length dimension of a vapour slug is the disk diameter because the entirety of the disk is covered before the vapour slug departs. This observation is especially true at higher heat fluxes. From the vantage point of new nucleated bubbles in the low end of the heater, the obstruction to venting is the projection of the disk diameter to the vertical axis. These newly formed bubbles gain kinetic energy as they rise along the heater surface – whether or not they have enough energy to overcome the obstruction depends, to a first approximation, on the perceived obstruction height.

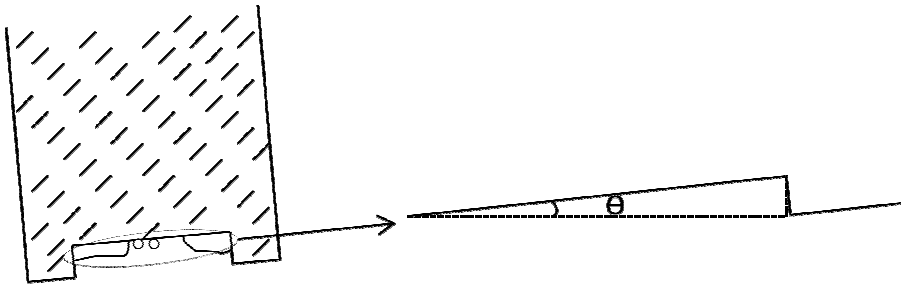


**Figure 5.6: Perceived Obstruction Height**

It is illuminating to consider how the Bond number arises in studies of bubble dynamics. Consider a simplified model where energy is balanced for a vapour slug located below the superheated microlayer:

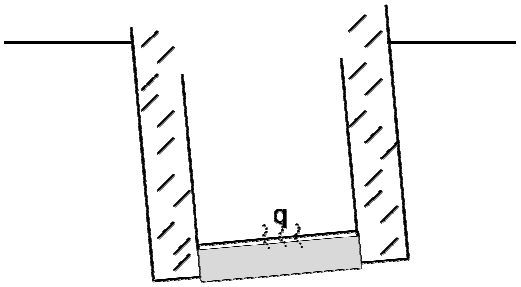


**Figure 5.7: Energy Balance On Vapour Slug**

Heat is transferred from the heated surface through the microlayer and into the two-phase mixture. The surface is covered such that a pancake like vapour bubble is formed prior to departure and venting. Performing an energy balance on the vapour slug just before it departs the surface and enters the pool gives:

Energy Input = Gravitational Potential Energy + Interfacial Tension Energy + Latent Heat of Vaporization

Gravitational Potential Energy ~$\Delta\rho g D^4$

The reference point is taken between the water-air interface and the separation distance between the free surface and the vapour slug is on the order of the disk diameter. Also, the vapour slug height is on the order of the disk diameter (as can be seen from the figure).

Interfacial Tension Energy ~$\sigma D^2$

This can be seen by noting that the surface tension is defined along a line – the physical property has units of N/m. The work required to create the interface and propagate it is on the order of the disk diameter squared.

When comparing the two competing effects, the latent heat of vaporization is moved into the left hand side of the equation:

$$Q_{in} - Mh_{fg} \quad \Delta\rho g D^2 D^2 + \sigma D^2 \qquad \text{(Equation 5.4)}$$

Normalizing with respect to the surface tension:

$$\frac{Q_{in}-Mh_{fg}}{\sigma} \cong \frac{\Delta\rho g D^2}{\sigma} D^2 + D^2 \qquad \text{(Equation 5.5)}$$

Equating the first term in the right hand side to unity and solving for the critical diameter or length scale gives the capillary length as stated in equation 5.2. Inserting the capillary length, *L*, into Equation 5.5:

$$\frac{Q_{in}-Mh_{fg}}{\sigma} \cong LD^2 + D^2 \qquad \text{(Equation 5.6)}$$

In the lifetime of the vapour slug, it will encounter viscous forces. For example, drag is encountered when it moves up to the air-liquid interface.

For the inclined cases, the vapour slug will advance to the high end of the plate and contact the impeding wall. This, to a first approximation, can be treated as a one-time energy cost analogous to the latent heat of vaporization. Thus, the conservation of energy equation adds the following two terms:

Energy Dissipation = Viscous Fluid Flow + Obstruction

Drag ~ $\mu$ ($A_x C_D + A_L C_f$) $v$

Obstruction ~ $\gamma D \sin\Theta = \gamma s$

If viscosity is neglected then the vapour slug's conservation of energy just before it vents to the atmosphere is:

$$\frac{Q_{in}-Mh_{fg}}{\sigma} \cong LD^2 + D^2 - \gamma s \qquad \text{(Equation 5.7)}$$

Normalizing with respect to the confinement length, s:

$$\frac{Q_{in}-Mh_{fg}}{\sigma s} \cong \frac{L}{s} D^2 + \frac{D^2}{s} - \gamma \qquad \text{(Equation 5.8)}$$

$$\frac{Q_{in}-Mh_{fg}}{\sigma s} \cong \frac{1}{Bo} D^2 + \frac{D^2}{s} - \gamma \qquad \text{(Equation 5.9)}$$

Therefore, the Bond number has appeared from non-dimensionalization of an idealized energy equation. By developing this model insight is gained into what other factors might impact CHF; such as viscosity.

Note that condensation heat transfer has been neglected in the treatment. As such, this model cannot be adequately used unless venting is the dominant mode of heat removal. For the flat inclination, $\Theta$=0˚, the above discussion does not apply.

## 5.3 Taylor-Helmholtz Instability in the Unconfined Variation

Zuber (1959) developed a theory to predict the CHF. In his dissertation he compared the results predicted by his theory to earlier experimental data—most notably data as obtained by Kutateladze (1952). The results were in very good agreement, and the so called hydrodynamic limit as discussed by Zuber is currently the accepted explanation of the dry-out phenomenon.

Zuber's theory was based on an upwards facing infinite surface in a pool of saturated liquid. He showed that the instigation of film boiling was caused by insufficient liquid replenishment due to the rate at which vapour leaves the surface. For well wetting surfaces, such as water on Brass, the hydrodynamic theory is still consistent with more recent experimental evidence (Dhir 1992).

A mathematical study and treatment of Zuber's theory is outside the scope of this thesis. However, the CHF phenomenon is qualitatively discussed. In Zuber's discussion he postulates that the instigation of film boiling is Taylor-Helmholtz unstable.

Helmholtz instability occurs when velocity shear of sufficient magnitude can overcome surface tension and manifests an unbounded wave. A physical example is found on oceans subjected to a large velocity shear.

Taylor instability arises when a less dense fluid is beneath a more dense fluid. A practical example of such a state is found in film boiling on an upwards facing surface.

Zuber postulated that both instabilities occur at the CHF point. It is argued here that similar influences exist for a downwards facing plate.

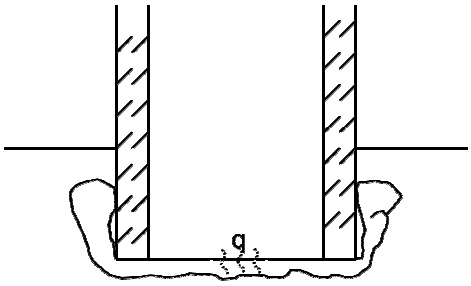


**Figure 5.8: Helmholtz Instability for the Unconfined Orientation**

Vapour slugs slide along the heater surface to one end before venting or becoming vapour jets along the periphery of the heater. It is expected that the Helmholtz instability exists similar to an upwards facing surface but is manifest at a lower heat flux as higher shear stresses will be experienced by the liquid along the liquid-vapour

interface as the slugs migrate to one side and vent. Taylor instability does not exist as vapour is below the superheated microlayer. The superheated liquid layer instead must be depleting until vapour contacts the surface at dryout.

## 5.4 Experimental Data Comparison for the Confined Variation

To the authors knowledge the experiment performed here with regards to the confined variation is novel. Confined boiling experiments have been performed in the literature and the results available are compared to data obtained here. Nucleate boiling curves and then CHF data is compared with published results. A correlation is presented and key observations are provided in the sections that follow.

Note that only data with $T_\infty$=30°C is included in all comparisons. As is evidenced in the Experimental Results chapter, there was no substantial impact at different pool temperatures. Thus, the most complete and convenient data set with $T_\infty$=30°C is the only one compared.

### 5.4.1 Nucleate Boiling Curves

Su *et. al.* (2008) published results on nucleate boiling for a downwards facing plate in a confined space. The confined space in their study was a gap of varying size. The disk diameter in the author's work and Su *et. al.* (2008) is similar, as are the confinement levels. Cases that have a basis for overlap are compared in Figure 5.9.

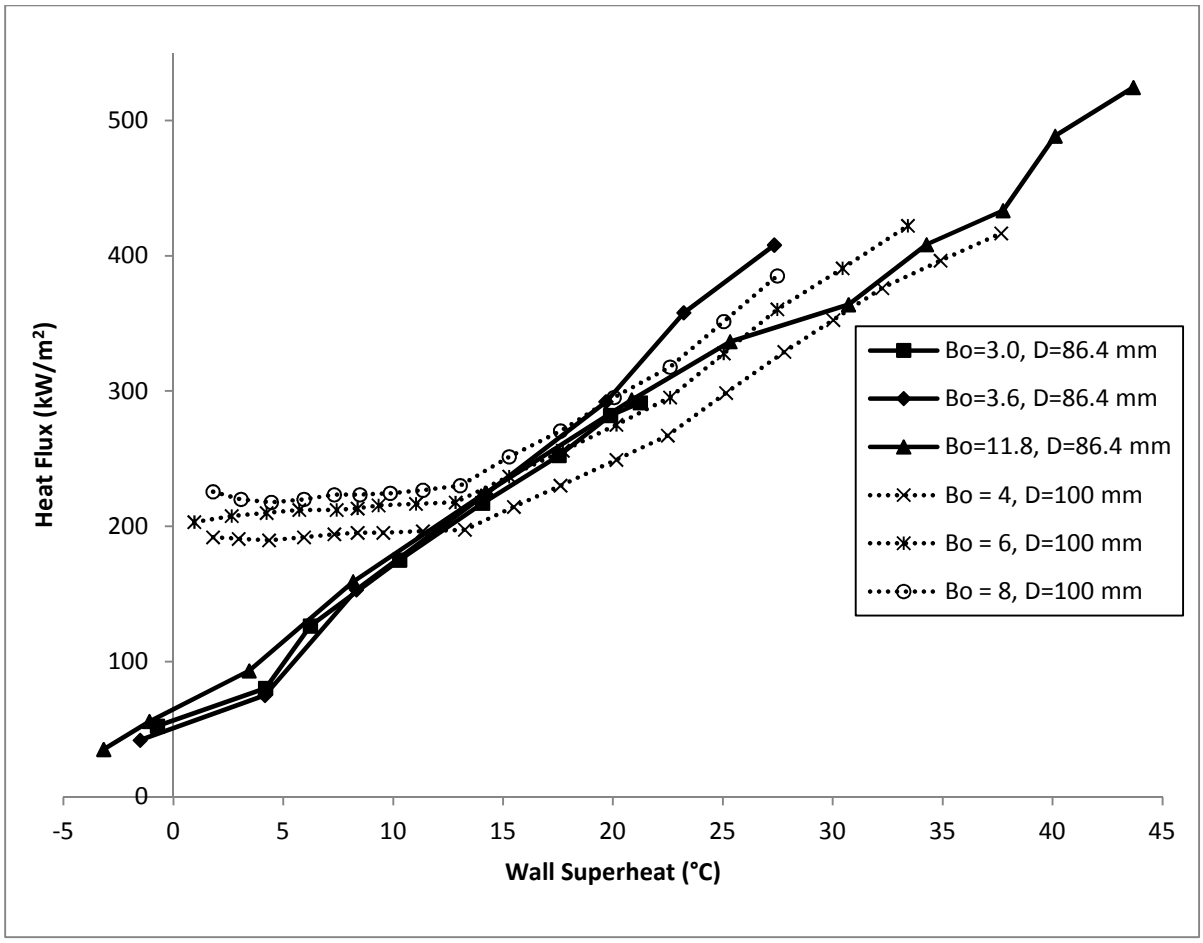


**Figure 5.9: Comparison of Author's Data (Solid Lines) to Su et. al. 2008 (Dashed Lines)**

The experimental results show excellent agreement in the medium to high heat flux regions with poor agreement in the low heat flux region. The technique used in measuring the heat flux relied upon in the study of Su *et. al.* (2008) has some bias as the heat flux through the middle of the disk will be at a maximum relative to all other locations. Thus, it is thought that the heat flux values quoted by Su *et. al.* (2008) have a positive bias relative to the true flux. In the authors study, some bias likely exists as well, but since the heat flux is measured over the entire plate it is argued that this bias is statistically smeared. This explanation is somewhat negative to the published study of Su *et. al.* (2008), and doesn't explain the agreement seen at medium to high heat fluxes. Another cause of the discrepancy could have been due to the poor definition of steady state. Su *et. al.* (2008) may not have waited as long as the author to acquire data. This is very possible as the steady state is poorly defined – a hot liquid layer near saturation begins to settle at the top of the pool similar to the behaviour seen in immiscible liquids and the temperature continues to slowly rise. As will be discussed however, when venting begins to dominate the time

scales become a great deal shorter and hence agreement is obtained between the author's study and Su *et. al.* (2008). The discrepancy seen in Figure 5.9 as well as the matching of nucleate boiling curves is of little practical importance for the designer or safety analyst. What is of utmost importance is the value of the critical heat flux, an event that leads to burnout and defines the safe and practical operation of a device.

### 5.4.2 CHF

Confined boiling CHF studies are available in the open literature. Theofanous *et. al.* (1994) completed a full scale study on the departure of nucleate boiling for a facility representative of a LWR lower head utilizing stainless steel as the heated plate under saturated boiling conditions. Note that the lower head is actually in a confined space and that the CHF is determined azimuthally. Theofanous *et. al.* (1994) relied on the direct joule heating method. The data obtained by the author is compared to that of Theofanous *et. al.* (1994) in Figure 5.14.

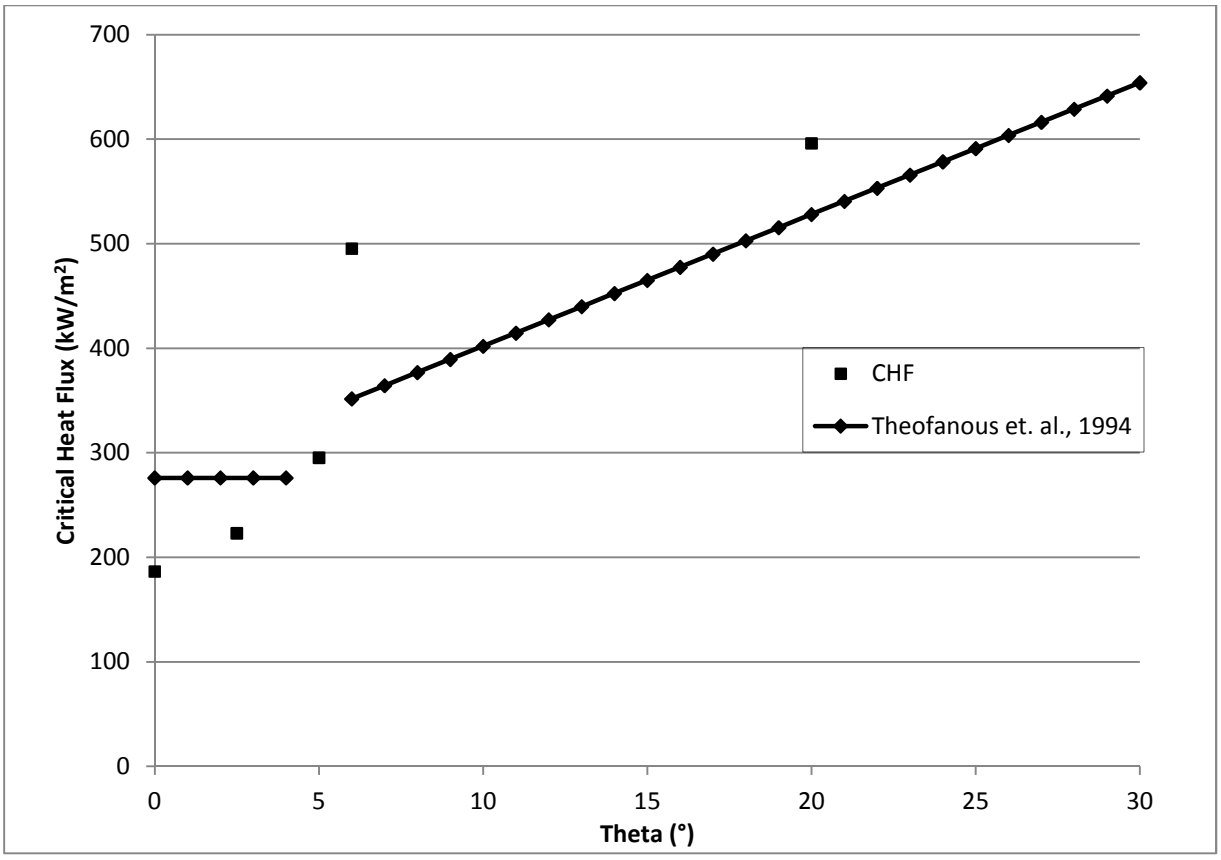


**Figure 5.10: CHF as a function of θ Comparison**

Considering the differences in the two experiments—one is full scale and a slightly curved plate and the other is scaled down and confined differently, the results are remarkable in their agreement. Also, a sharp increase in CHF,

the transition angle, for Theofanous *et. al.* (1994) occurred at 5° while the author's transition angle occurs at 5.5°. This is a remarkable result and is a very good indication that the experiment was scaled down correctly – i.e. without losing the important physical behaviours.

### 5.4.3 The Subcooling Impact on CHF

The data indicates that CHF is weakly impacted by subcooling. This is contrary to what is accepted, but there are some plausible explanations. Either the studied range of bulk fluid temperatures is too narrow to permit any sort of conclusion within experimental error or a sufficient layer of hot fluid near saturation exists for all cases and the recorded pool temperature is not representative of the temperature in the vicinity of the heater. Further experimentation and improvements are needed before a conclusions can be drawn.

### 5.4.4 CHF Correlation

A correlation is developed for easy and quick predication of CHF in a confined space. Linear interpolation is used for inclination angle θ≥6° and a least squares fit is used for θ≤5°. The resulting graph is plotted in Figure 5.11.

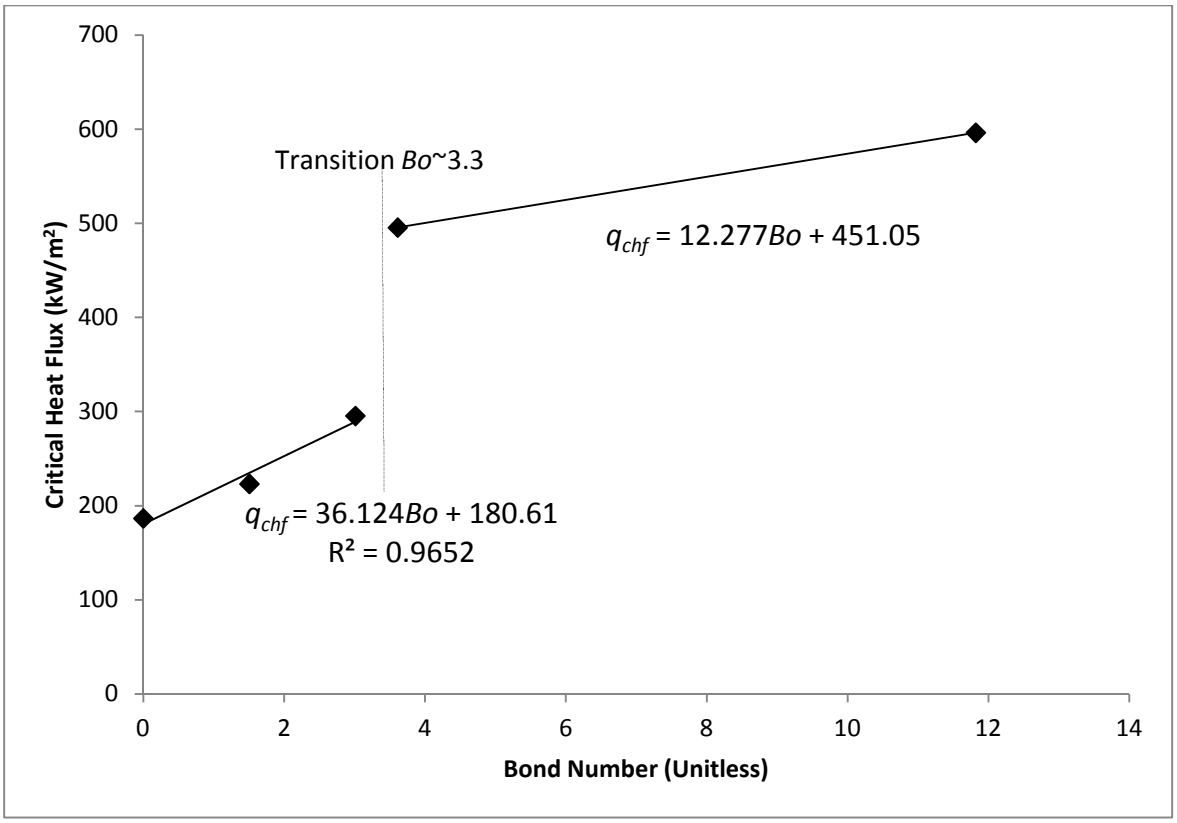


**Figure 5.11: CHF Correlation with Bond Number**

The critical heat flux, $q_{chf}$, for Bo<3.3 [kW/m$^2$]:

$$q_{CHF} = 36.1Bo + 180.61 \qquad \text{(Equation 5.10)}$$

The critical heat flux, $q_{chf}$, for Bo<3.3 [kW/m$^2$]:

$$q_{CHF} = 12.3Bo + 451.05 \qquad \text{(Equation 5.11)}$$

### 5.4.5 Observations on Heat Transfer Effectiveness

At low heat fluxes venting is not prominent and the effectiveness of heat transfer is similar for all inclinations. Small bubbles nucleate, grow and then collapse or reach some equilibrium size and transfer heat to the cold fluid by condensation through the vapour-liquid interface. A large vapour bubble does begin to collect in the cavity of the heated element with small vapour bubbles in the low end. After some time a vapour slug appears to cover the majority of the surface but then quickly collapses into the pool without venting. The scatter of the heat transfer rate at low heat fluxes is confirmed to be small as shown in Figure 5.12.

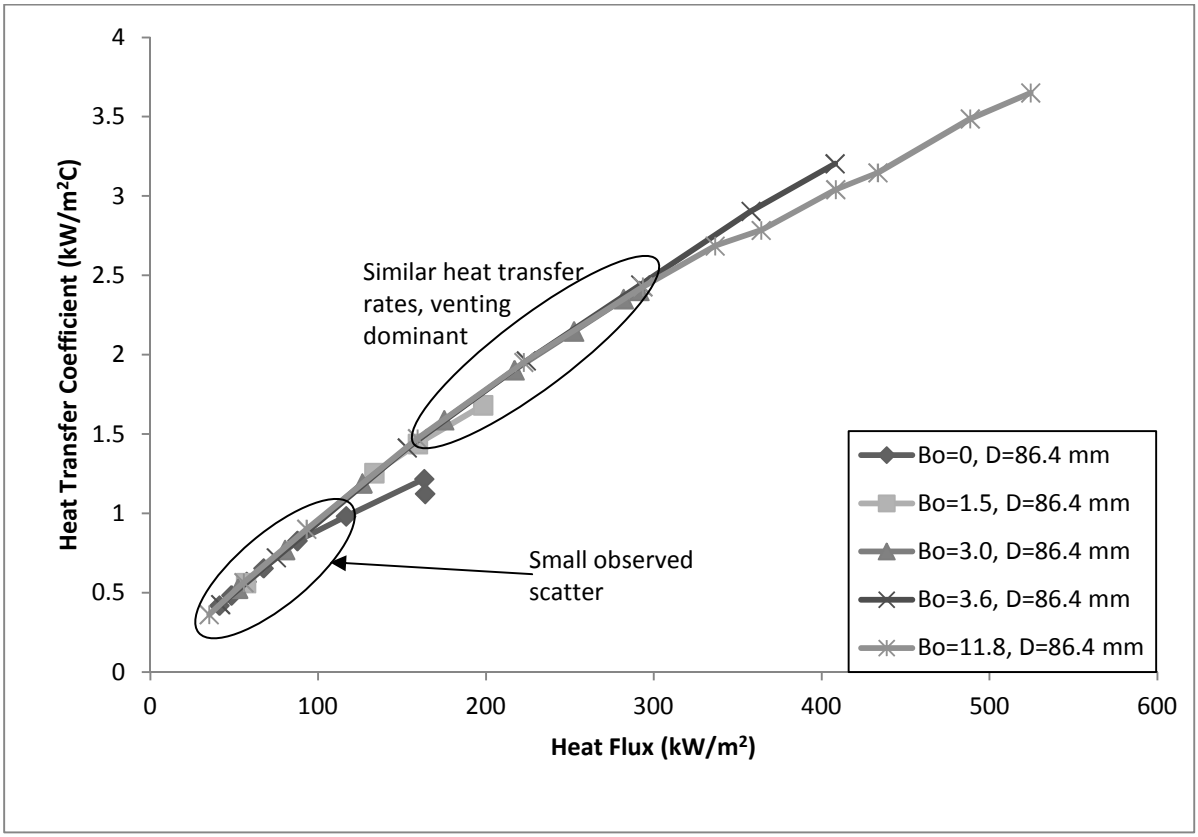


**Figure 5.12: Heat Transfer Rates**

When venting does not proceed, the required time to reach equilibrium is on the order of tens of minutes. Venting begins to occur above a heat flux of ~150 kW/m$^2$ and is observed for all inclinations except θ=0°. Since a vapour slug vents in approximately 0.5 seconds the required time to reach equilibrium is smaller. Venting is the most effective method of heat removal and thus the most important to understand. To the naked eye it appears that a vapour slug envelopes the entire heated surface and then vents with the leading front being at the high end of the heated element. See Figure 5.7.

The heat transfer rates at medium heat fluxes are very similar as the effectiveness is dominated by venting. As the inclination angle is increased the impediment to venting is correspondingly decreased. In this region of the nucleate boiling curve, however, this is unimportant. At medium heat inputs the capillary action of the vapour slug is able to overcome the impediment before the superheated liquid layer is depleted. This explains why the transfer rates are invariant with respect to inclination.

Thus whether or not film boiling is instigated depends on whether or not the capillary action of the vapour slug can overcome the impediment in the time it takes for the superheated liquid layer to deplete. An alternative explanation is that it is the force of buoyancy that causes the vapour slug to expand and eventually escape the cavity. If this escape is made before the superheated liquid layer is depleted then film boiling is not instigated. Regardless, the impediment is geometric in nature and is reduced with increasing inclination angle. Predictably the CHF and the heat transfer rates increase as the angle of inclination is increased.

### 5.4.6 Instigation of Film Boiling

Film boiling is instigated in the cavity of the heated element for all inclinations expect θ=0°. Film boiling is known to be localized to the cavity as visual observations have been made and confirm that at least a portion of the heater is rewet. Thermocouples located directly above the cavity show a large temperature excursion. It is believed that the cavity is under stable film boiling, the low end of the heater is rewet and the two regions are separated by a continually growing and shrinking (unsteady) film. The size of the stable film layer is expected to be greatest for θ=2.5° and decrease with increasing inclination angle.

The behaviour is markedly different for the θ=0° orientation as the capillary action of the vapour slug is not able to overcome the impediment. Indeed the transition angle is believed to be ~2.5° as an experiment with 1.3°

inclination was performed qualitatively and yielded essentially identical results. When the capillary action cannot overcome the impediment and the heater surface is facing down, film boiling is slowly instigated around the circumference of the disk and then spreads to the entire surface.

Note that film boiling was never allowed to stabilize in any experiment as this would result in damage to the assembly.

## 5.5 Experimental Data Comparison for the Unconfined Variation

The boiling heat transfer for a downwards facing plate has been studied extensively in the open literature. Experimental results obtained in this experiment are compared with available data and are compared to a general correlation in the sections that follow.

### 5.5.1 Nucleate Boiling Curves

Nishikawa *et. al.* (1984) studied the effects of inclination angle on the heat transfer behaviour for a Copper plate and discovered that the boiling curve only differed at low heat fluxes for varying inclination angles. This data is reproduced in Figure 5.13:

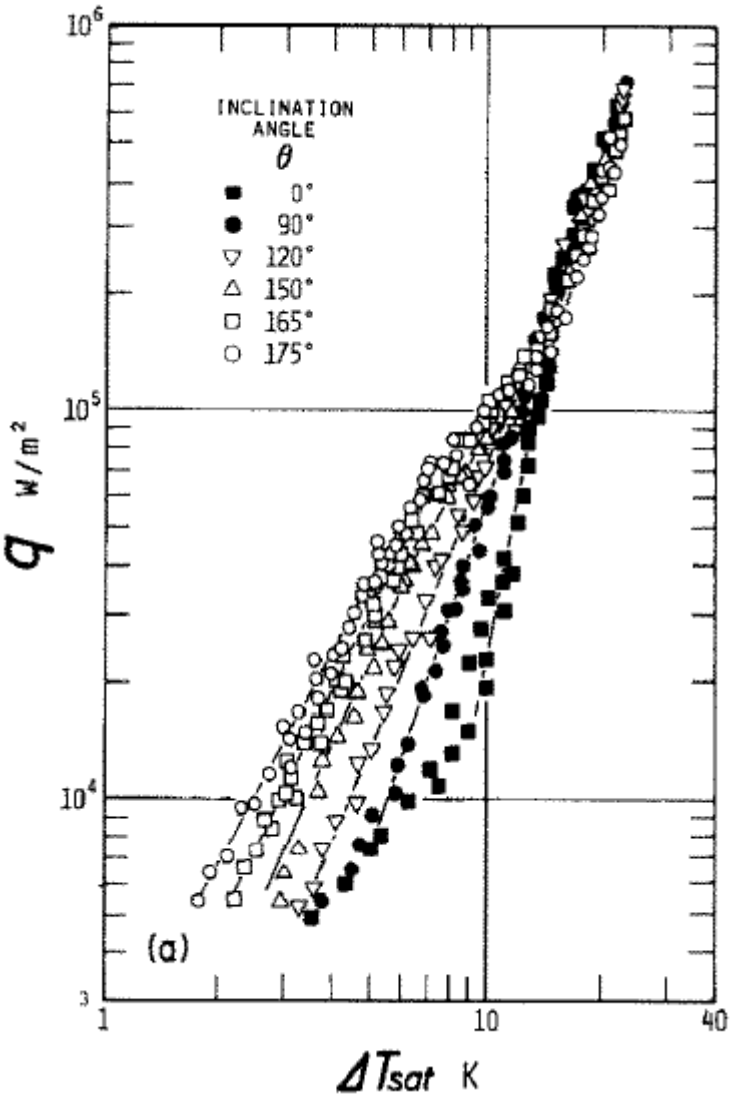


**Figure 5.13: Nucleate Boiling Data from Nishikawa *et. al.* (1984)**

Note that the angle convention for Nishikawa *et. al.* (1984) was different as θ=180° is downwards facing and θ=0° is upwards facing. The researchers concluded that the boiling curves for all inclination angles converge to the same line as medium to high heat fluxes are approached.

Data obtained in this experiment is plotted with the Nishikawa *et. al.* (1984) data and once again remarkable agreement is observed. See Figure 5.14.

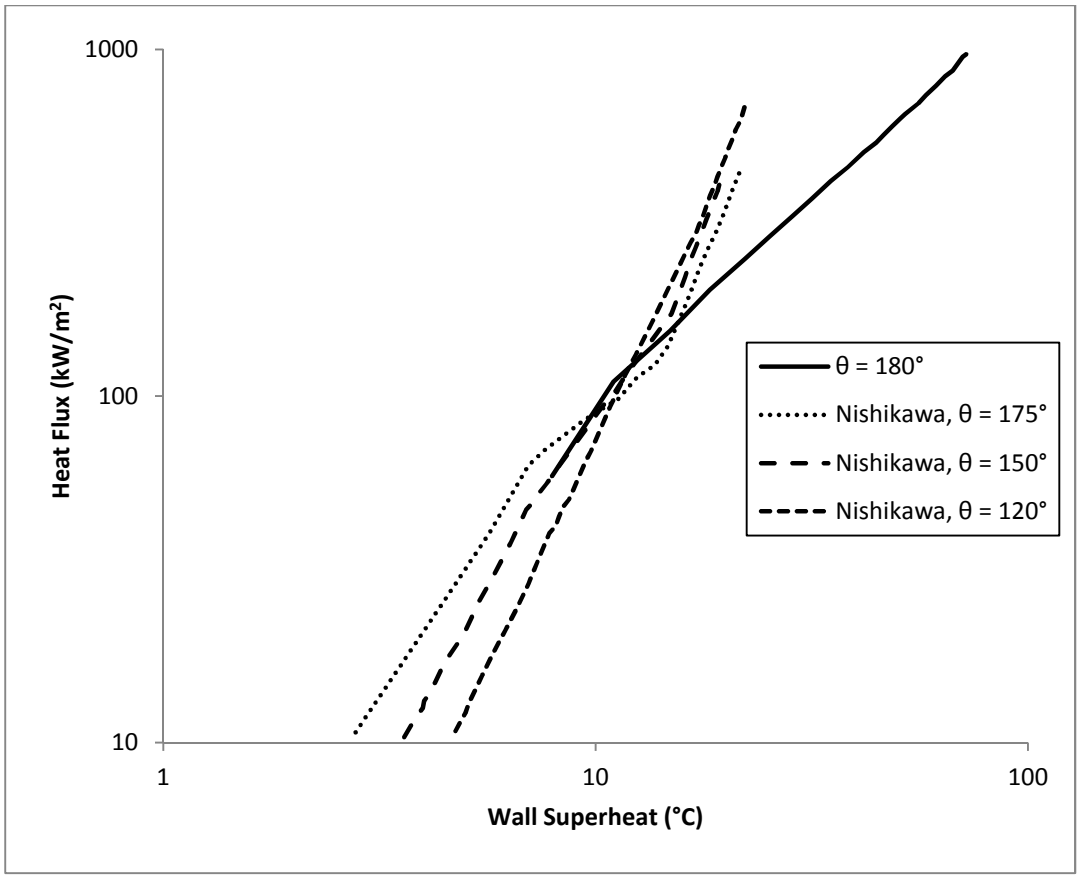


**Figure 5.14: Unconfined Boiling Curve Comparison**

At first glance there may appear to be a large discrepancy between the two data sets. This is not the case at all, as both downwards facing curves indicate a similar kink in the data at medium heat fluxes, as well there is strong agreement in the low to medium heat flux range. Also, there is evidence to believe that surface characteristics, for example the oxide film formed on the surface, actually is the key factor in determining heat transfer rates (Zysina-Molozhen (1953)). Indeed from a design or safety analysis perspective the wall superheat is a relatively unimportant quantity, the conclusion of Nishikawa *et. al.* (1984) is that at high heat fluxes the boiling curves converge to the same line.

The Stephan-Andelsalam correlation is the most widely used correlation in boiling heat transfer and it is used here as well. The heat transfer rates as calculated from the experimental data and as predicted by the Stephan-Andelsalam correlation is presented in Figure 5.15.

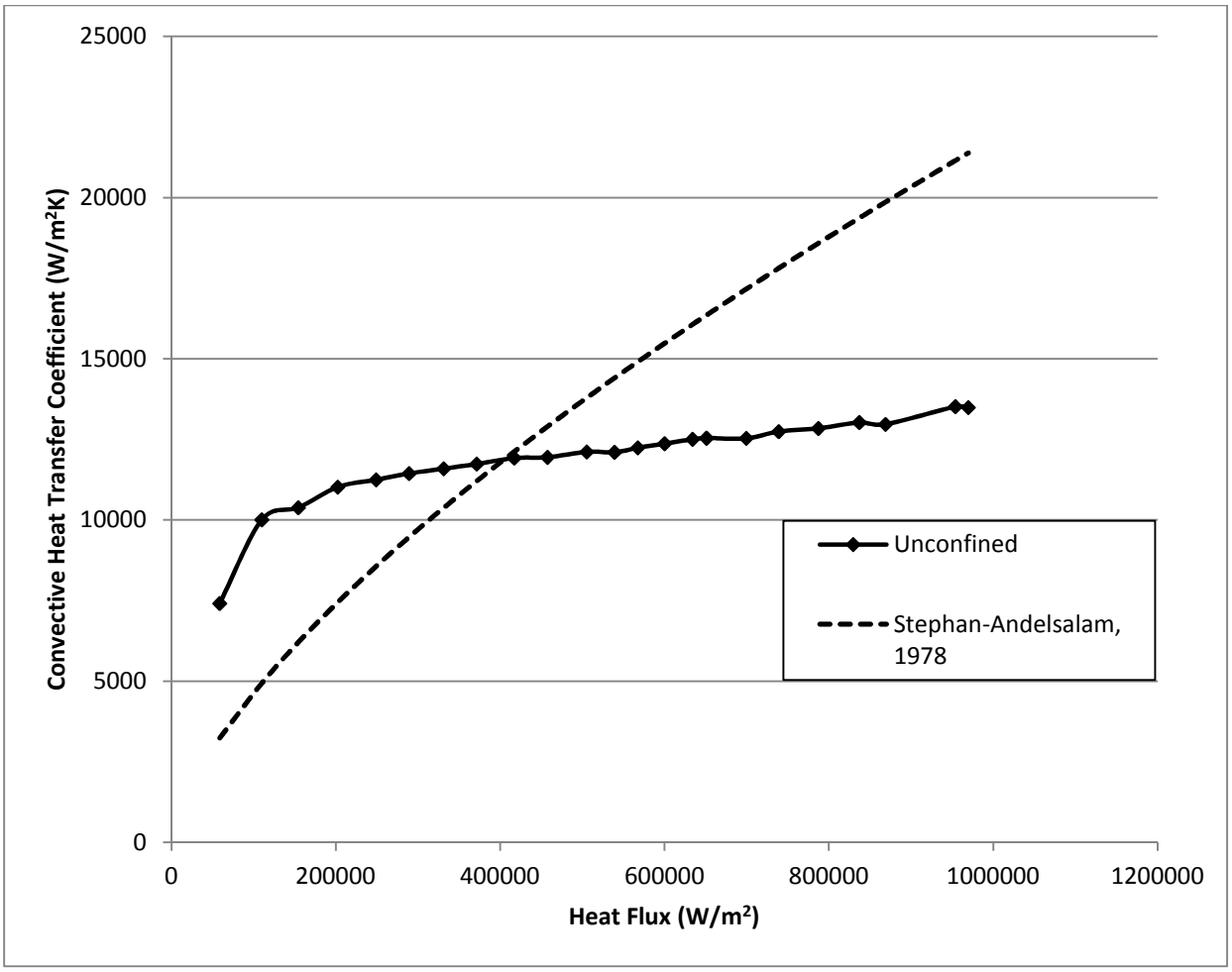


**Figure 5.15: Stephan-Andelsalam Correlation Comparison with Data**

The discrepancy is calculated using:

$$e = \left|\frac{h_{predicted}}{h_{data}} - 1\right| \times 100\% \qquad \text{(Equation 5.12)}$$

There is some agreement between the data and the predicted heat transfer rates but there are large discrepancies particularly in the high heat flux region. The error ranges from~2% to ~60% with a mean of 31% and the functions do not trend the same way. Note that this is not necessarily a negative result as the Stephan-Andelsalam correlation is general and was constructed using varied experimental data (different fluids and geometries).

### 5.5.2 CHF

The hydrodynamic limit as derived by Zuber (1959) and experimentally confirmed by Kutateladze (1952):

$$q_{CHF} = C\rho_G^{1/2} h_{LG} \sqrt[4]{g(\rho_L - \rho_G)\sigma} \qquad \text{(Equation 5.13)}$$

For water at atmospheric pressure the hydrodynamic limit is evaluated to be ~1100 kW/m$^2$. This theory assumes an upwards facing infinite plate at saturated pool conditions. This theory may be applicable for unconfined downwards facing boiling as well. Data from Nishikawa *et. al.* (1984) implies this; as well, experimental data presented here also seems to support the thought that the physics of the hydrodynamic limit are applicable to downwards facing surfaces.

There is a significant amount of experimental data available in the open literature and it is summarized in Table 5.1:

**Table 5.1: Experimental CHF Studies – Saturated Conditions**

| Author(s) | Surface and Environment | Method | CHF (kW/m$^2$) |
|---|---|---|---|
| Yang et. al. 1997 | Downwards Facing Plate, Stainless Steel | Direct Joule Heating | 776 |
| Guo and El-Genk 1992 | Downwards Facing Plate, Copper | Quench Cooling | 200-300 |
| Yang et. al. 2005 | Aluminum Hemisphere, Plain and Coated | Direct Joule Heating and Quench Cooling | 400-700 |

It is noted that all of the experiments quoted in Table 5.1 were for saturated conditions. As can be seen there are large differences in the CHF for what are similar experiments. A consensus in the academic community does not exist yet for the CHF of a downwards facing plate.

The CHF values as reported by Yang *et. al.* (1997) is found to be the CHF value that agrees most closely with the observed result in this thesis. The discrepancy maybe due to the possibility that the researchers did not adequately take into account the temperature drop between the thermocouples and the surface exposed to water. Note that stainless steel is a poor thermal conductor.

The data obtained by Guo and El-Genk (1992) relied on the quench cooling method, which is prone to transient effects as discussed earlier. The method of quench cooling isn't applicable to the CANDU response as the Shield Tank Water surrounds the Calandria Vessel throughout the postulated accident.

The last quoted study, Yang et. al. (2005), may have been biased. It is seen that the plain vessel and the coated vessel achieved CHFs of 400 and 700 kW/m$^2$, respectively. A considerably higher wall superheat was quoted in the

latter case. This may indicate a bias on the behalf of the experimenters to show a significant CHF enhancement when a surface coating is applied.

The experimental results quoted in Table 5.1 can be converted to applicable values for subcooled water. Unfortunately, as it will be shown later, the currently accepted methodology used to convert CHF values at saturation to an equivalent subcooled value result in extreme values and is likely not applicable for a downwards facing surface in pool boiling.

The experimental data obtained here indicated that CHF is greater than 1 MW/m$^2$. An appeal is made to the hydrodynamic limit as well as the yet to be determined impact that subcooling makes on the CHF for the particular geometry studied.

### 5.5.3 Observations on Heat Transfer Effectiveness

At low heat fluxes, bubbles nucleate and reach an equilibrium size without detaching from the surface. As the heat flux is increased the bubbles will begin to coalesce and form a vapour slug. The vapour slug will collapse back into the pool without venting.

At medium heat fluxes, the vapour slug begins to vent and steam is released into the atmosphere. As the heat flux is increased the frequency of venting is observed to also increase. The flow patterns do not change as the heat flux is increased to~1 MW/m$^2$. A venting vapour slug continues to remove heat from the surface and dryout is not observed.

Condensation heat transfer, wherein the vapour slug collapses into the pool, is observed to be of significance. For high heat fluxes, as the vapour slug departs the surface and rises through in a jet like pattern there is likely thinning of the jet due to condensation heat transfer. The maximum vapour removal rate is likely linked to this as well as Taylor-Helmholtz instability.

## 5.6 The Effect of Subcooling and the Miller-Ivey Correlation

Saturated CHF pool boiling experiments can be extrapolated for subcooled conditions using:

$$q_{CHF}^{\Delta T_{sub}} = q_{CHF}[1 + B\Delta T_{SUB}] \qquad \text{(Equation 5.14)}$$

Where *B* is given by Ivey and Morris (1962):

$$B = 0.1\left(\frac{\rho_f}{\rho_g}\right)^{0.75}\left(\frac{c_{pf}}{h_{LG}}\right) \qquad \text{(Equation 5.15)}$$

For subcoolings of ~60 °C, the correction factor $B\Delta T$ is ~2.5. This means that the data reported in Table 5.1, for example, when converted to subcooled conditions would result in exorbitant heat fluxes.

Earlier experimental data has also shown that the CHF is insensitive to subcooling for the case of confined boiling. These results do not mesh well with the predictions of equation 5.14. Numerically the CHF is predicted to increase by approximately 20% for each 5˚C increase in subcooling. Equation 5.14 may not be applicable to the geometry studied in this thesis as the Miller-Ivey correlation was constructed from cylindrical geometries. It was investigated here based on the direction provided in Zuber's dissertation.

In addition to the geometrical argument, Equation 5.14 may not be applicable on the premise that fluid near saturation exists around the heated surface and that what leads to dryout is a vapour slug that stops the replenishment of the superheated liquid layer. In the steady state, fluid near saturation rises to the top of the free surface and in essence this experiment becomes one conducted at saturation conditions. In other words, there may not be a subcooling margin at all.

Lastly, subcooling is difficult to measure as the location is not clear. In contrast to the upwards facing heated surface, the re-circulation pathway for downwards facing surfaces is not well defined (Su *et. al.* 2008). Further study is warranted. A potential method relies on using non-invasive temperature and flow measurements to discover where the re-circulation pathway is and measure the temperature of the bulk at this location.

## 5.7 The Effect of Heater Surface Oxidation

The formation of an oxide layer on the heated surface is expected to have an impact on the boiling curve and CHF. A marked impact for an oxidized (i.e. aged) surface versus a freshly polished surface was not observed. This result is easily explainable and supported by other independent research. The surface roughness for Brass doesn't change appreciably over short times scales (~5 hours) for water near saturation and the oxide layer is also narrow (Zhdan and Castle). Given the short times scales and low temperatures of the experiments presented here, corrosion of the heated surface was minimal and thus had no appreciable impact on the results.

## 5.8 In-Vessel Retention

Since the CANDU reactor most closely resembles the unconfined variation the data here indicates that melt relocation through wall-melt-through is physically unreasonable given that the CHF is approximately an order of magnitude greater than the heat fluxes that would be seen by the Shield Tank Water.

In the confined study, significant impediment to heat removal exists. At the lowest inclination, the most effective removal method (through venting) does not occur and still the CHF is greater than what would be seen by the Shield Tank Water (D. L. Luxat and J. C. Luxat (2007)). These are remarkably good results for the CANDU design.

## 5.9 Recommendations on Future Work

This thesis raised some interesting questions, but by no means is definitive. The tools are here to enable one to undertake a definitive study in pool boiling on downwards facing surfaces. The direction of future study should include:

- Studying the effect disk diameter has on nucleate boiling and CHF in an unconfined and confined variation. Current electrical capacity in the EPBF is able to accommodate such an expansion.
- Thermocouple structures can be built around the heated element in an attempt to study how vent frequency impacts boiling heat transfer (see Equation 1.4). There may be a critical frequency that once surpassed results in film boiling.
- Boiling heat transfer in gaps, applicable to LWR designs, can easily implemented by adding a plate beneath the heated surface.
- A non-invasive study of the temperature and flow fields near the heated element can be made so that a location indicative of a re-circulation pathway can be identified. Following this, one can define subcooling for downwards facing surfaces and then the effect that subcooling has on CHF can be studied.
- Capturing high speed images of the boiling process.

A more immediate need that can be undertaken by a summer student is as follows:

- A level control system needs to be designed and constructed such that the water level in the test section tank and auxiliary tank are within 1 mm of each other and a specified set point. The system cannot rely on

operator intervention. A filter should also be added to remove any particulates that may exist in the working fluid.

- The confined boiling experiments should be repeated and the results confirmed.
- Further analysis of the obtained data, as desired (note all utilized data is attached on the accompanying CD).

# 6 Conclusion

A successful experimental investigation of the physical feasibility of Calandria Vessel failure by wall-melt-through under thermal loads has been completed. The experimental facility was designed and constructed to study boiling heat transfer on downwards facing surfaces. Boiling heat transfer was studied using the gradual heating technique for surfaces that were under confined and unconfined boiling conditions.

The level of confinement was adjusted by varying the inclination angle for a surface in which venting was obstructed by the placement of a lip surrounding the heated surface. This was a novel confinement technique that also allowed the separation of condensation and venting as a method of heat removal. The confined variation is intended to conservatively represent the Calandria Vessel at the point of stagnation with significant obstruction to vapour slug movement. The lip obstruction was practically intended to conservatively represent obstructions due to moderator piping found in the Shield Tank Water. The obtained nucleate boiling curve has been compared with that of Su *et. al.* (2008) and excellent agreement was obtained at medium to high heat fluxes. The obtained CHF results as a function of inclination angle were compared to data presented by Theofanous *et. al.* (1994) and good agreement was reached. Similar results were also obtained with regards to an observed transition angle in the CHF-Angle of Inclination plot. The obtained CHF value for the $\theta=0°$ inclination was higher than the heat flux expected to be present through the Calandria Wall in the event of a prolonged severe accident (D. L. Luxat and J. C. Luxat (2007)). This implies that film boiling will not be instigated even in the event that venting cannot be relied upon. The argument that the Calandria Vessel will not fail due to thermal loading can be made. Physically, it is reasonable to expect that venting, or vapour slug movement due to gravitational forces, can be relied upon as a method of heat removal in the Shield Tank Water. The critical angle that allowed for venting was $\theta=2.5°$ with CHF increasing as the angle of inclination is increased.

The unconfined variation was intended to represent the behaviour of the Calandria Vessel wall at the stagnation point. The geometry is still thought to have some conservatism. In the best estimate the curvature in the Calandria Vessel wall will assist in heat removal. The nucleate boiling curve was compared to data as obtained by Nishikawa *et. al.* (1984) and acceptable agreement was found. The power requirement to instigate film boiling was not met and as such it can be stated that for the unconfined geometry the CHF is greater than 1 $MW/m^2$.

Thus, Calandria Vessel rupture due to thermal loading is physically unreasonable as the CHF is approximately one order of magnitude greater than the anticipated heat flux from the core debris in the best estimate experimental representation of the scenario. Core debris relocation through wall-melt-through is thought and experimentally supported here to be physically unreasonable.

# 7 References

[1] Dhir, V.K. (1992), Some Observations from Maximum Heat Flux Data Obtained on Surfaces Having Different Degrees of Wettability, *Pool and External Flow Boiling: Proceedings of Engineering Foundations Conference*.

[2] Dhir, V.K. (1998), Boiling Heat Transfer, *Annual Review of Fluid Mechanics*, pp 365-401.

[3] Dupleac, D., Mladin, M. and Prisecaru, I. (2009), Generic CANDU 6 plant severe accident analysis employing SCAPSIM/RELAP5 code, *Nuclear Engineering and Design*, pp 2093-2103.

[4] Guo, Z., El-Genk, M. (1992), An experimental study of saturated pool boiling from downward facing and inclined surfaces, *International Journal of Heat and Mass Transfer*, pp 2109-2117.

[5] Henry, C.D., and Kim, J. (2004), A study of the effects of heater size, subcooling, and gravity level on pool boiling heat transfer, International Journal of Heat and Mass Transfer, pp 262-273.

[6] Hohl, R., Blum, J., Buchholz, M., Luttich, T., Auracher, H., and Marquardt, W. (2001), Model-based Experimental Analysis of Pool Boiling Heat Transfer with Controlled Wall Temperature Transients, *International Journal of Heat and Mass Transfer*, pp 2225-2238.

[7] Ivey, H. J., and Morris, D.J. (1962), On the relevance of the vapour-liquid exchange mechanism for subcooled boiling heat transfer at high pressure, *British Rep. AEEW-R-137*, Atomic Energy Establishment, Winfrith.

[8] Kutateladze, S.S. (1952), Heat Transfer in Condensation and Boiling, *USAEC Report AEC-tr-3770*.

[9] Luxat, D.L., and Luxat, J.C. (2007), Calandria Vessel Integrity under Severe Accident Loads, *Transactions of SMiRT* 19.

[10] Luxat, J.C. (2007), Thermalhydraulic Aspects of Profession to Severe Accidents in CANDU Reactors, *Proceedings of the 12$^{th}$ International Topical Meeting on Nuclear Reactor Thermalhydraulics (NURETH-12)*.

[11] MacKenzie, H., Judd, R.L. and Shoukri, M.S.M. (1999), Experiments in narrow gap convective boiling, Proceedings of the 17$^{th}$ Canadian Congress of Applied Mechanics, pp 269-270.

[12] Mathew, P.M., Nitheanandan, T. and Bushby, S. J., *Severe Core Damage Accident Progression within a CANDU 6 Calandria Vessel*, www.sar-net.org/upload/4-1_candu.pdf.

[13] McDanel Advanced Ceramic Technologies (2009), *Ceramic Tubes and Rods*, Beaver Falls, Pennsylvania, 2009, http://mcdanelceramics.thomasnet.com/category/ceramic-tubes-rods?

[14] Mikic, B.B. and Rohsenow, W.M. (1969), A New Correlation of Pool Boiling Data Including the Effect of Heating Surface Characteristics, *Journal of Heat Transfer*, pp 245-250.

[15] Nishikawa, K., Fujita, Y., Uchida, S. and Ohta, H. (1984), Effect of surface configuration on nucleate boiling heat transfer, International Journal of Heat and Mass Transfer, pp1559-1571.

[16] Omega (2011), Type K: Revised Thermocouple Reference Tables, Laval, Quebec, http://www.omega.com/temperature/z/pdf/z218-220.pdf

[17] Petrovic, S., Robinson, T. and Judd, R.L. (2004), Marangoni heat transfer in subcooled nucleate pool boiling, International Journal of Heat and Mass Transfer, pp5115-5128.

[18] Qui, D., and Dhir, V.K. (2002), Experimental study of flow pattern and heat transfer associated with a bubble sliding on downward facing inclined surfaces, *Experimental Thermal and Fluid Science*, pp 605-616.

[19] Stephan, K. and Andelsalam, M. (1978), Heat Transfer Correlations for Natural Convection Boiling, International Journal of Heat and Mass Transfer, pp 73-87.

[20] Su. G.H., Wu, Y. W., and Sugiyama, K. (2008), Subcooled pool boiling of water on a downward-facing stainless steel disk in a gap, *International Journal of Multiphase Flow*, pp 1058-1066.

[21] Theofanous, T.G., Dinh, T.N., Tu, J.P., and Dinh, A.T. (2002), The boiling crisis phenomenon Part II: dryout dynamics and burnout, *Experimental Thermal and Fluid Science*, pp793-810.

[22] Theofanous, T.G., Liu, C. Additon, S., Angelini, S, Kymalainen, O., and Salmassi, T. (1997), In-vessel coolability and retention of a core melt, *Nuclear Engineering and Design*, pp 1-48.

[23] Theofanous, T.G., Syri, S., Salmassi, T., Kymalainen, O., Tuomisto, H. (1994), `Critical heat flux through curved, downward facing, thick walls`, Nuclear Engineering and Design, 151, 247-258.

[24] Theofanous, T.G., Tu, J.P., Dinh, A.T., and Dinh, T.N. (2002), The boiling crisis phenomenon Part I: nucleation and nucleate boiling heat transfer, *Experimental Thermal and Fluid Science*, pp 775-792.

[25] Touloukian, Y. S., and C. Y. Ho, Eds. (1972), *Thermophysical Properties of Matter*, Vol. 1, *Thermal Conductivity of Metallic Solids*, Plenum Press, New York.

[26] Yang, J., Dizon, M.B., Cheung, F.B., Rempe, J. L., Suh, K. Y. and Kim, S.B. (2005) `Critical Heat Flux for Downward Facing Boiling on a Coated Hemispherical Surface`, Experimental Heat Transfer, 18: 4, 223-242.

[27] Yang, S.H., Baek, W.P, Chang, S.H. (1997), Pool-boiling critical heat flux of water on small plates: effects of surface orientation and size, *International Communications in Heat and Mass Transfer*, pp 1093-1102.

[28] Zhdan, P.A. and Castle, J.E. (2001), Corrosion of Brass in Ultrapure Water, *Surface and Interface Analysis*, pp 180-184.

[29] Zuber, N. (1959), Hydrodynamics of Boiling Heat Transfer. AEC Report AECU-4439.

[30] Zysina-Molozhen, L.M. (1953), Some Data on the Number of Centres of Vaporization in Boiling on Industrial Heating Surfaces, *Problems of Heat Transfer During A Change of State*, Moscow.

# 8 Appendix A: Time Series Plots and Unreduced Data

This Appendix contains plots of the raw data temperatures for the unconfined and confined variations. Plots and tables are thought to be representative for the unconfined variation. Two times series plots for the confined variation are presented and are thought to be bounding in terms of temperature variability.

## 8.1 Unconfined, $T_\infty$=30 ˚C, P=3.4 kW

*Description*: Time series plot when temperatures have stabilized. Table of values is obtained at the last sampling point.

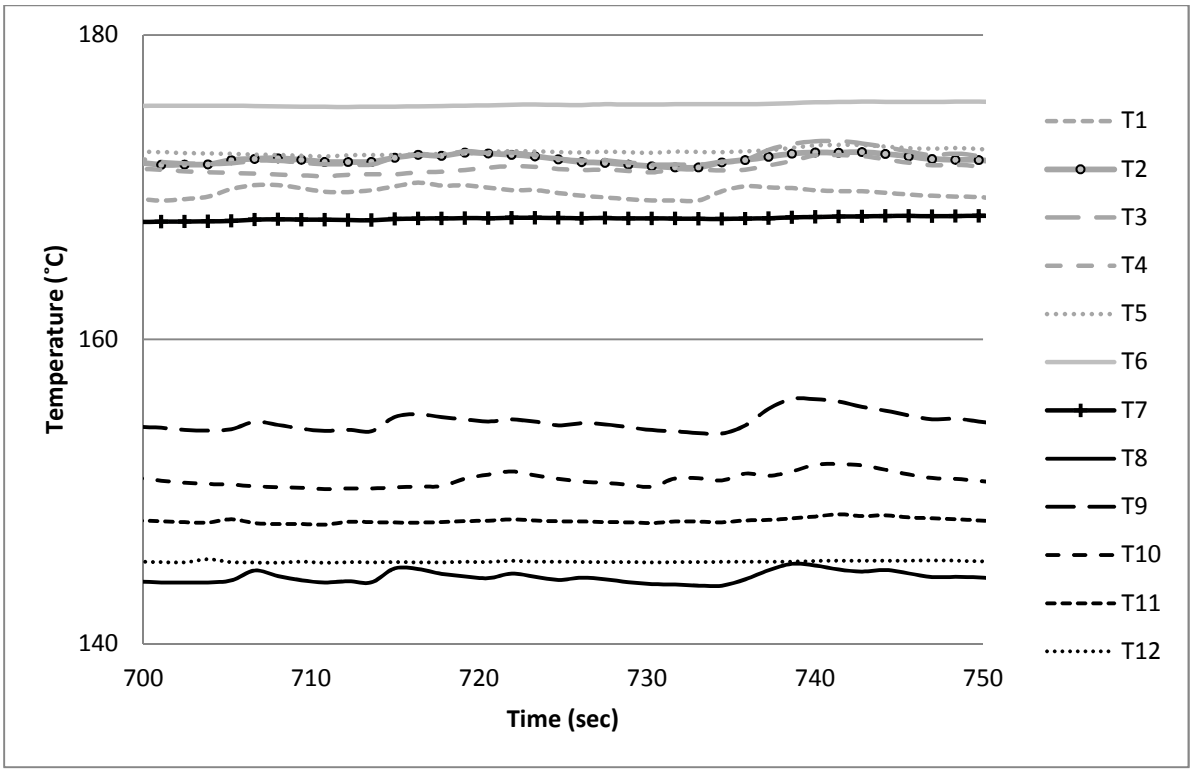


**Figure 8.1: Time Series Plot of Temperatures, Unconfined**

In Figure 8.1 grey lines are temperature recordings at the thermocouple depth closer to the heater surface-water interface (denoted as T1-T6). The black lines are temperature recordings deeper in the heated element (T7-T12).

**Table 8.1: Unreduced Data at Last Sampled Point**

| | $\langle T_{1,2} \rangle$ | k(W/mK) | $\langle T_2 \rangle$ | $\langle T_1 \rangle$ | q (kW/m$^2$) | $T_{wall}$ |
|---|---|---|---|---|---|---|
| Value | 162.06 | 127.3 | 172.06 | 152.05 | 501.5 | 142.04 |
| Variance | | - | 2.02 | 2.39 | - | - |

A top view of the heated element is shown in Figure 8.2 with an accompanying table. These in tandem are used to find specific thermocouple locations and the associated depths.

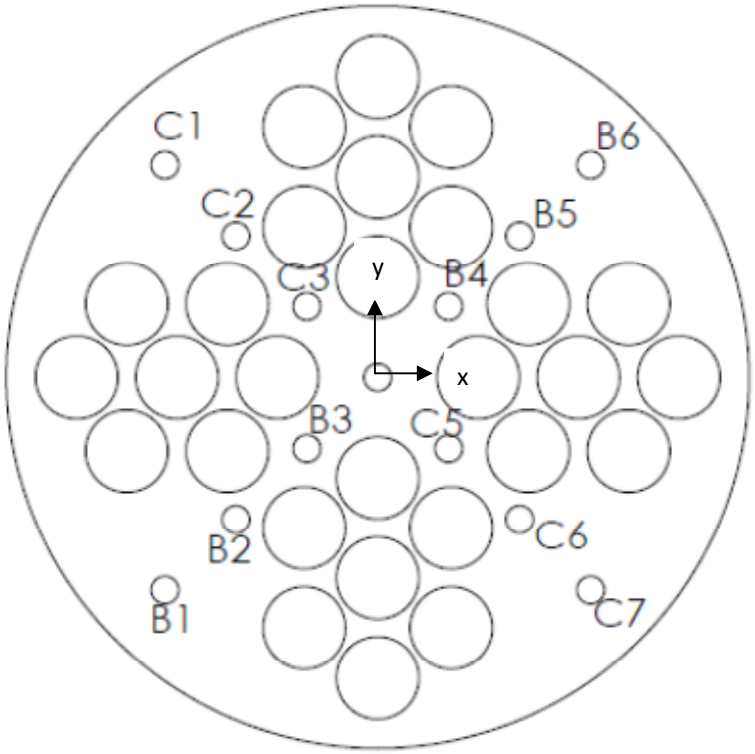


**Figure 8.2: Thermocouple Locations**

**Table 8.2: Thermocouple Access Hole Location and Depth**

| Tag | Thermocouple Label | X Location from Geometric Centre (inches) | X Location from Geometric Centre (inches) | Depth (inches) |
|---|---|---|---|---|
| C1 | T1 | -0.967 | 0.967 | 3.7 |
| C2 | T2 | -0.645 | 0.645 | 3.7 |
| C3 | T3 | -0.322 | 0.322 | 3.7 |
| C5 | T4 | 0.322 | -0.322 | 3.7 |
| C6 | T5 | 0.645 | -0.645 | 3.7 |
| C7 | T6 | 0.967 | -0.967 | 3.7 |
| B1 | T7 | -0.967 | -0.967 | 3.9 |
| B2 | T8 | -0.645 | -0.645 | 3.9 |
| B3 | T9 | -0.322 | -0.322 | 3.9 |
| B4 | T10 | 0.322 | 0.322 | 3.9 |
| B5 | T11 | 0.645 | 0.645 | 3.9 |
| B6 | T12 | 0.967 | 0.967 | 3.9 |

## 8.2 Thermocouple Locations for the Confined Variation

Note that the thermocouple labels were altered for the two confined and unconfined studies. This was done intentionally to ensure that the two sets of data would not be confused. See Table 8.3 for the confined variation thermocouple tags. Table 8.3 and Figure 8.2 can be used in tandem if one desires to know a particular thermocouple location and depth.

**Table 8.3: Thermocouple Labels for the Confined Variation**

| Tag | Thermocouple Label |
|---|---|
| C1 | T1 |
| C2 | T2 |
| C3 | T3 |
| C5 | T7 |
| C6 | T8 |
| C7 | T9 |
| B1 | T4 |
| B2 | T5 |
| B3 | T6 |
| B4 | T10 |
| B5 | T11 |
| B6 | T12 |

## 8.3 Angle of Inclination = 0˚, $T_\infty$=30 ˚C, P=1.4 kW

*Description*: Time series plot when temperatures have stabilized. Table of values is obtained at the last sampling point.

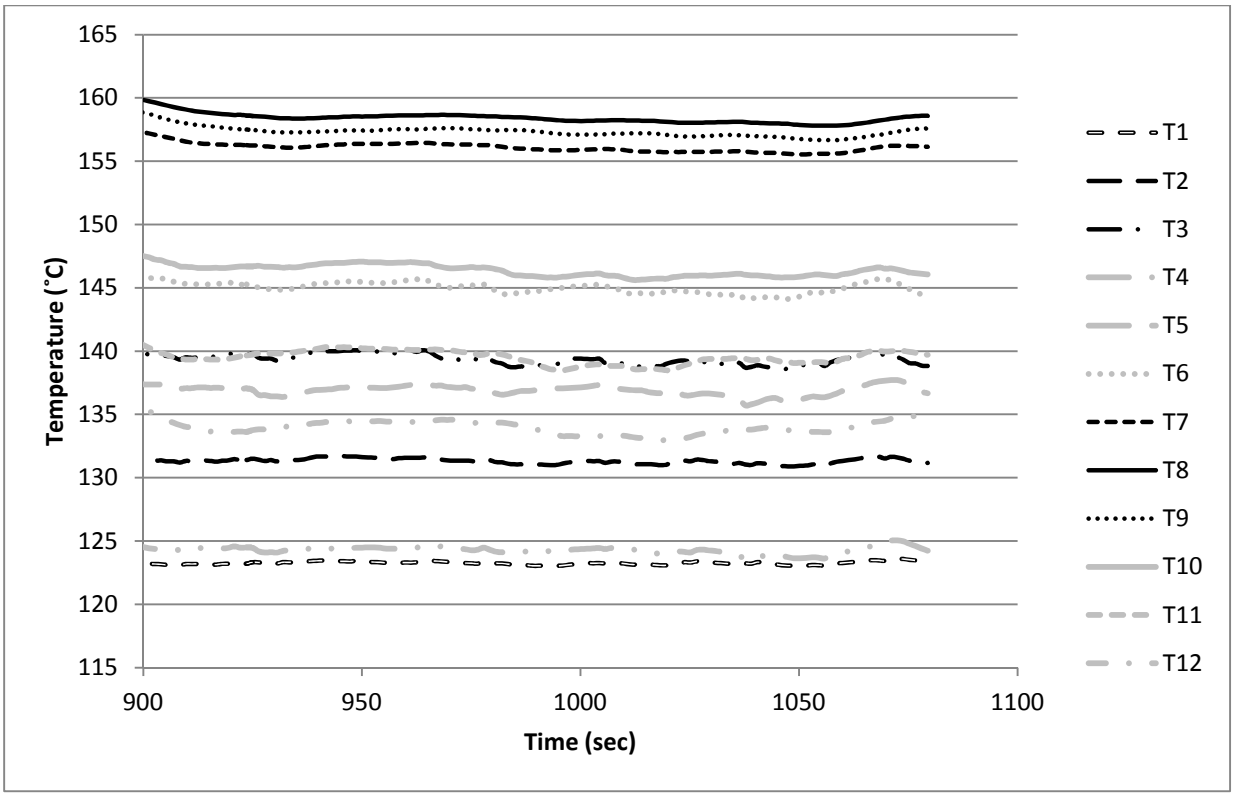


**Figure 8.3: Time Series Plot of Temperatures, Angle of Inclination = 0˚**

In Figure 8.3 grey lines are temperature recordings at the thermocouple depth closer to the heater surface-water interface (denoted as T4-T6 and T10-T12). The black lines are temperature recordings deeper in the heated element (T1-T3 and T7-T9).

**Table 8.4: Unreduced Data at Last Sampled Point**

| | $\langle T_{1,2} \rangle$ | k(W/mK) | $\langle T_2 \rangle$ | $\langle T_1 \rangle$ | q (kW/m$^2$) | $T_{wall}$ |
|---|---|---|---|---|---|---|
| Value | 140.97 | 124.80 | 144.29 | 137.65 | 163 | 134.34 |
| Variance | 12.07 | N/A | 15.23 | 7.87 | 568 | N/A |

## 8.4 Angle of Inclination = 6˚, $T_\infty$=30 ˚C, P=1.6 kW

In Figure 8.4 grey lines are temperature recordings at the thermocouple depth closer to the heater surface-water interface (denoted as T4-T6 and T10-T12). The black lines are temperature recordings deeper in the heated element (T1-T3 and T7-T9).

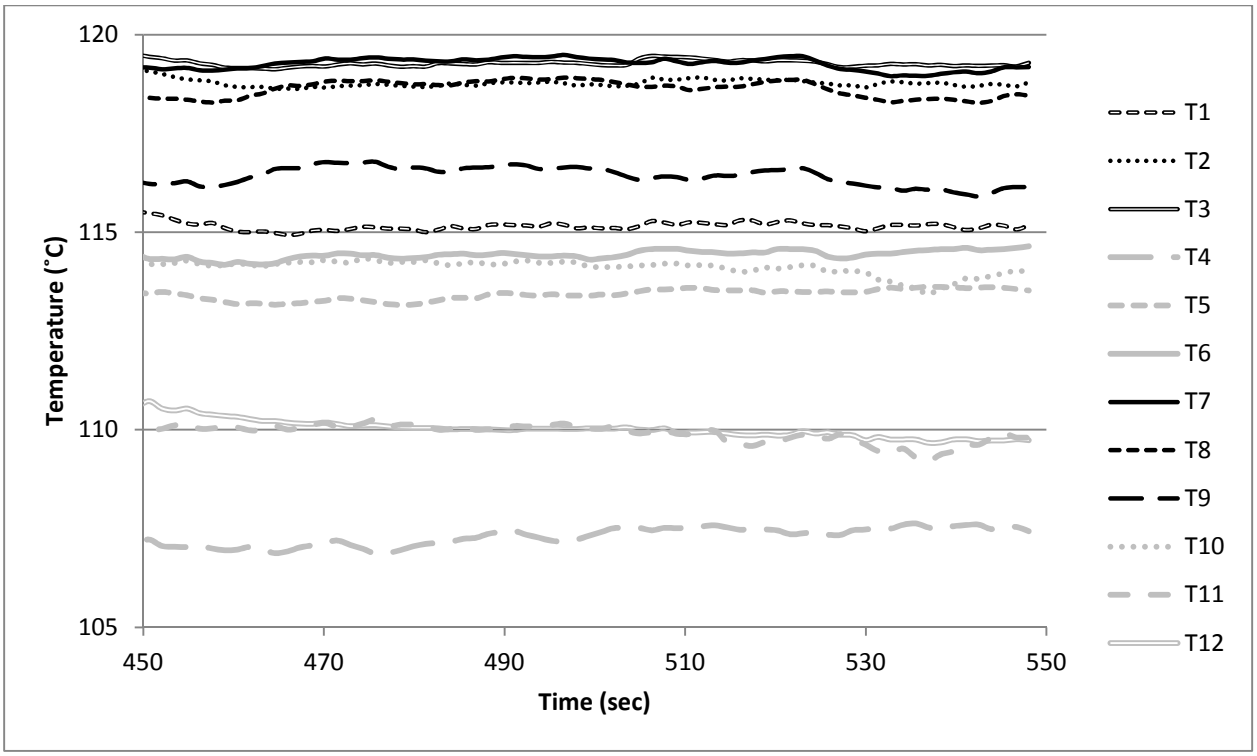


**Figure 8.4: Time Series Plot of Temperature Values, Angle of Inclination = 6˚**

**Table 8.5: Unreduced Data at Last Sampled Point**

| | $<T_{1,2}>$ | k(W/mK) | $<T_2>$ | $<T_1>$ | q (kW/m$^2$) | $T_{wall}$ |
|---|---|---|---|---|---|---|
| Value | 114.68 | 121.69 | 117.84 | 111.52 | 151 | 108.37 |
| Variance | 4.02 | N/A | 1.74 | 2.92 | 112 | N/A |

## 8.5 Angle of Inclination = 6˚, 5˚ and 2.5˚ Location of High and Low End

For the above-specified angles of inclination the high end of the heated element (relative to the ground) was located closest to the T1 thermocouple and the low end was closest to the T9 thermocouple. This is noteworthy as the raw data showed that the temperature reading of the T1 thermocouple was at all times the highest reading or was close to being the highest reading. The temperature excursion usually occurred first for the T1 thermocouple.